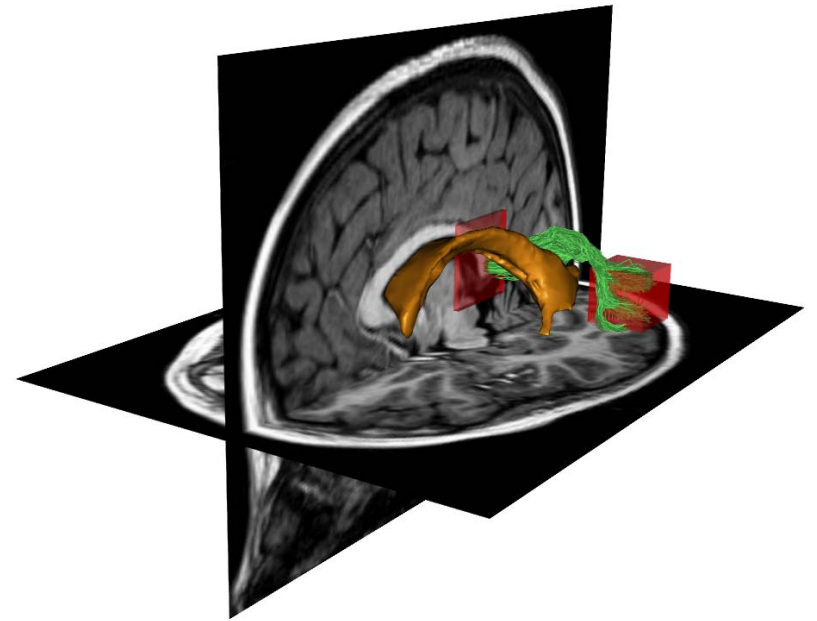
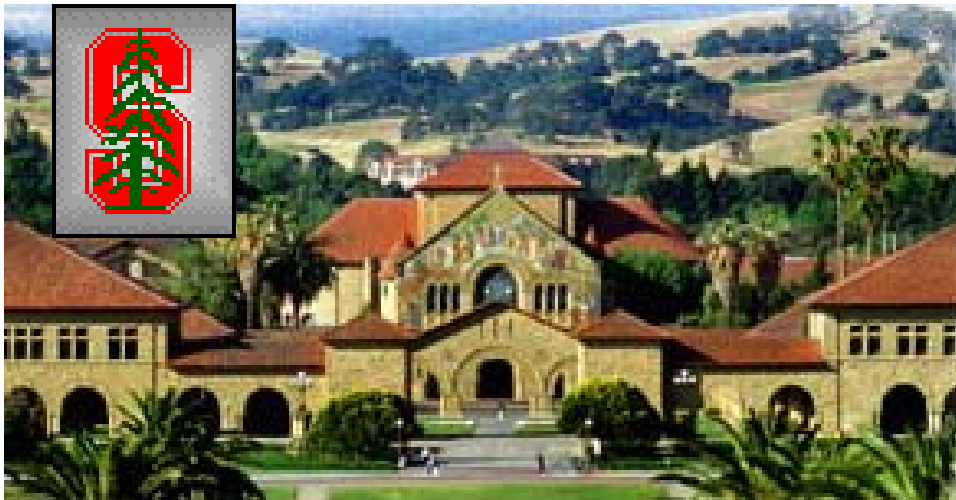


Diffusion tensor imaging and fiber tractography of human brain pathways



Brian Wandell

Anthony Sherbondy, Robert Dougherty, Michal Ben-Shachar
Psychology Department
Stanford University

Abstract

Diffusion tensor imaging and fiber tractography of human brain pathways **Brian Wandell, Anthony Sherbondy, Robert Dougherty, Michal Ben-Shachar** **Psychology, Stanford University**

The astonishing hypothesis of neuroscience is that thoughts and emotions are the interactions of neuronal signals. The synapses that mediate interactions between cortical neurons are located within a thin layer of cells that covers the surface of the brain. The local results of these interactions in the gray matter are communicated to distant brain regions along pathways comprising many axons. Mapping these pathways- the white matter tracts- is an essential part of understanding brain function. Until recently, there have been no non-invasive methods to estimate white matter tracts in the living human brain. New magnetic resonance and computational methods have emerged that provide a great deal of information about these structures in healthy and diseased brains. These Diffusion Tensor Imaging (DTI) methods measure water diffusion throughout the brain. These measurements provide an aggregate measure of the microscopic structure of living brain tissue that has sparked the development of statistical algorithms to compare the local diffusion properties in different brains, such as those of healthy and diseased groups. Further, a number of labs have developed Fiber Tractography (FT) algorithms that use the diffusion measurements to estimate the pathways followed by the white matter fiber tracts as they course their way from one gray matter region to another. In this tutorial, we will describe (a) the measurements, (b) the statistical algorithms, (c) the FT algorithms, and (d) various applications.

Diffusion tensor imaging and fiber tractography of human brain pathways

- The brain (~ 5 slides)
- MR - diffusion weighted imaging (~ 20 slides)
- The diffusion surface (~30 slides)
 - The surface shape
 - Statistical analysis
 - Visualization: Diffusion surfaces
- Fiber tractography – The algorithms (~30 slides)
 - Deterministic algorithms
 - Probabilistic wavefront algorithms
 - Most likely pathway

The Brain

Neurons – Cells; in cortex they are within a sheet on the surface;
 10^{13} in human

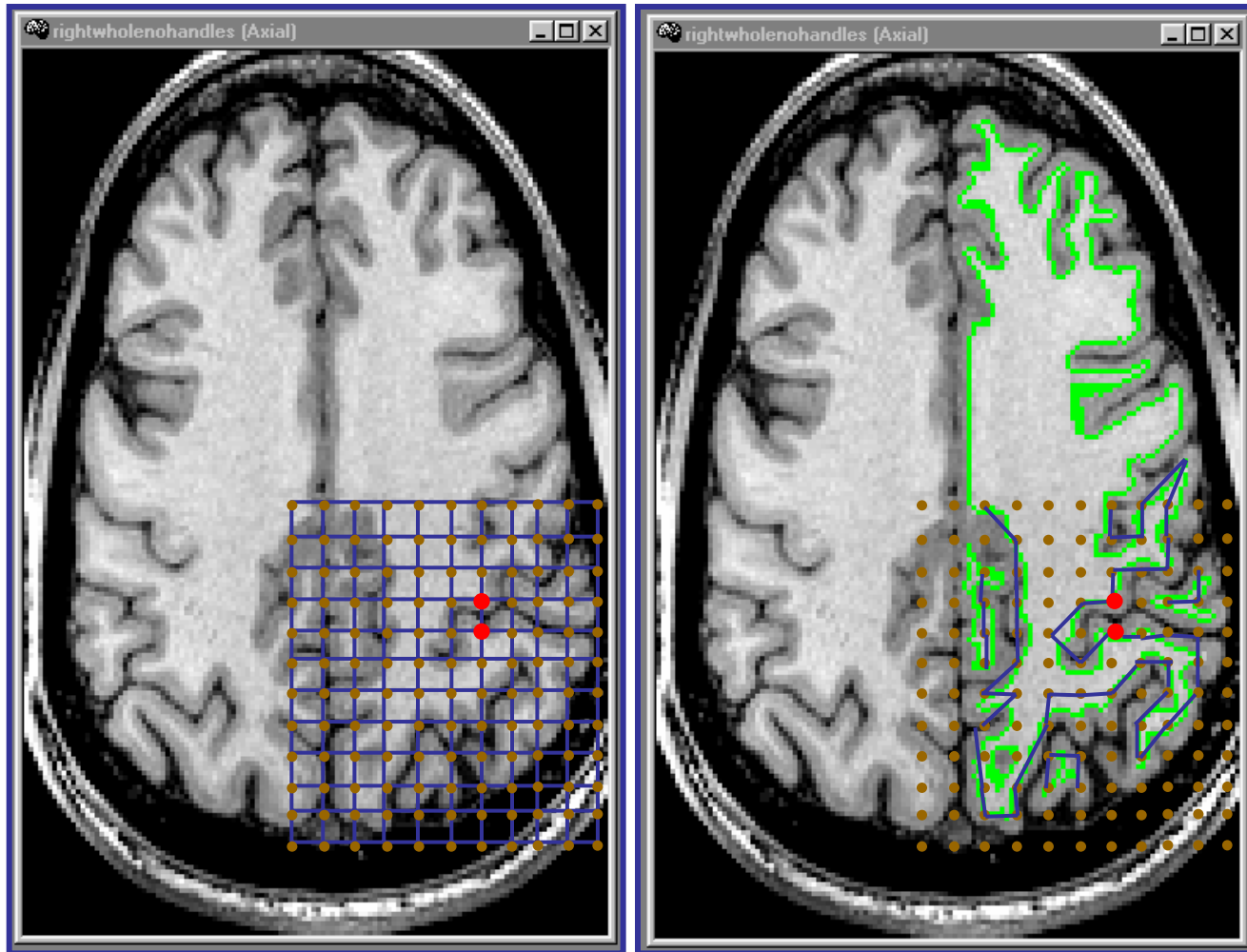
Synapses – Connections between cells; 10^{16} in human

Columns – Groups of neurons with similar properties

Axons – Carry cell output signals; various lengths from a fraction of a millimeter to many centimeters

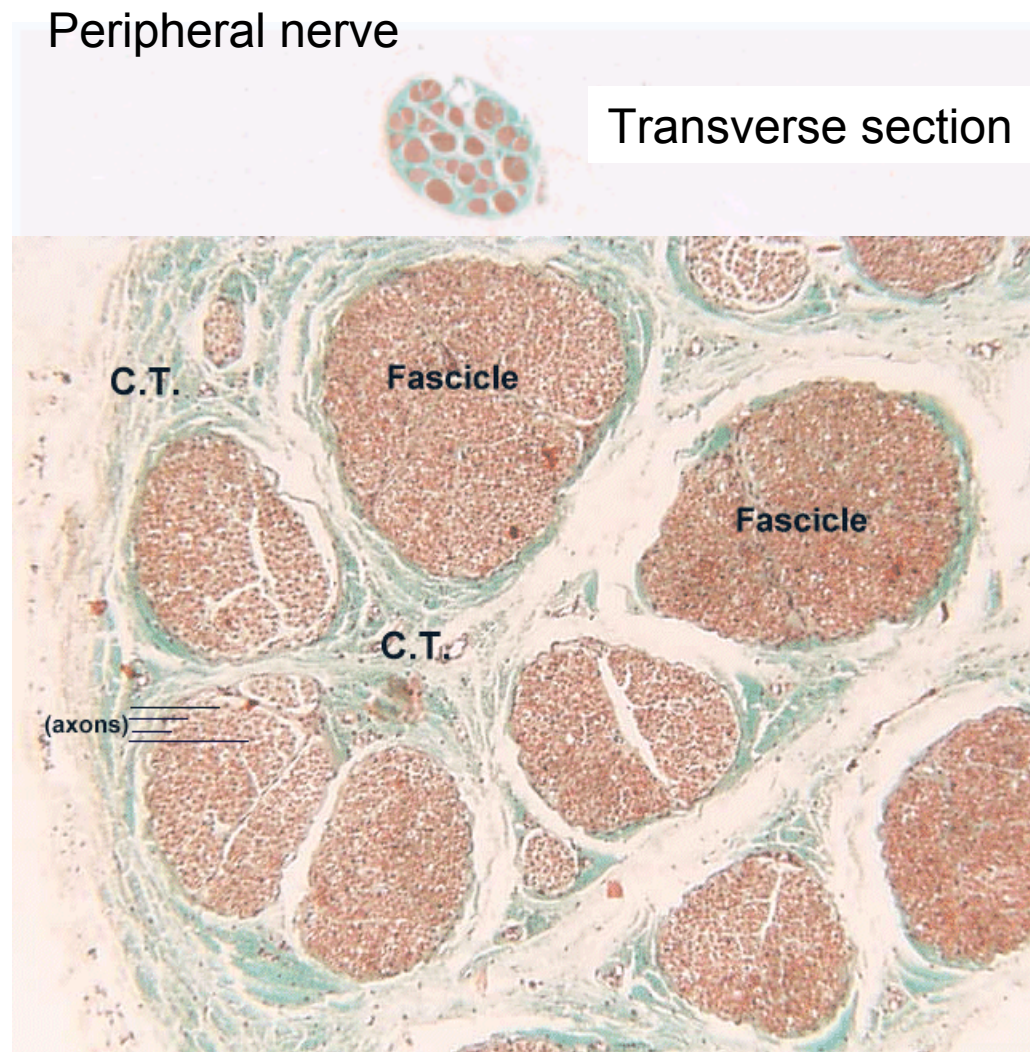
Fascicles – Multiple axons traveling together; single cells do not find a single projection cell.

MR Signal Processing: Respect The Cortical Surface

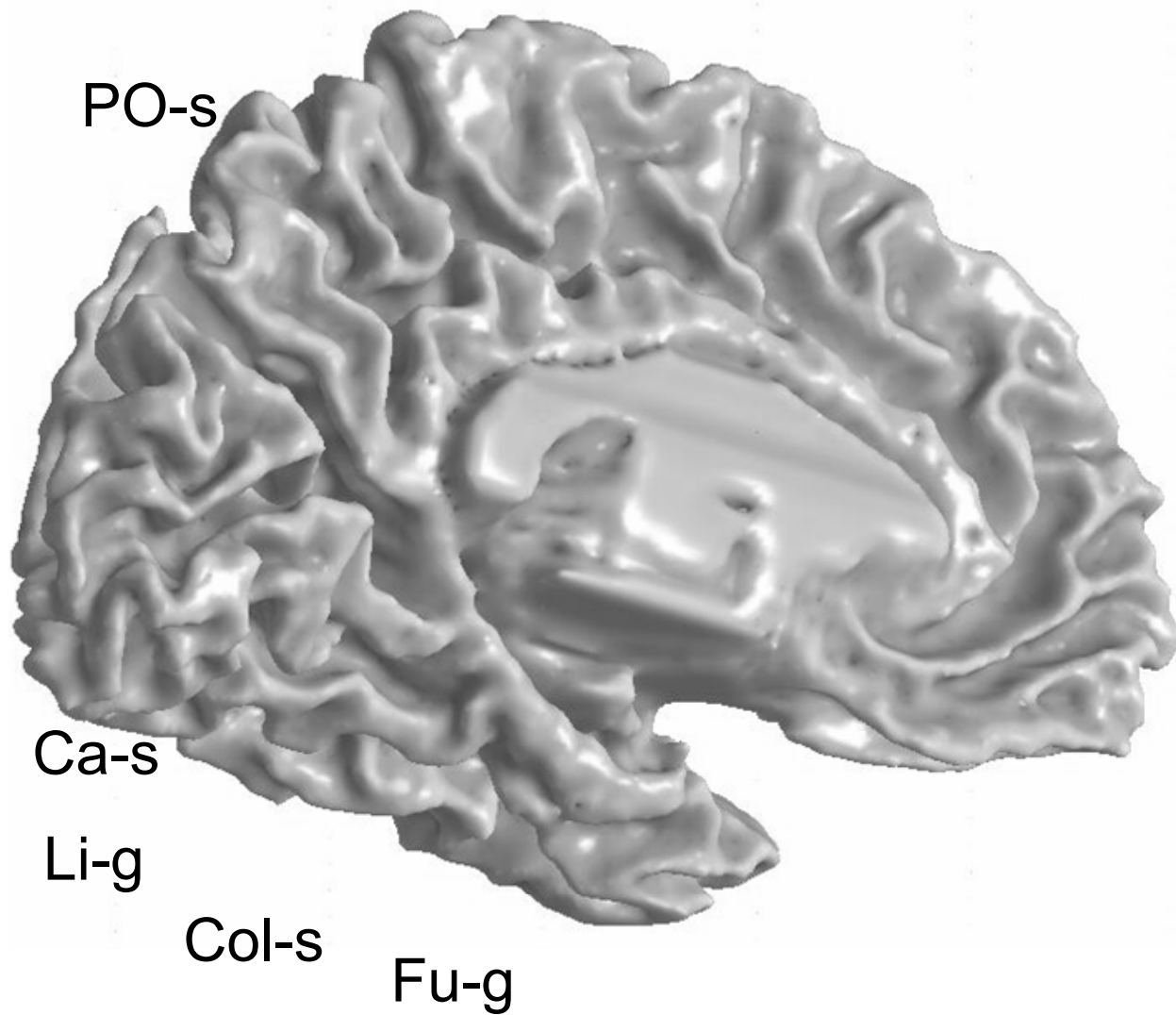


White Matter: Axons and Fascicles (Axon bundles)

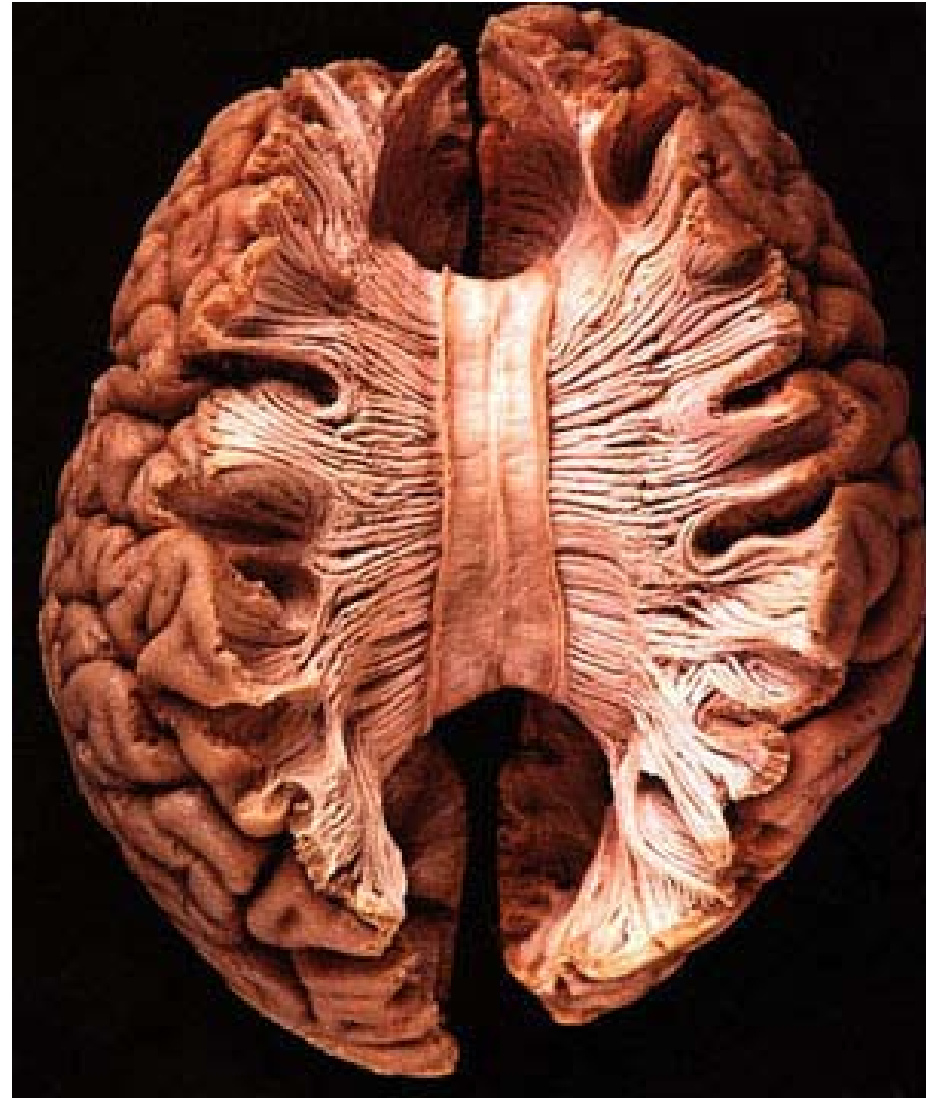
Axons are very fine
They appear to travel
together in bundles called
fascicles
The functionality of these
fascicles is unknown
There are regular properties
of these fascicles identified
in histology



Gray/white
surface
boundary



The White Matter



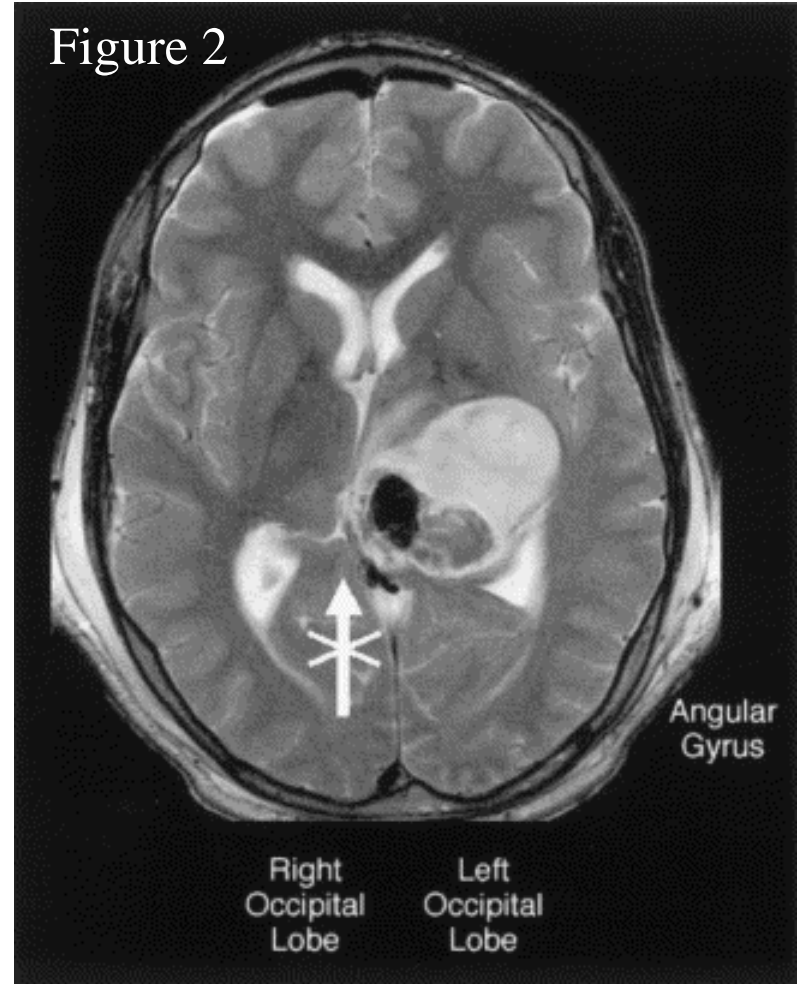
From: The Virtual Hospital (www.vh.org); TH Williams, N Gluhbegovic, JY Jew

White matter damage is common

Figure 1



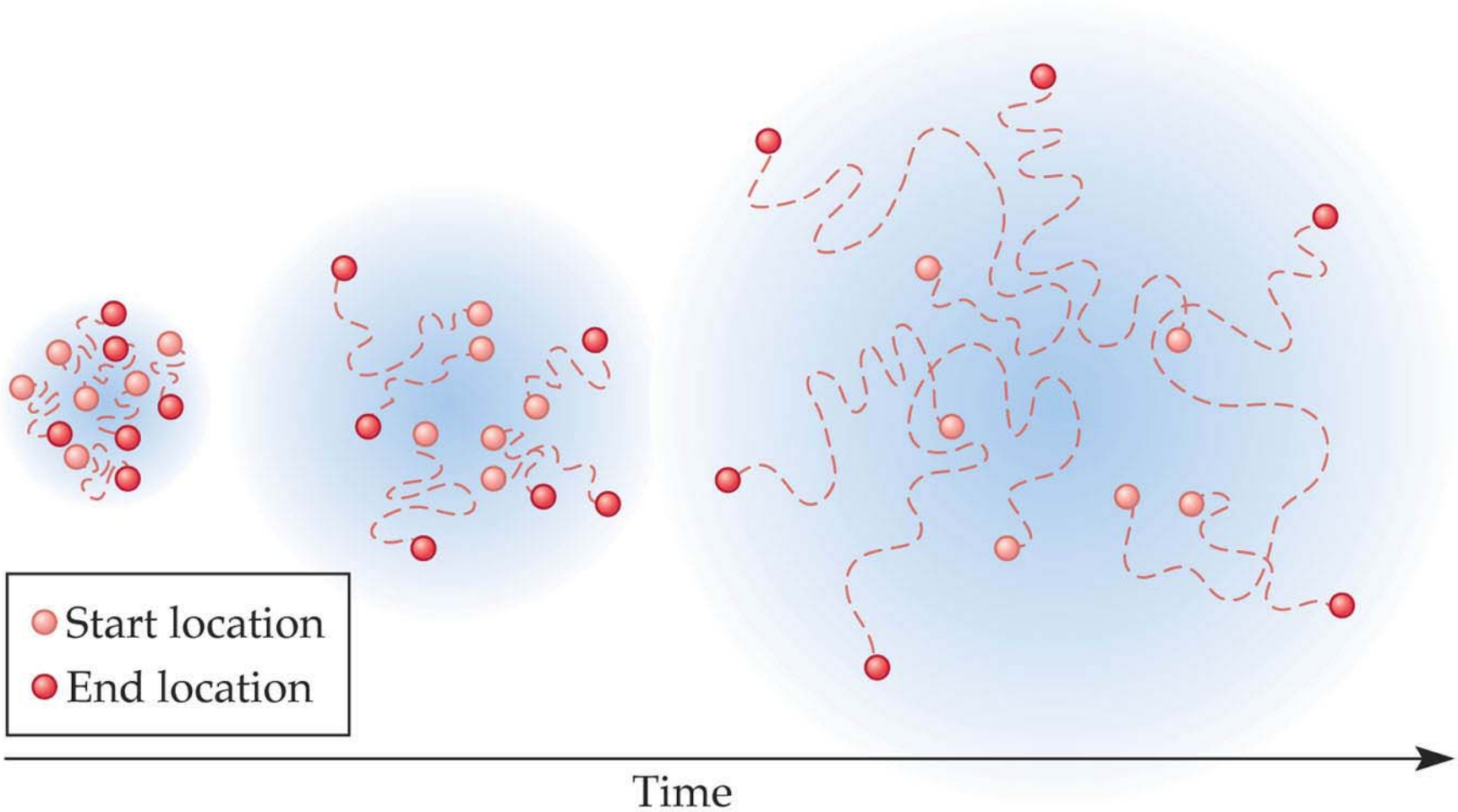
Figure 2



MR: Diffusion Weighted Imaging

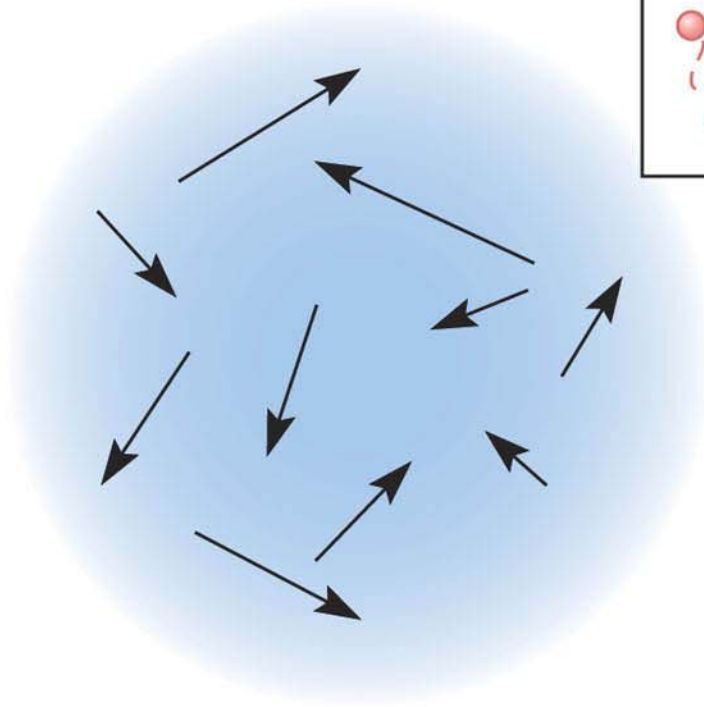
Description of diffusion within a voxel

5.17 Diffusion. Over time, molecules within gases or liquids will move freely through the medium.

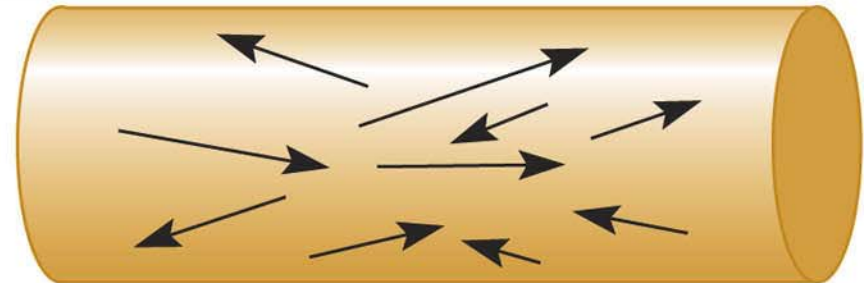
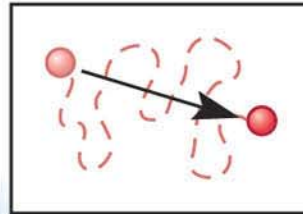


5.18 Isotropic and anisotropic diffusion.

(A)



(B)



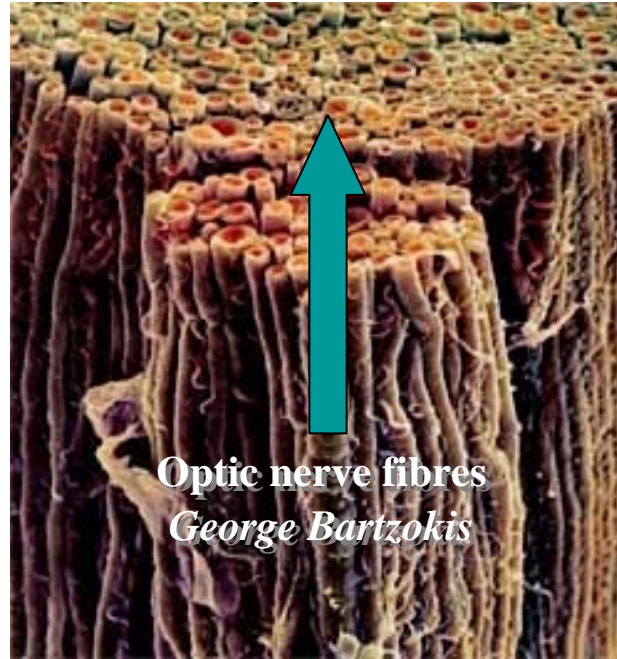
Diffusion Tensor Imaging: Concepts and Applications

Denis Le Bihan, MD, PhD,^{1*} Jean-François Mangin, PhD,¹ Cyril Poupon, PhD,¹ Chris A. Clark, PhD,¹ Sabina Pappata, MD, PhD,¹ Nicolas Molko, MD,^{1,2} and Hughes Chabriat, MD^{1,2}

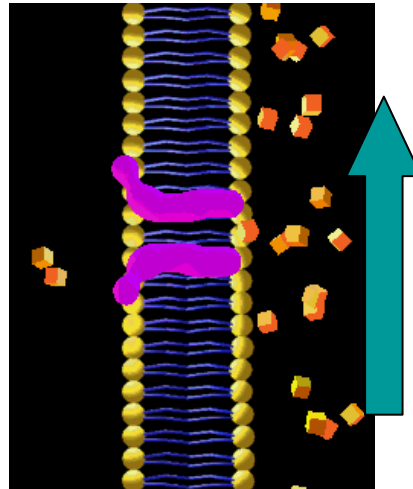
“The success of diffusion MRI is deeply rooted in the powerful concept that during their random, diffusion driven displacements molecules probe tissue structure at a microscopic scale well beyond the usual image resolution: during typical diffusion times of about 50 msec (Le Bihan)”

- Diffusion imaging is the only non-invasive measurement of diffusion
- Diffusion image doesn't interfere with diffusion
- Diffusion is an intrinsic process that does not depend on the distortions introduced into the local magnetic field; hence it is unlike the T1, T2 or fMRI (BOLD) effects

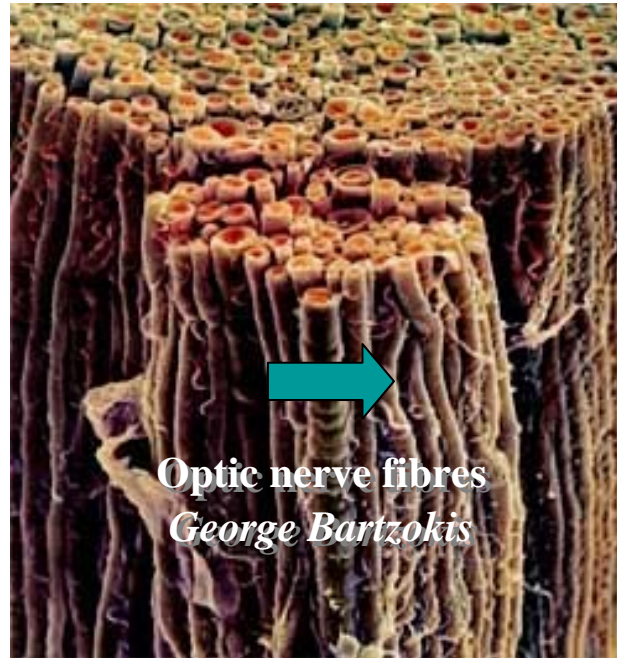
H₂O
Diffusion
Probes
Microscopic
Structures
In the Brain



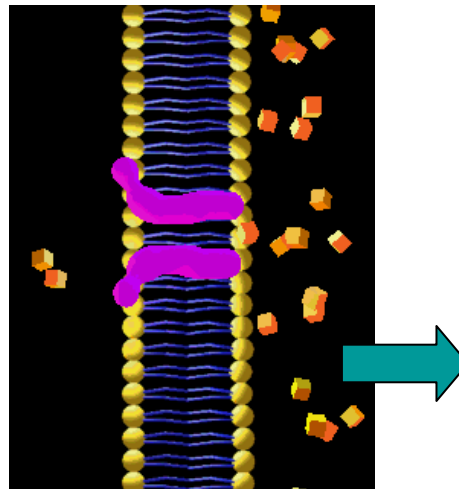
*Along the axon, within
the cytoskeleton, there
is a large
Apparent Diffusion
Coefficient (ADC)*



H₂O Diffusion Probes Microscopic Structures In the Brain



*Bi-lipid cell membranes
limit diffusion.
Hence, perpendicular to
the length the ADC is
smaller*

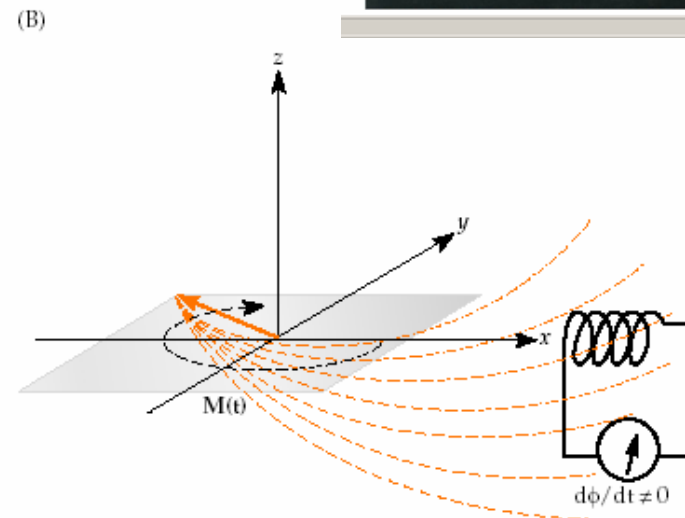
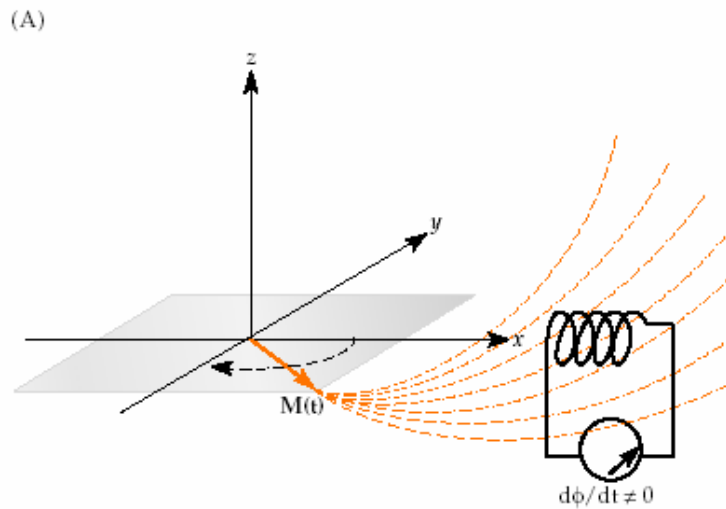
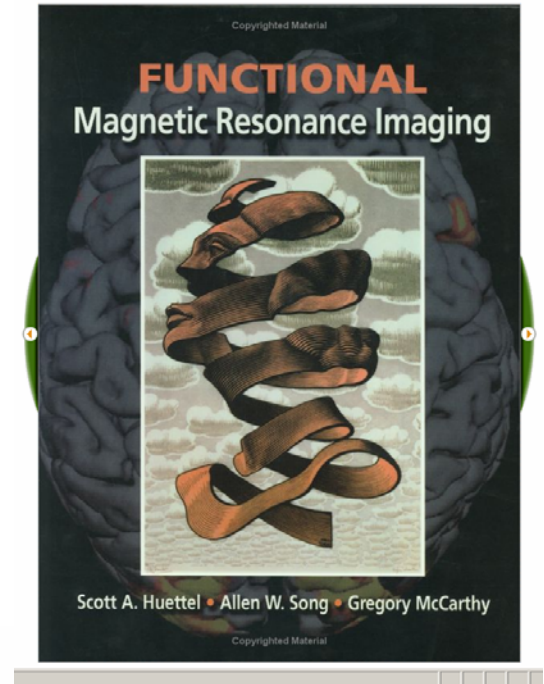


Diffusing Water Probes Microscopic Tissue Structure

- Tissue structures affect diffusion
- MR diffusion measures depend on microscopic structure within voxel
- Diffusion through white matter probes:
 - density of axons
 - degree of myelination
 - average fiber diameter
 - directional similarity of axons

MR Principles

- MR signals measure how excited spins decay over time
- These spins (usually hydrogen) decay at a rate that depends on their (a) environment and (b) diffusion



Stejskal-Tanner equation is essential for measuring diffusion

THE JOURNAL OF CHEMICAL PHYSICS

VOLUME 42, NUMBER 1

1 JANUARY 1965

Spin Diffusion Measurements: Spin Echoes in the Presence of a Time-Dependent Field Gradient*

E. O. STEJSKAL† AND J. E. TANNER

Department of Chemistry, University of Wisconsin, Madison, Wisconsin

(Received 20 July 1964)

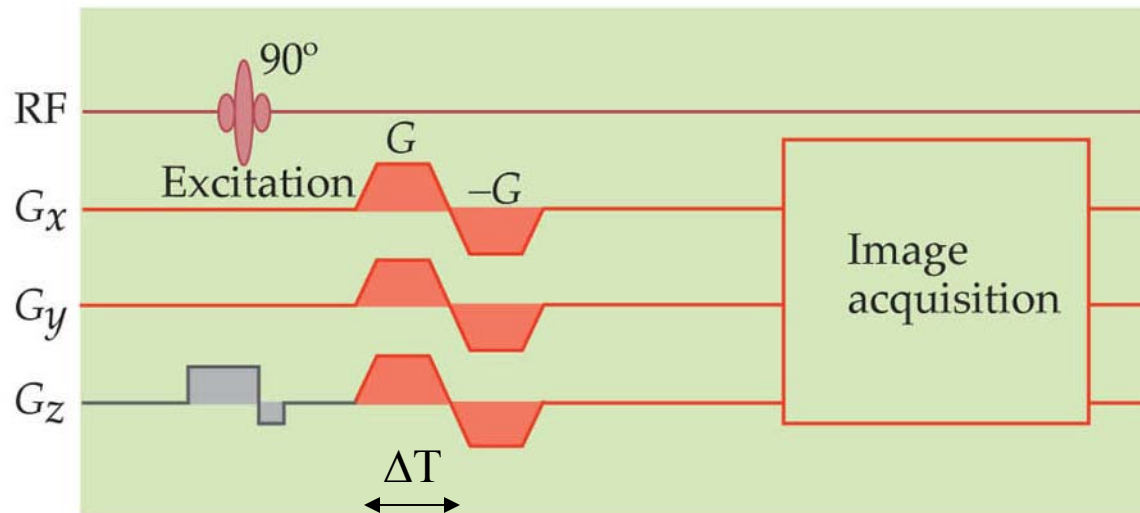
A derivation is given of the effect of a time-dependent magnetic field gradient on the spin-echo experiment, particularly in the presence of spin diffusion. There are several reasons for preferring certain kinds of time-dependent magnetic field gradients to the more usual steady gradient. If the gradient is reduced during the rf pulses, H_1 need not be particularly large; if the gradient is small at the time of the echo, the echo will be broad and its amplitude easy to measure. Both of these relaxations of restrictions on the measurement of diffusion coefficients by the spin-echo technique serve to extend its range of applicability. Furthermore, a pulsed gradient can be recommended when it is critical to define the precise time period over which diffusion is being measured.

The theoretical expression derived has been verified experimentally for several choices of time dependent magnetic field gradient. An apparatus is described suitable for the production of pulsed gradients with amplitudes as large as 100 G cm^{-1} . The diffusion coefficient of dry glycerol at $26^\circ \pm 1^\circ \text{C}$ has been found to be $(2.5 \pm 0.2) \times 10^{-8} \text{ cm}^2 \text{ sec}^{-1}$, a value smaller than can ordinarily be measured by the steady gradient method.

$$\text{Signal attenuation} = \exp(-b * \text{ADC})$$

Diffusion-weighted gradient echo sequence (Stejskal-Tanner)

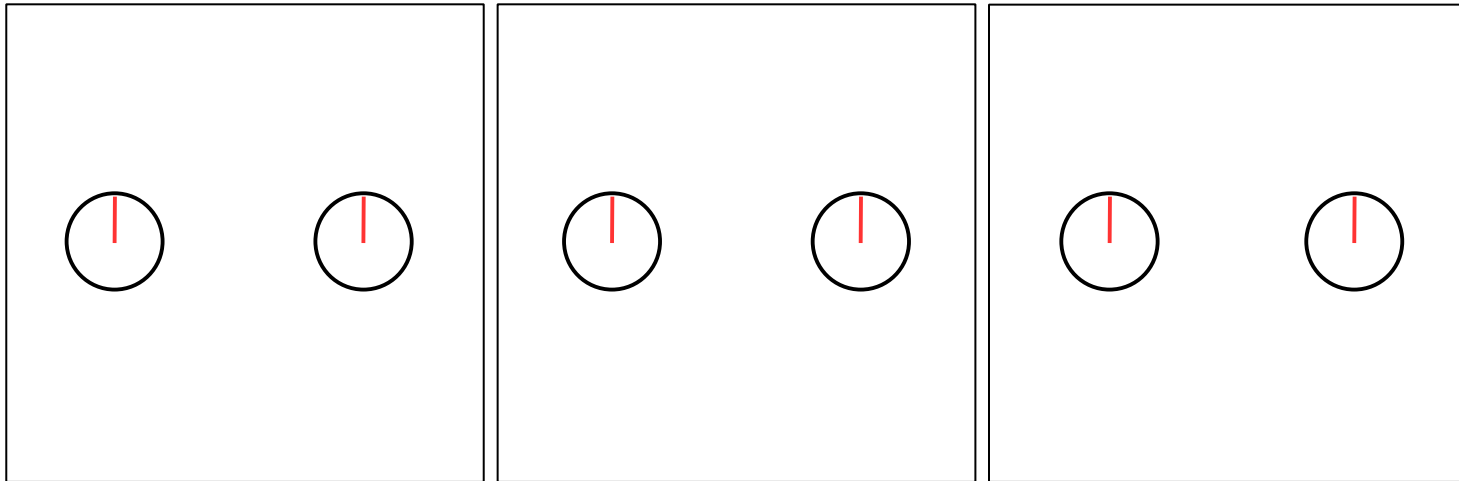
- Gradient pair ($G, -G$) has no net effect on stationary spin
- Second pulse undoes first
- Moving spins are not re-phased by second pulse
- Phase-shift causes a signal decay that depends on the distance moved during time ΔT (diffusion time)



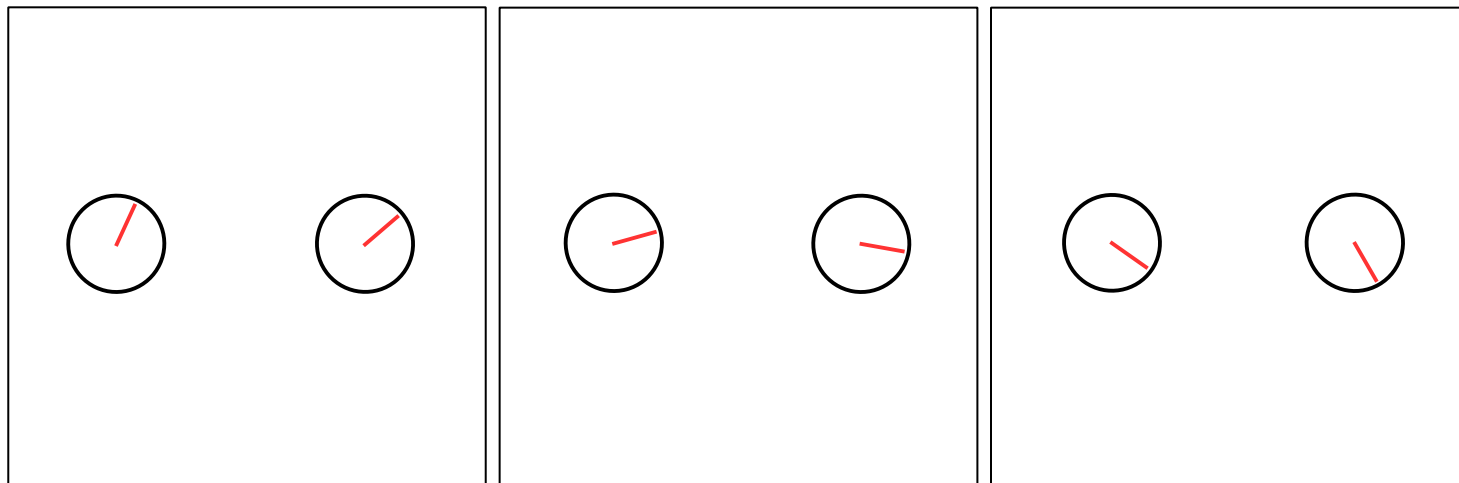
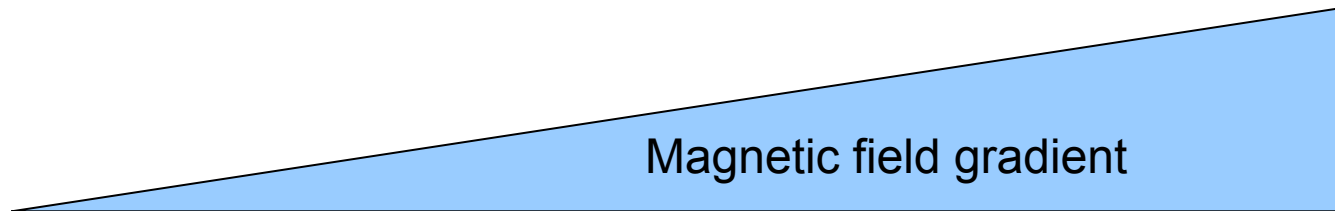
Not used in recent years, but good for explanation.

“The truth, you can’t handle the truth.”

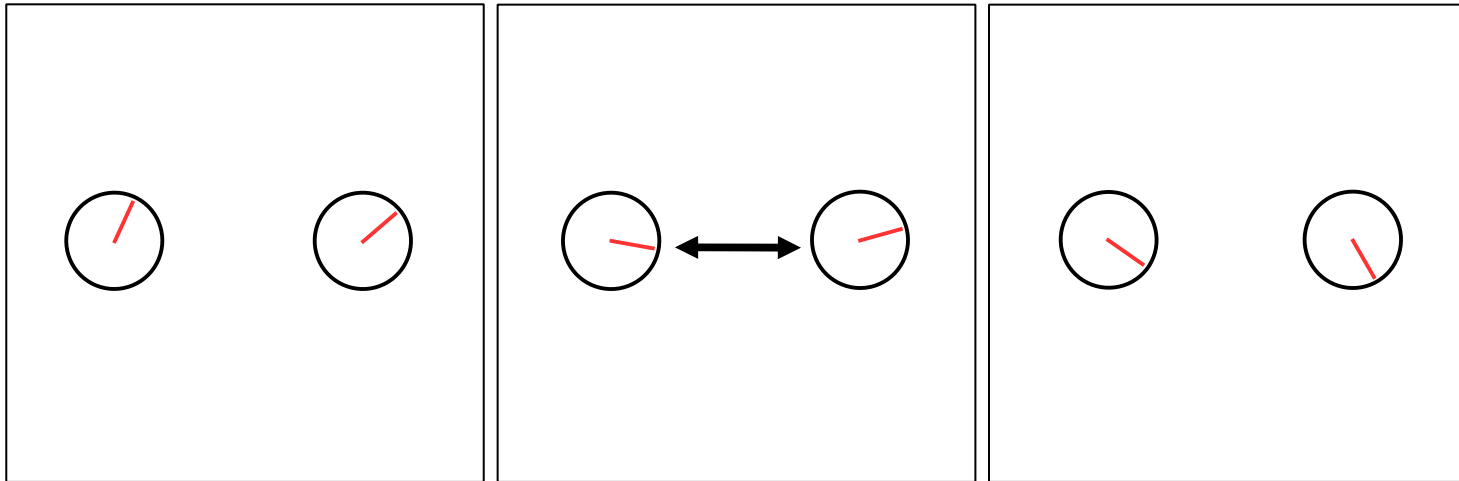
Protons Precessing in Phase



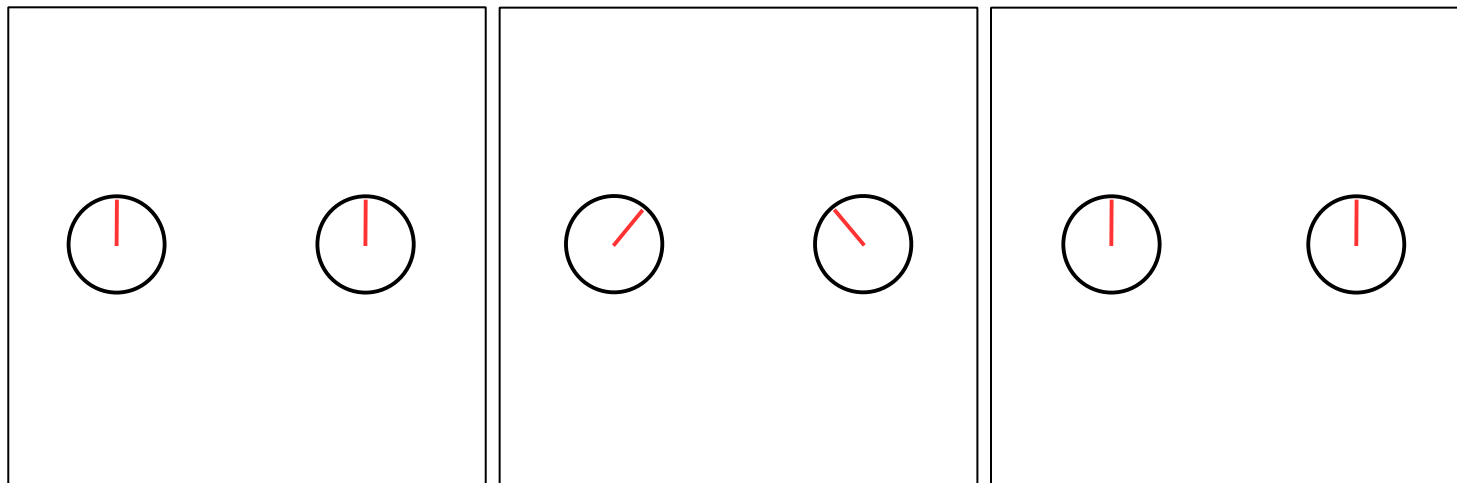
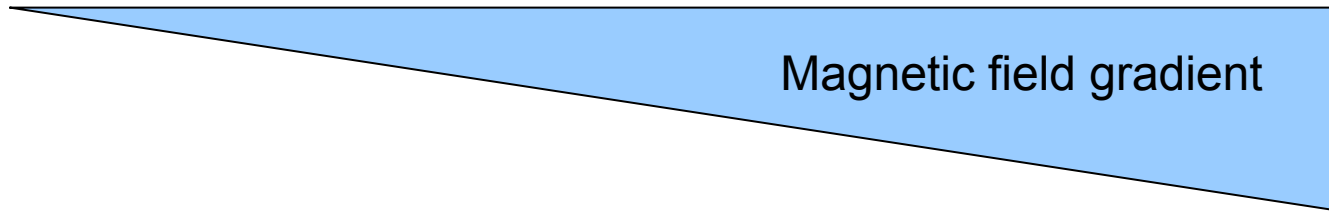
Diffusion Weighting: First Pulse



Time to Diffuse

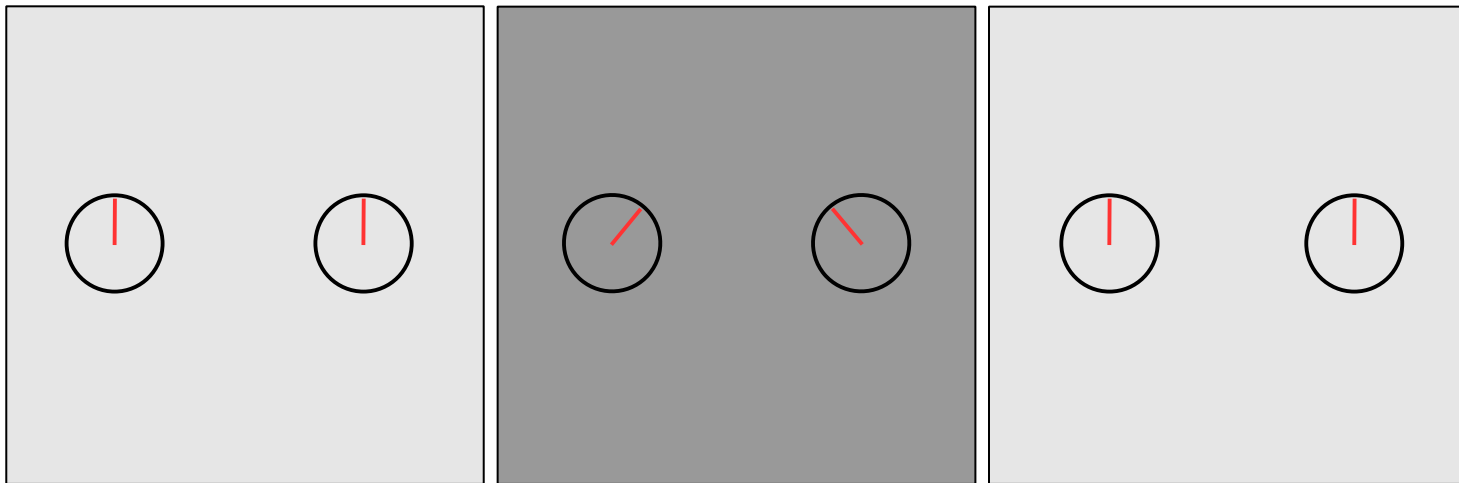


Diffusion Weighting: Second Pulse



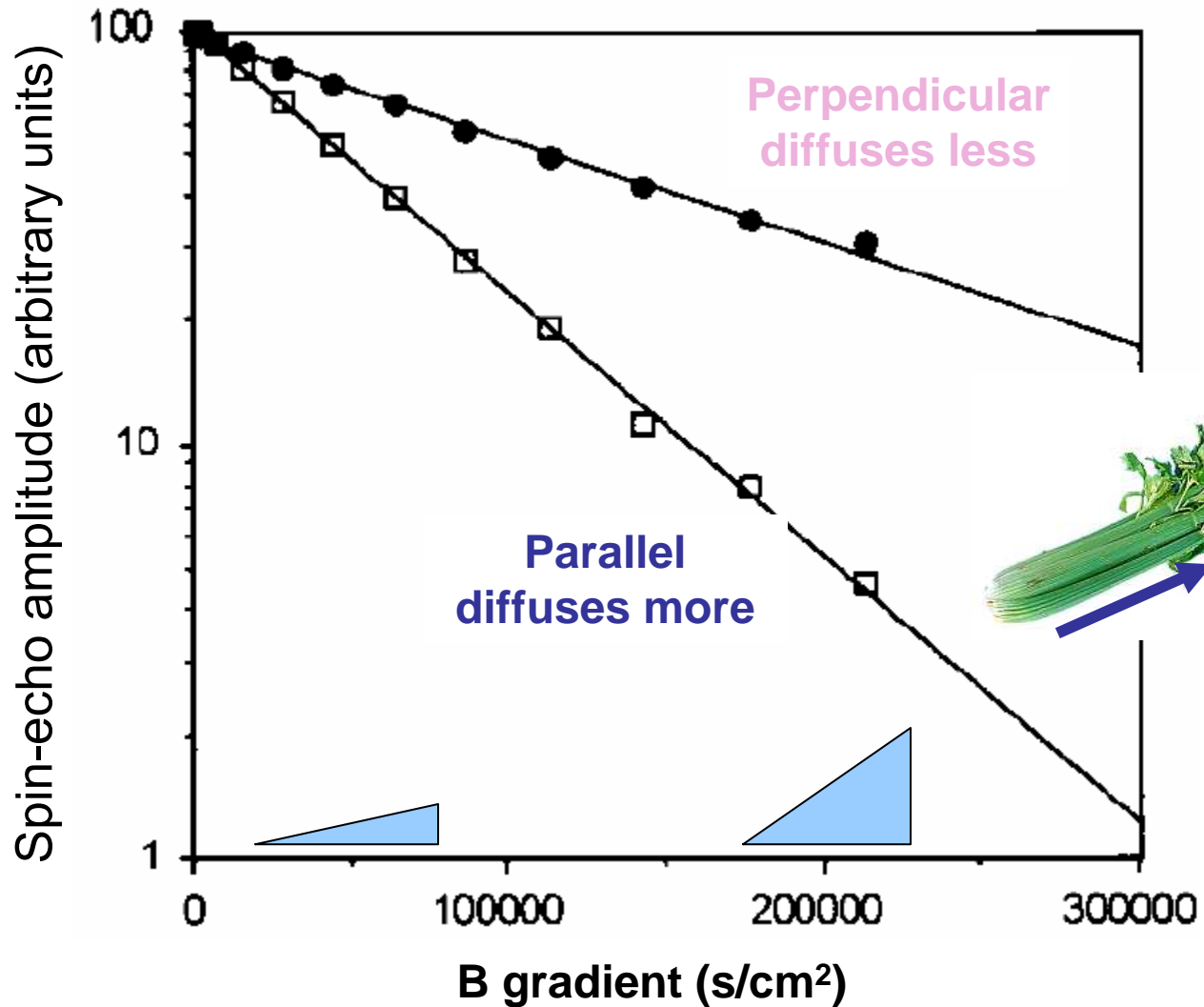
Reduced signal from spin dephasing

Stejskal-Tanner equation:
Signal attenuation = $\exp(-b * ADC)$



Diffusion measured in celery

(Beaulieu, 2002)



Bloch-Torrey Equations

- The Bloch-Torrey equations specify how net magnetization depends on these several factors

$$\underbrace{\frac{dM}{dt}}_{\text{Signal}} = \underbrace{\gamma M \times B}_{\text{Longitudinal}} + \underbrace{\frac{M_0 - M_z}{T_1}}_{\text{Longitudinal}} - \underbrace{\frac{M_x + M_y}{T_2}}_{\text{Transverse}} + \underbrace{\nabla \cdot D \nabla (M - M_0)}_{\text{Diffusion}}$$

M – Net magnetization

γ – Gyromagnetic constant

B – Magnetic field

D – Diffusion parameter

T_1, T_2 – Longitudinal and transverse decay constants

Diffusion coefficient

Sequence-
dependent
constant

Diffusion coefficient

$$M_+ = M_0 e^{-t/T2} e^{-bD}$$

with a constant b
that depends on the sequence

The T1 term
contributes very little
for reasons not
explained here.

It turns out that
diffusion disturbs the
T2 image

Diffusion coefficient

Sequence-
dependent
constant

Diffusion coefficient

$$M_+ = M_0 e^{-t/T2} e^{-bD}$$

with a constant b
that depends on the sequence

So we measure two
T2 images at different
 b levels.

Once measure the
gradients as shown
(M_+). Then measure
again with $b=0$ ($M_{b=0}$)

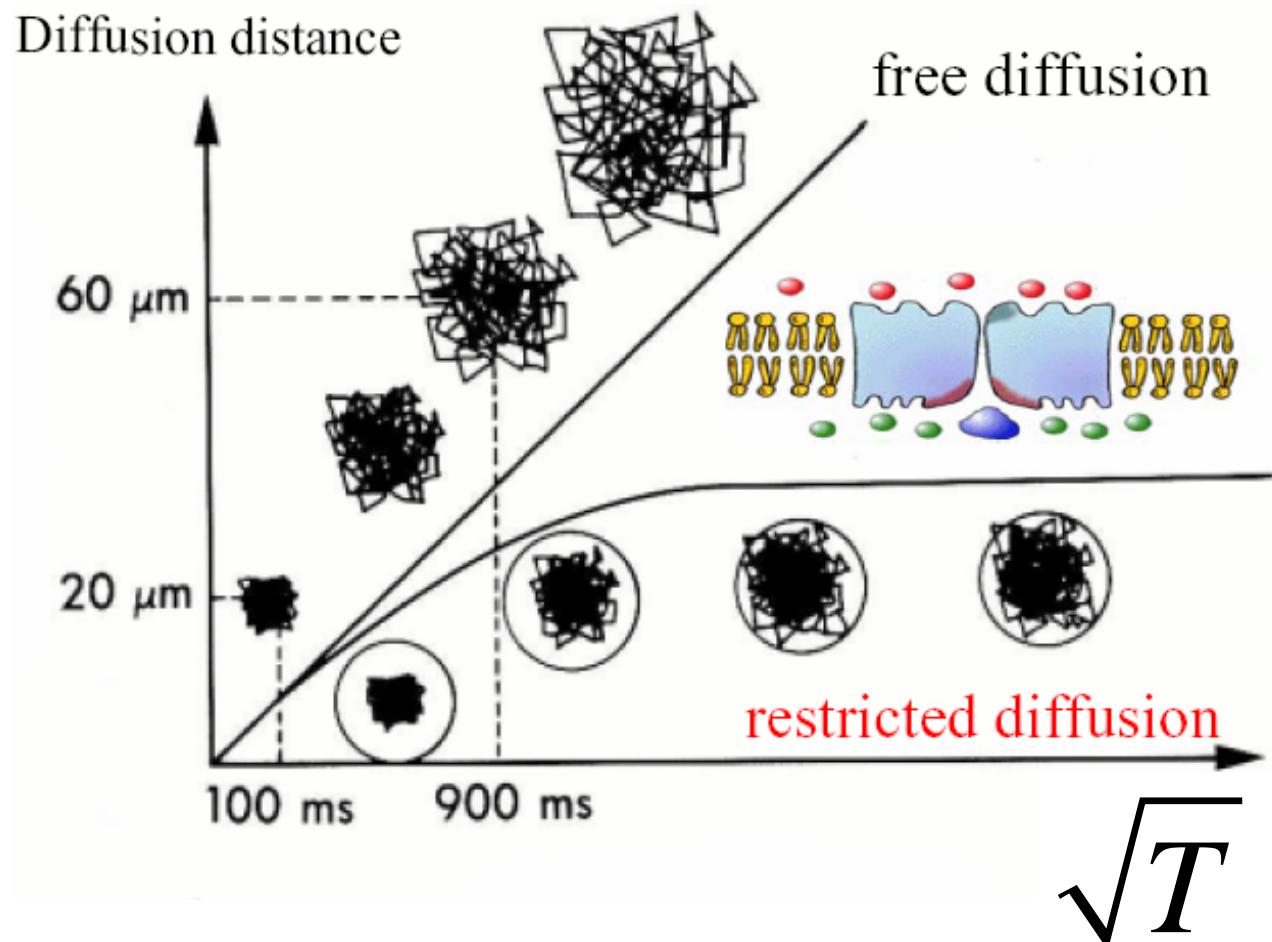
$$\ln\left(\frac{M_+}{M_{b=0}}\right) = -bD$$

$$D = \frac{1}{-b} \ln\left(\frac{M_+}{M_{b=0}}\right)$$

Diffusion distances

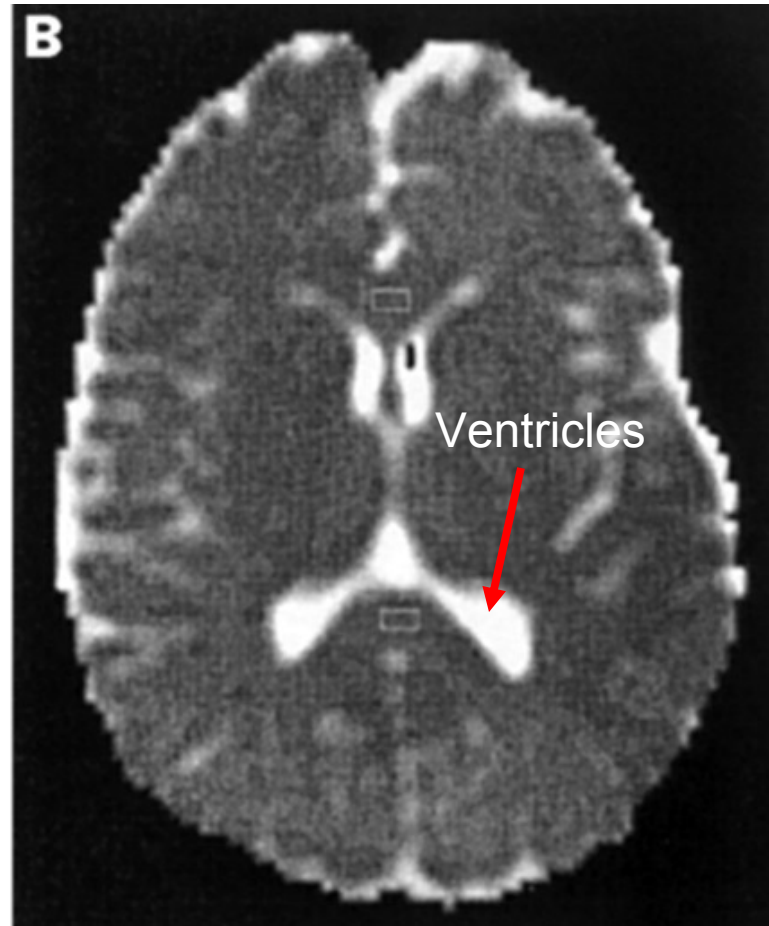
- ~ 3 $\mu\text{m}^2/\text{ms}$ – Body temperature in water (CSF)
- ~ 2.1 $\mu\text{m}^2/\text{ms}$ – Body temperature in axoplasm

• In isotropic case, an average water molecule will diffuse a distance of $\sqrt{2Dt}$ in a time t , and D is the scalar apparent diffusion coefficient.



Mean diffusivity (MD) summarizes the diffusion in all directions

- MD has units of m^2/sec
- Diffusion-weighted imaging (DWI) is commonly used in clinical applications
- For many years, clinicians made measurements in the three principal directions



Diffusion Tensor Imaging Diffusion: a
model of measurements in multiple
directions

Diffusion Tensor Imaging Point-wise Analyses

Biophysical Journal Volume 66 January 1994 259–267

259

MR Diffusion *Tensor* Spectroscopy and Imaging

Peter J. Basser,* James Mattiello,* and Denis LeBihan†

*Biomedical Engineering and Instrumentation Program, National Center for Research Resources, and †Diagnostic Radiology Department, The Warren G. Magnuson Clinical Center, National Institutes of Health, Bethesda, Maryland 20892 USA

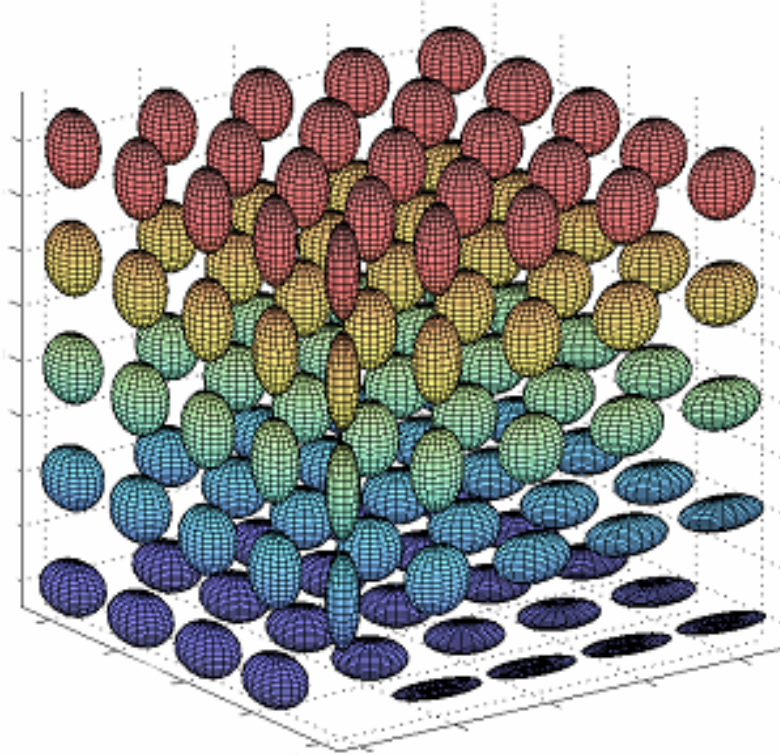
ABSTRACT This paper describes a new NMR imaging method for measuring the effective diffusion tensor, \mathbf{D} , of anisotropic diffusion of water molecules in biological tissue. The method exploits the anisotropy of the diffusion tensor to determine the principal axes of the tensor by using a series of pulsed-gradient, spin-echo NMR measurements. The principal axes are the eigenvectors of \mathbf{D}_{eff} , while the principal values are the eigenvalues. The principal axes are constructed in each voxel by using a series of NMR measurements. Moreover, the three scalar principal values reveal useful information about the underlying transport process. The apparent diffusivity, D_{app} , is the sum of the three principal values.

Short version:
**Measure in multiple
directions and summarize
iso-diffusion surface as
an ellipsoid**

ing. It consists of estimating an effective diffusion tensor, \mathbf{D} . We show how the phenomenon of anisotropic diffusion is measured by these NMR methods, is estimated from a series of NMR measurements. They coincide with the eigenvalues of \mathbf{D}_{eff} . Diffusion ellipsoids, which are defined by the principal values, are distances in these directions. The principal axes are defined in the laboratory frame of reference, and the principal values are defined in the principal axes. Inherently, tensors (like \mathbf{D}_{eff}) are defined in the principal axes. *opic voxel* that scalars (such as

DTI Data Sets Are Volumes of Diffusion Surfaces

DTI data are surfaces

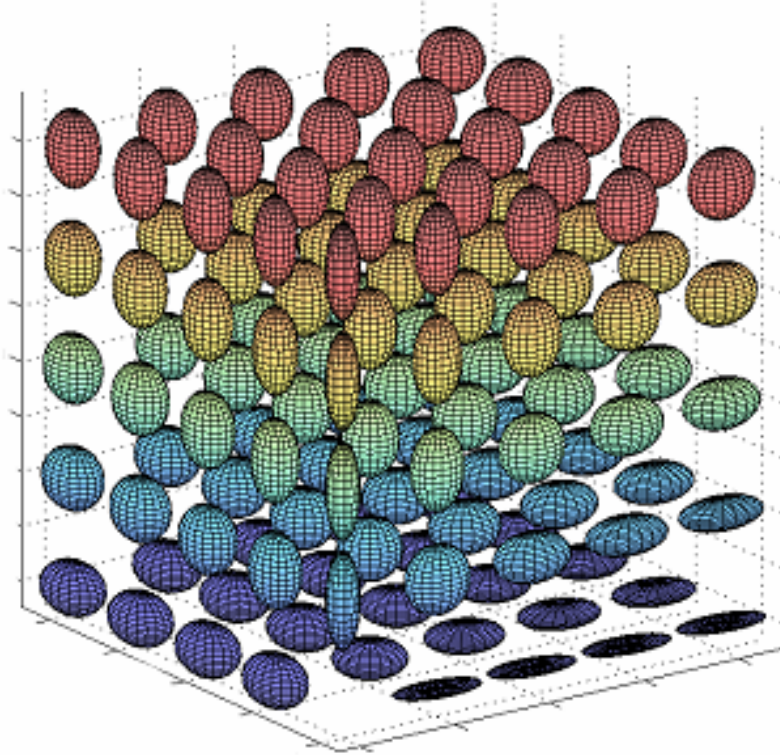


*Conventional MR volumes
are real-valued*



DTI Data Sets Are Volumes of Diffusion Surfaces

DTI data are surfaces



“The shape of the effective diffusion ellipsoid has a useful physical interpretation. ... a diffusion tensor ... defines a surface of constant mean translational displacement of spin-labelled particles.”

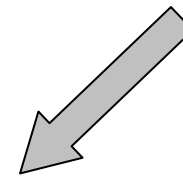
*Basser, Mattiello & LeBihan
(1994) Biophysical Journal,
pg. 261.*

Mathematical Description: An ellipsoid (Diffusion tensor)

- Water molecules move in physical Brownian motion ($t = \text{time}$).

$$p(x, t) = \frac{1}{\sqrt{(2\pi)^3 |2Dt|}} \exp\left(-\left(\frac{1}{2}\right) x^t (2Dt)^{-1} x\right)$$

Key term



x - the position in 3-space (m)

t - time (sec)

D - 3x3 Diffusion tensor (m^2/sec)

$p(x,t)$ - probability density of a molecule being at location x at time t

The std. dev. of this Gaussian is the mean diffusion distance

Mathematical Description: An Ellipsoid (Diffusion Tensor)

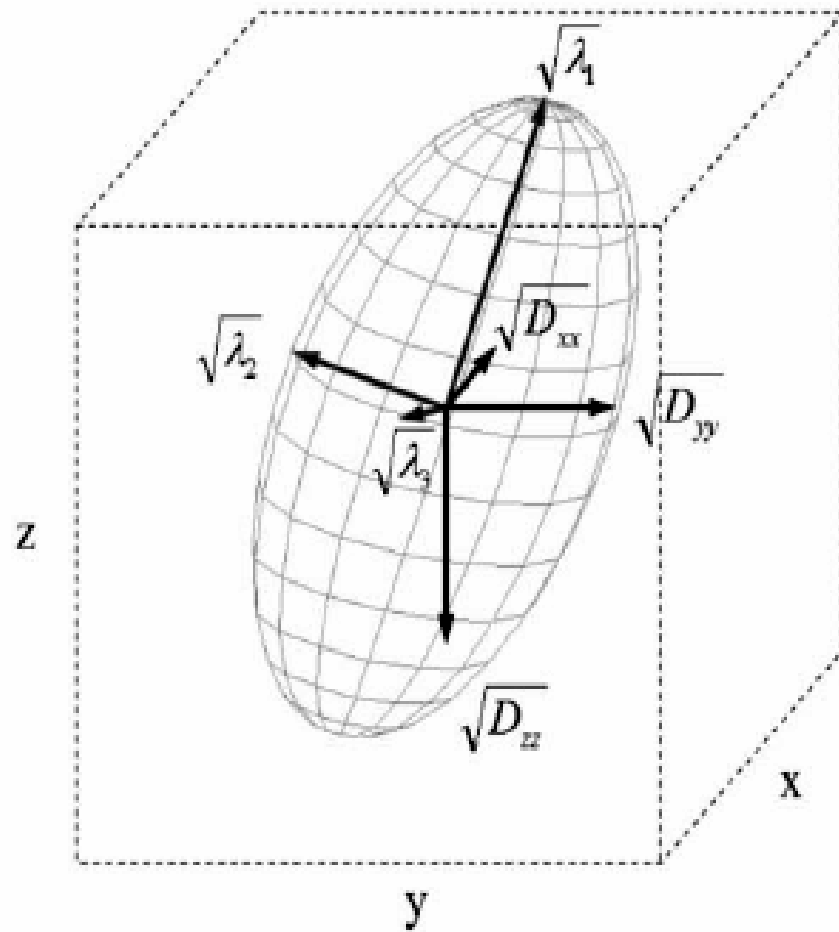
- The diffusion at each sample location is represented by a 3x3 covariance (positive, semi-definite) matrix .

$$D = A^t A, A \text{ is non-singular}$$

$$A = U^t S V$$

$$D = V^t S^2 V$$

Mathematical Description: An Ellipsoid (Diffusion Tensor)



This surface summarizes the mean distance from the starting position that a typical particle (water molecule) will travel in diffusion time $T = \frac{1}{2}$

Mathematical Description: An Ellipsoid (Diffusion Tensor)

- The local diffusion is represented by a 3x3 covariance matrix (positive, semi-definite).

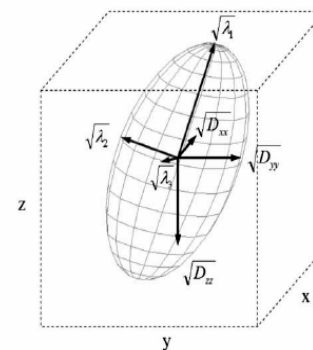
$$D = \begin{pmatrix} D_{xx} & D_{xy} & D_{xz} \\ D_{xy} & D_{yy} & D_{yz} \\ D_{xz} & D_{yz} & D_{zz} \end{pmatrix} = \begin{pmatrix} \vdots & \vdots & \vdots \\ v_1 & v_2 & v_3 \\ \vdots & \vdots & \vdots \end{pmatrix} \begin{pmatrix} \lambda_1 & 0 & 0 \\ 0 & \lambda_2 & 0 \\ 0 & 0 & \lambda_3 \end{pmatrix} \begin{pmatrix} \cdots & v_1 & \cdots \\ \cdots & v_2 & \cdots \\ \cdots & v_3 & \cdots \end{pmatrix}$$

Apparent diffusion coefficients (ADC)

SVD decomposition

Eigenvalues: $\lambda_1 \geq \lambda_2 \geq \lambda_3 > 0$

Eigenvectors: $v_i \perp v_j \quad i \neq j$



Visualization ideas

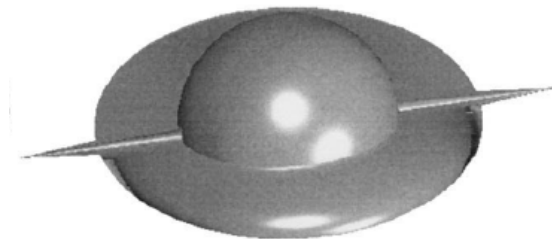
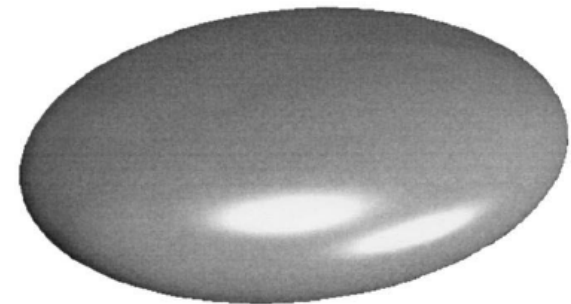
Represent the tensor in terms of three components: linear, spherical and planar. These components are derived from the eigenvalues.

This figure compares the ellipsoidal representation of a tensor (above) with the authors' proposed composite shape that includes a linear, planar and spherical component (below). These components are scaled according to the eigenvalues,

Processing and visualization for diffusion tensor MRI

C.-F. Westin*, S.E. Maier, H. Mamata, A. Nabavi, F.A. Jolesz, R. Kikinis

Brigham & Women's Hospital, Harvard Medical School, Department of Radiology, 75 Francis Street, Boston, MA 02115, USA

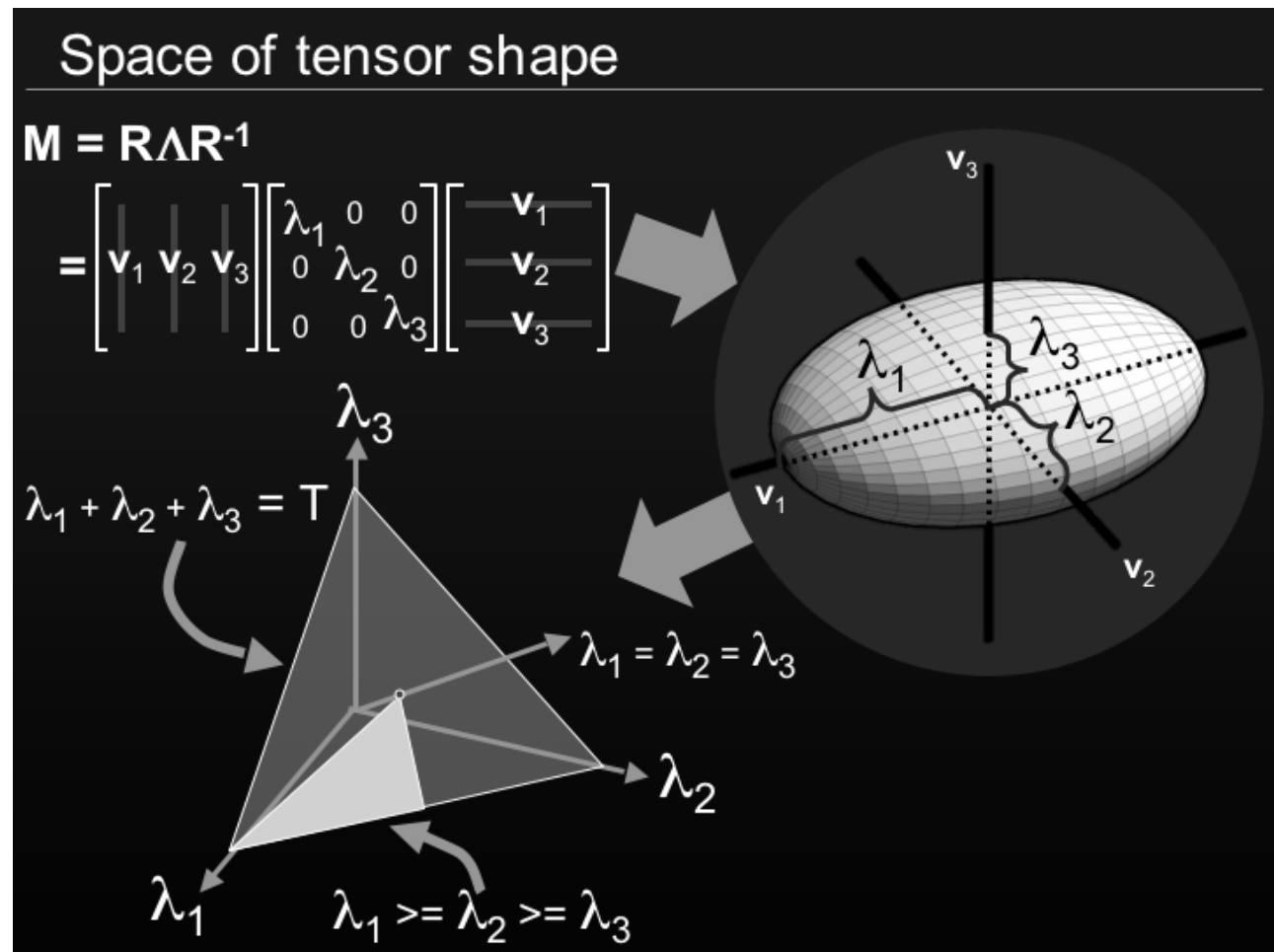


Visualization of the tensor data

(G-Glyphs; Kindlmann et al.)

<http://www.cs.utah.edu/~gk/papers/vissym04/web/slide003.html>

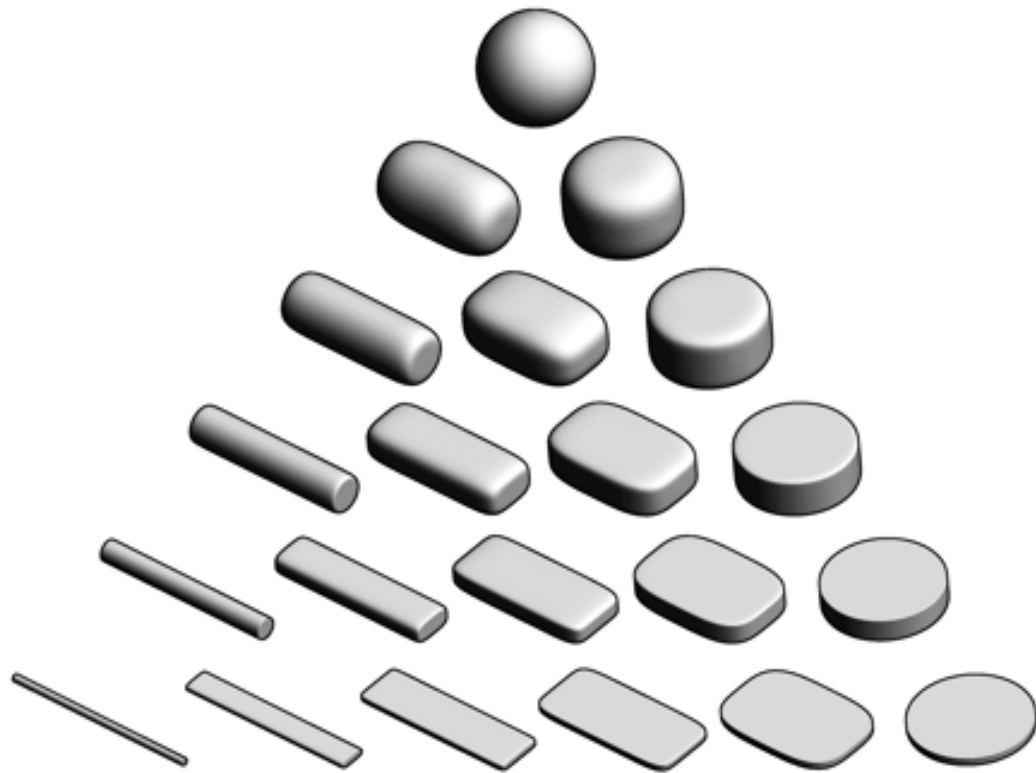
- We ignore rotation
- Keep size the size by equalizing the trace
- Account for required ordering



Visualization of the tensor data

(G-Glyphs; Kindlmann et al.)

They argue that we should summarize the information using super-quadratics rather than ellipsoids. I agree that they are easier to interpret. They don't, however, show the estimated iso-diffusion surface. But they are attractive and informative.



Visualization of Anatomic Covariance Tensor Fields

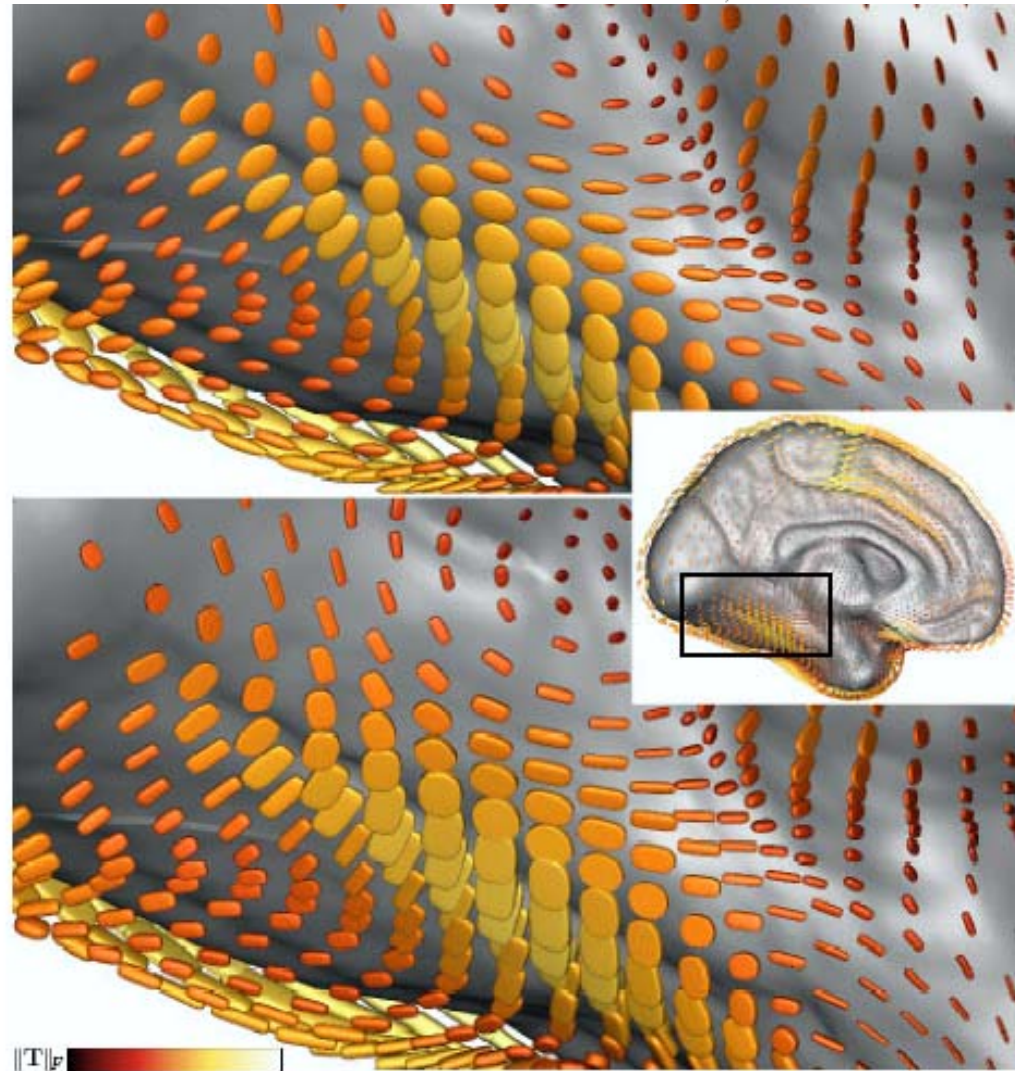
Gordon L. Kindlmann¹ David M. Weinstein¹ Agatha D. Lee²
Arthur W. Toga² Paul M. Thompson²

¹Scientific Computing and Imaging Institute, University of Utah, UT

²Laboratory of Neuro Imaging, Brain Mapping Division, Department of Neurology,
UCLA School of Medicine, CA

Example DTI Image Using G-Glyphs

*Comparison of
ellipsoid (top) and
superquadric
(bottom)
representation.*



Conceptual organization of the parameters

Eigenvalues: $\lambda_1 \geq \lambda_2 \geq \lambda_3 > 0$

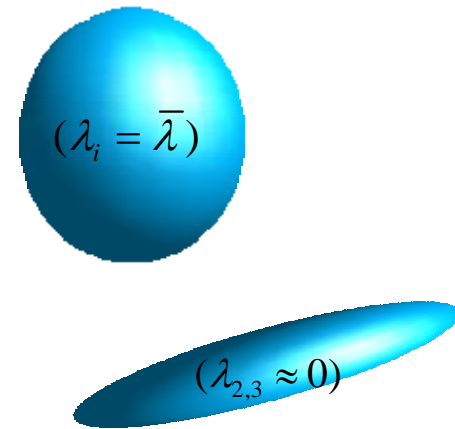
Eigenvectors: $v_i \perp v_j \quad i \neq j$

- There are 6 parameters in the diffusion tensor – 3 eigenvalues; 2 directions for first eigenvector; one direction for second.
- Research scientists need a way to think about these data.
- Physicists and mathematicians took the lead in defining summaries
- The best summaries will come from achieving a biologically-based parameterization.

Fractional Anisotropy

(Basser & Pierpaoli, 1996)

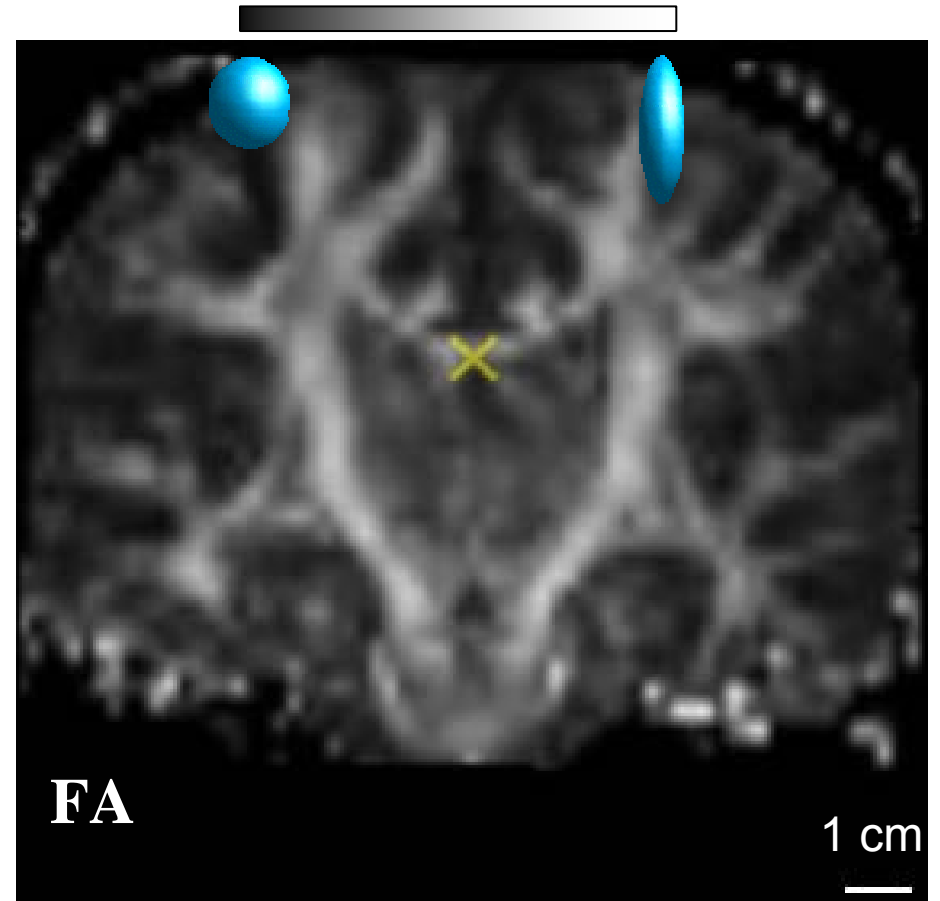
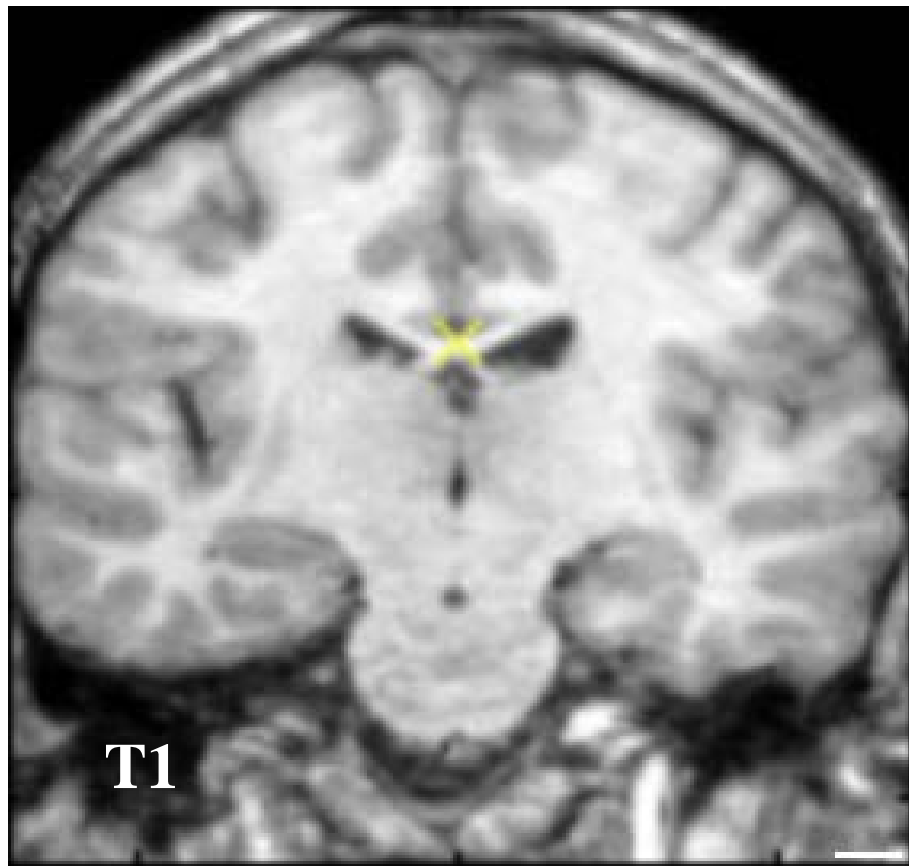
- Normalized variance of ellipsoid axis magnitudes
 - FA=0 for sphere
 - FA=1 for tube
 - FA is dimensionless



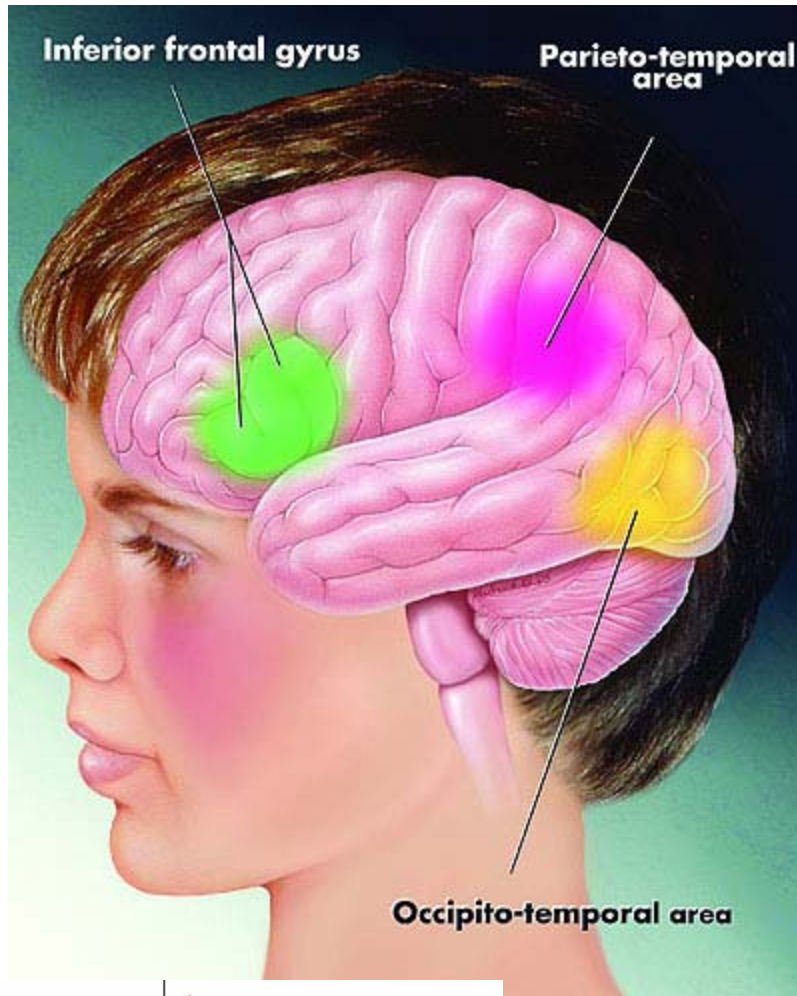
$$\sqrt{\frac{3}{2}} \sqrt{\frac{(\lambda_1 - \bar{\lambda})^2 + (\lambda_2 - \bar{\lambda})^2 + (\lambda_3 - \bar{\lambda})^2}{\lambda_1^2 + \lambda_2^2 + \lambda_3^2}}, \quad \bar{\lambda} = \frac{\lambda_1 + \lambda_2 + \lambda_3}{3}$$

Fractional Anisotropy (FA) summarizes one aspect of the diffusion surface

FA range: 0.1 – 0.7; dimensionless

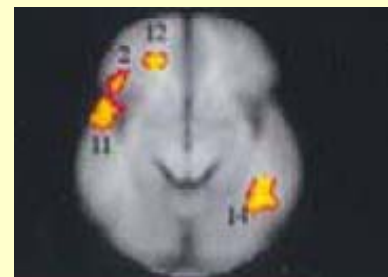
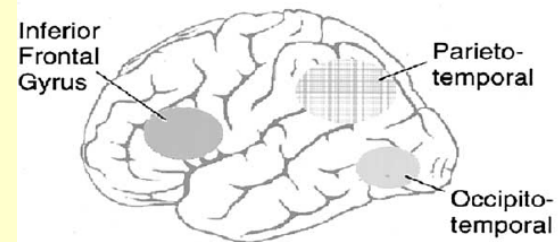


Reading



▲ SCIENTISTS THINK, BASED ON ACCUMULATING RESEARCH, THAT SKILLED READING REQUIRES CERTAIN PATTERNS OF ACTIVITY IN A NETWORK OF AREAS MOSTLY ON THE LEFT SIDE OF THE BRAIN. THESE BRAIN AREAS INCLUDE THE INFERIOR FRONTAL GYRUS, PARIETO-TEMPORAL AREA, AND OCCIPITO-TEMPORAL AREA. SOME EVIDENCE SUGGESTS THAT THE INFERIOR FRONTAL GYRUS BRAIN AREA AND THE PARIETO-TEMPORAL BRAIN AREA HELP A READER ANALYZE A WORD, WHILE THE OCCIPITO-TEMPORAL BRAIN AREA HELPS A READER QUICKLY RECOGNIZE KNOWN WORDS.

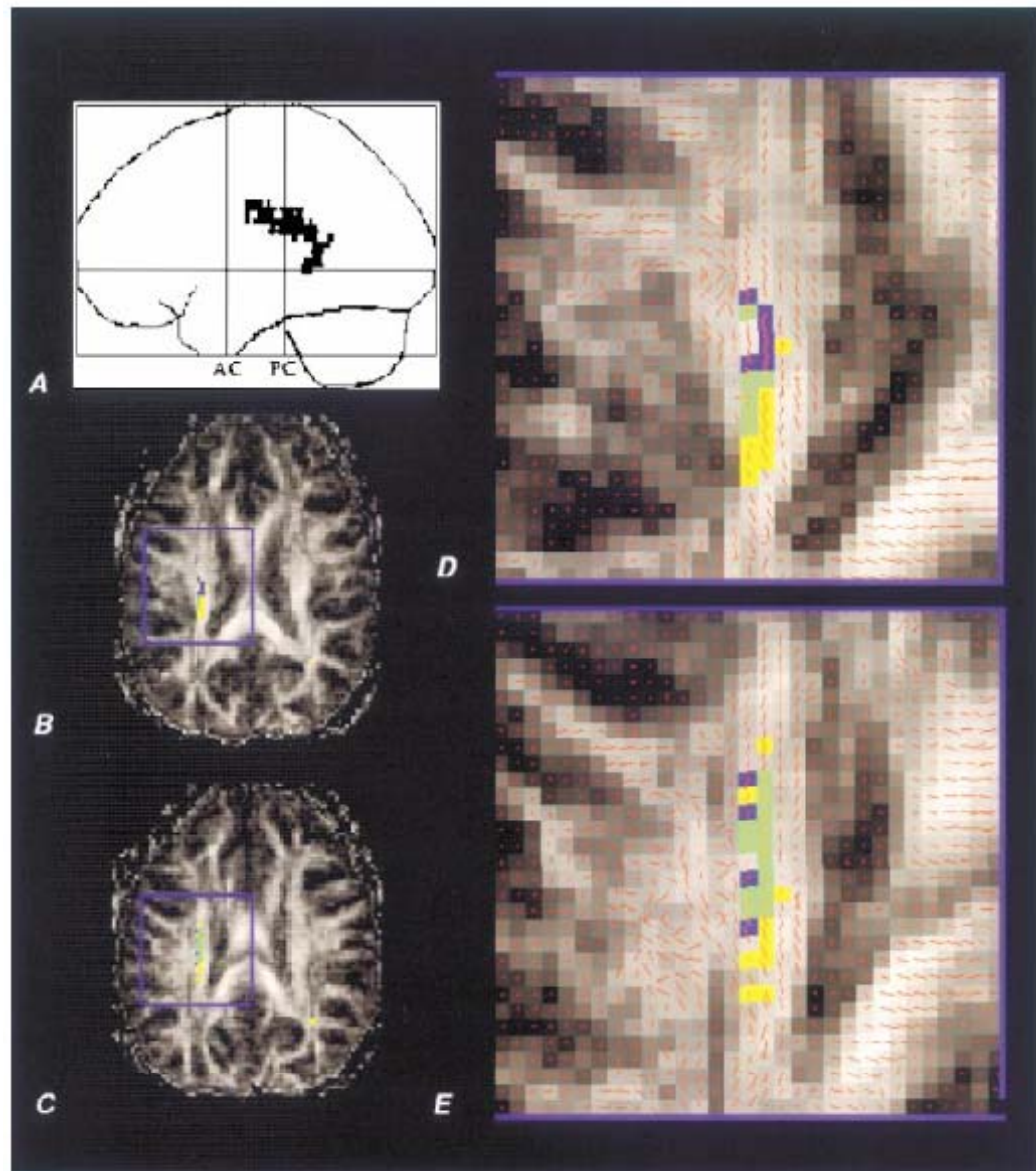
Shaywitz et al., 2002



*Controls > Dys
Non-word rhyming*

In Adults Correlations Exist Between Reading Performance and FA

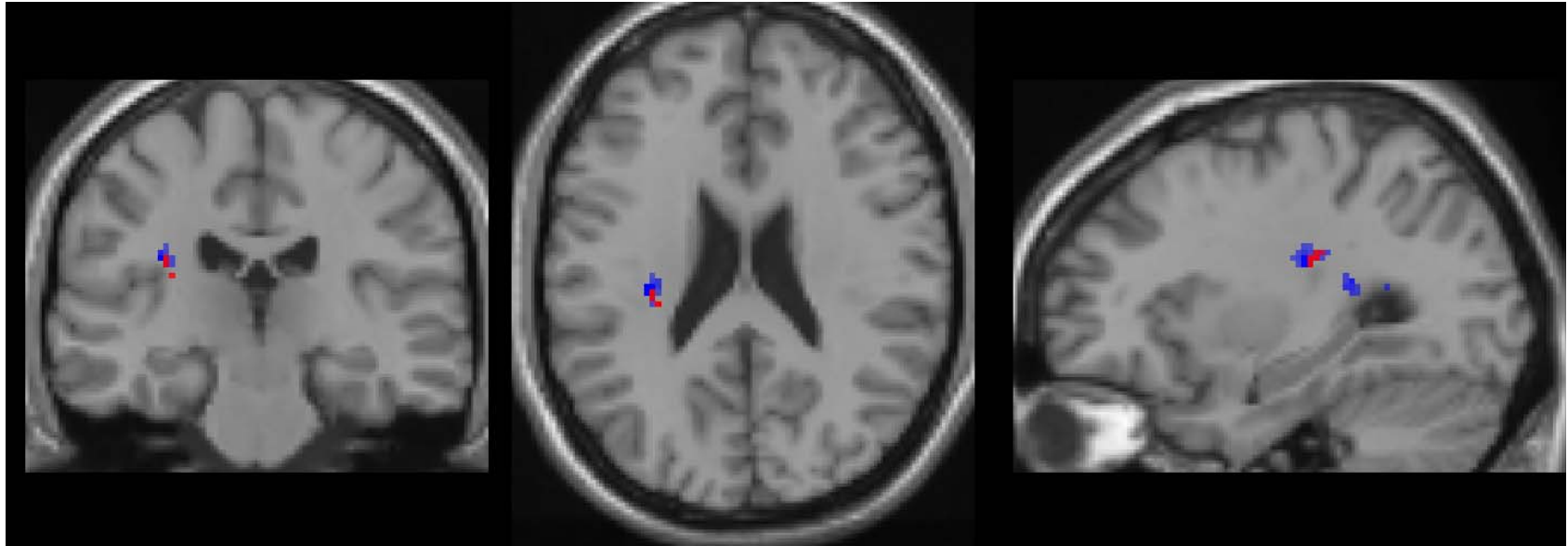
(Klingberg et al., 2000)



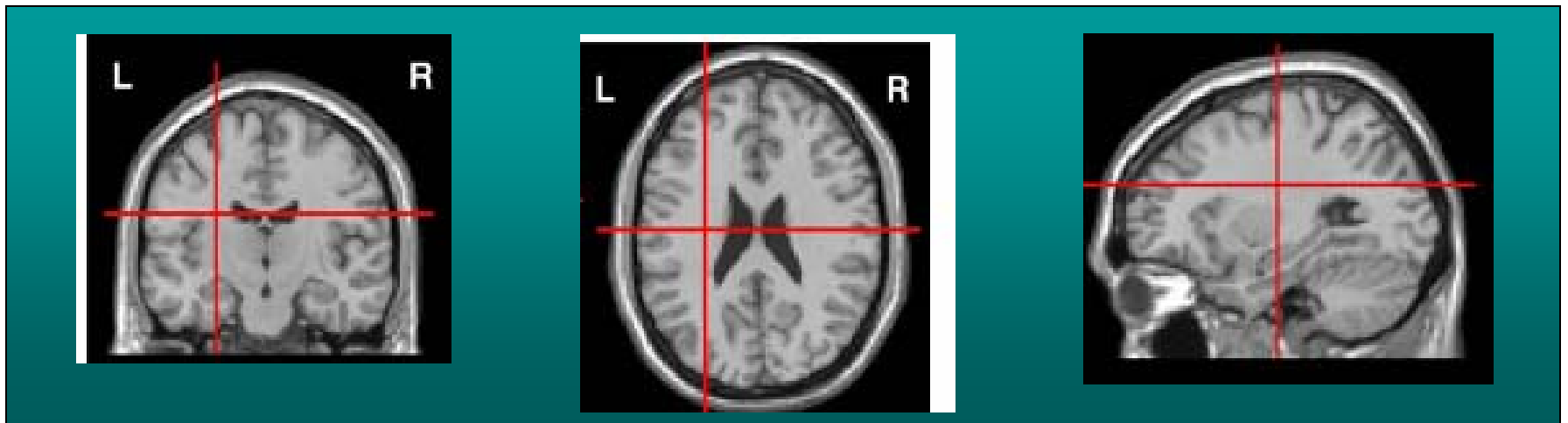
For the gray scale, lighter colors represent higher anisotropy. Green indicates voxels significant in both the between group analysis and the Word ID correlation analysis; yellow indicates voxels significant only in the between-group analysis; and blue indicates voxels significant only in the correlation analysis.

FA correlates with reading skill in children

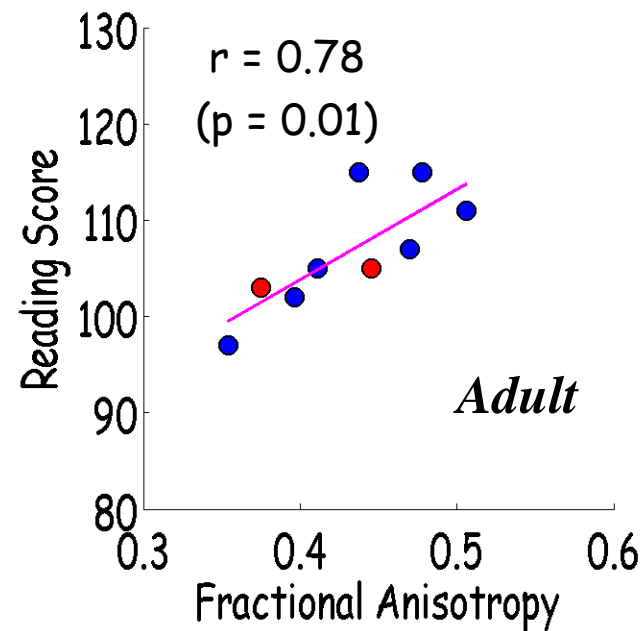
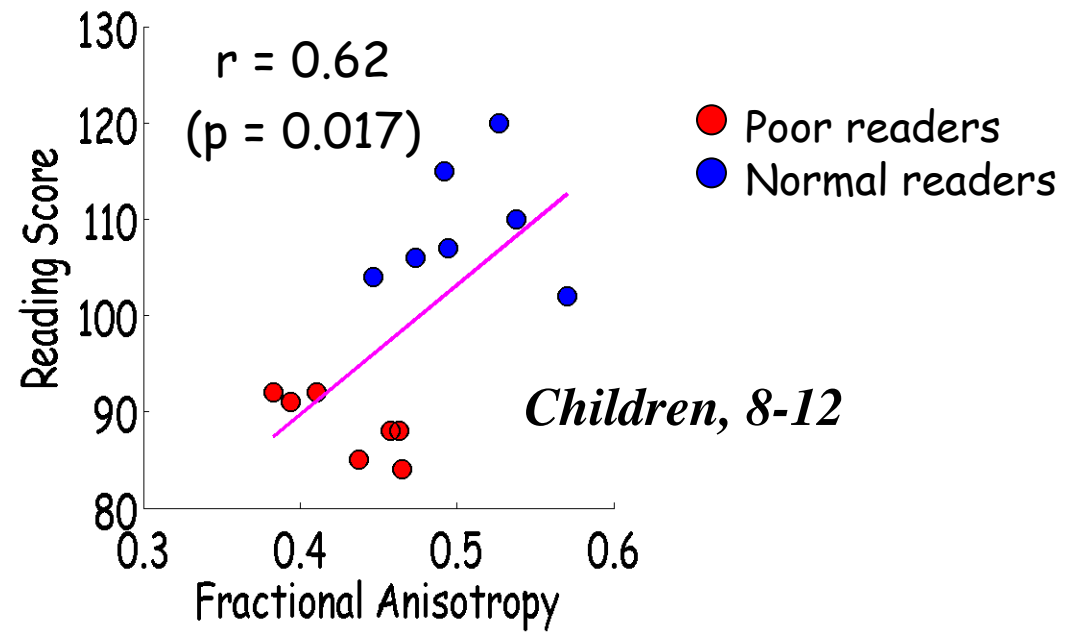
Deutsch, Dougherty, Bammer, Siok, Gabrieli, Wandell (2005)



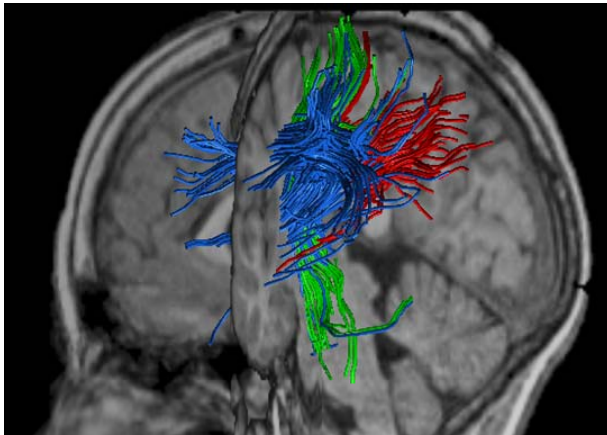
Beaulieu C, Plewes C, Paulson LA, Roy D, Snook L, Concha L, Phillips L. (2005).



We See This
Correlation
In Children
and Adults



Conclusions



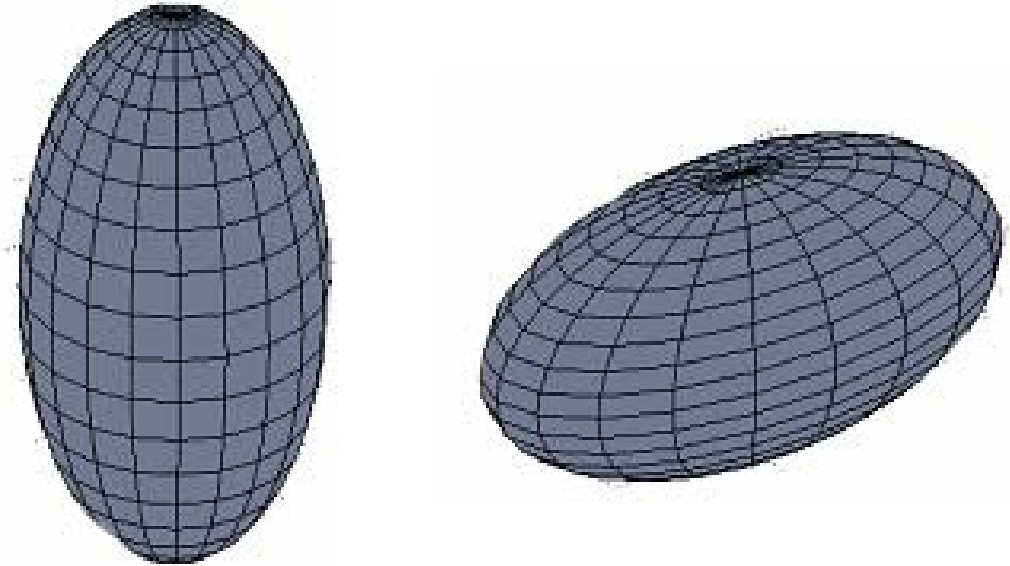
Diffusion tensor imaging can be used in a variety of ways, ranging from FA maps, direction maps, and fiber tracts

There is excellent agreement that certain white matter differences correlate with reading skill.

Interpreting these differences, by describing the data with respect to the natural brain structures (fiber bundle positions and properties) is underway, but still in its infancy.

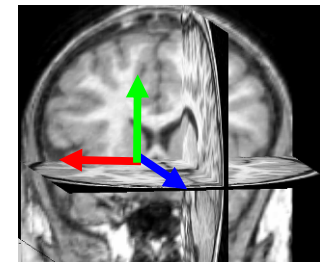
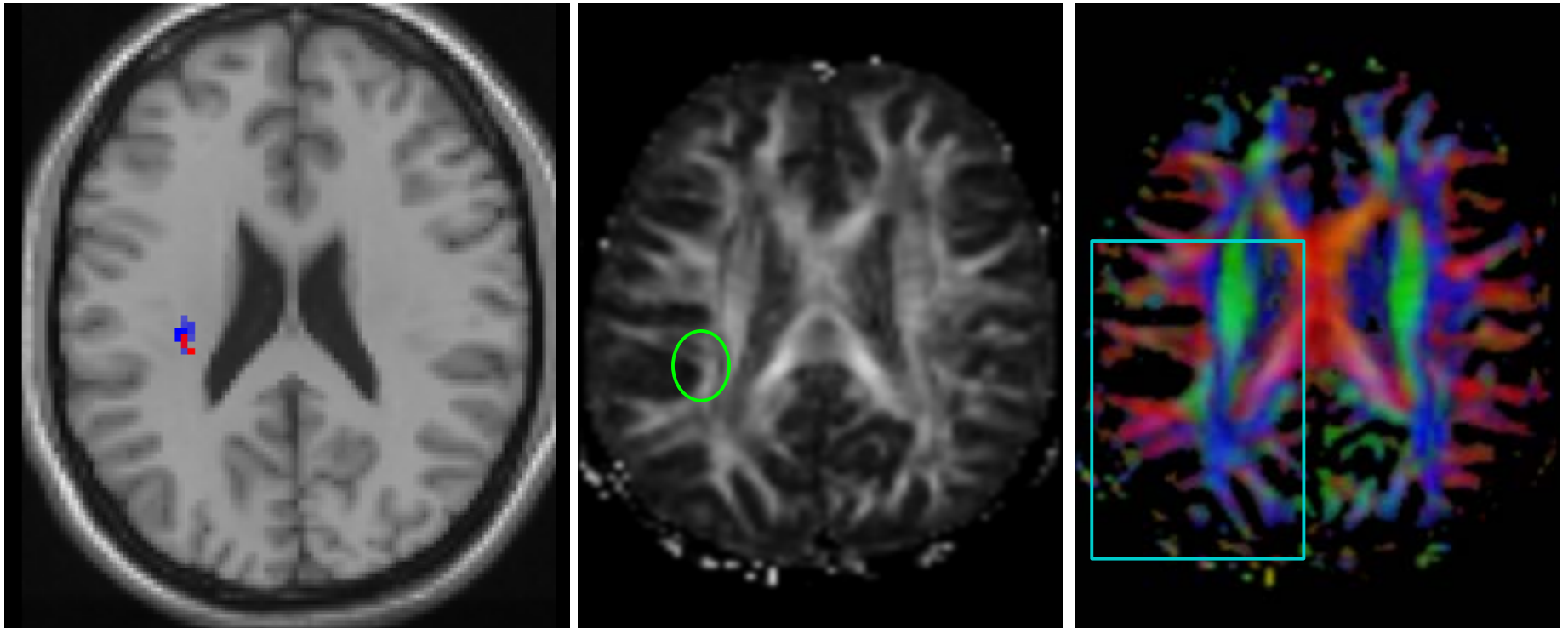
FA Does Not
Discriminate
Between
Ellipsoid
Orientations:
What More Can
We Learn From
Direction?

Fractional Anisotropy = 0.6
Directions differ



Using Direction We See Much More

Account for Directional Data Requires New Statistical Methods



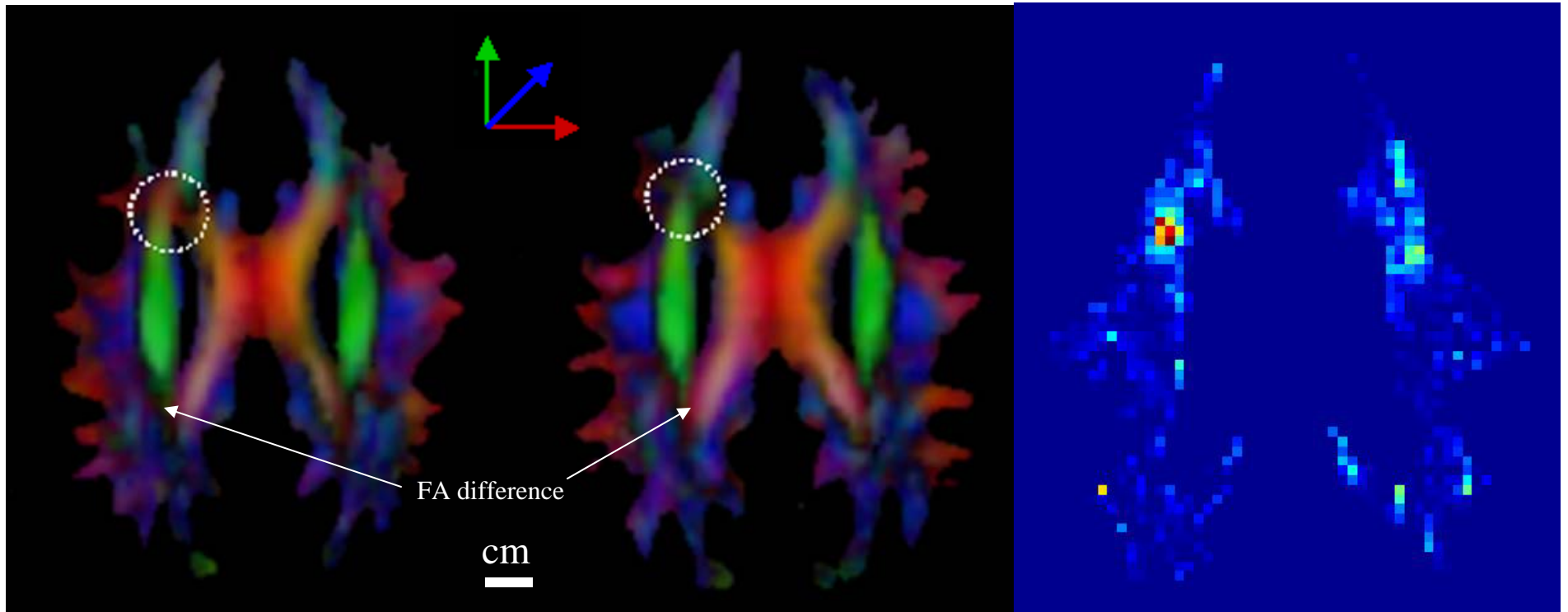
The Directional Difference Appears Occurs in Anterior Cortex (N=14)

(Schwartzmann, Dougherty, Taylor, 2005, MRM)

Good Readers

Poor Readers

Bipolar Watson Distribution



Diffusion MRI of Complex Neural Architecture

Neurotechnique

David S. Tuch,^{1,2,*} Timothy G. Reese,¹
Mette R. Wiegell,¹ and Van J. Wedeen¹
¹Athinoula A. Martinos Center for Biomedical
Imaging
Massachusetts General Hospital

surement of neural connectivity in the human brain
in vivo.

Over the past few years, investigators (Basser et al.,
2000; Conturo et al., 1999; Jones et al., 1999; Koch et
al., 2002; Manin et al., 2002; Mori et al., 1999; Mori and

“Accurate reconstruction of neural connectivity patterns from DTI has been hindered, however, by the inability of DTI to resolve more than a single axon direction within each imaging voxel. Here, we present a novel magnetic resonance imaging technique that can resolve multiple axon directions within a single voxel. The technique, called q-ball imaging, can resolve intravoxel white matter fiber crossing as well as white matter insertions into cortex. The ability of q-ball imaging to resolve complex intravoxel fiber architecture eliminates a key obstacle to mapping neural connectivity in the human brain noninvasively (Tuch et al., Neuron, 2003 abstract)”.

Q-Ball Imaging

David S. Tuch^{1,2*}

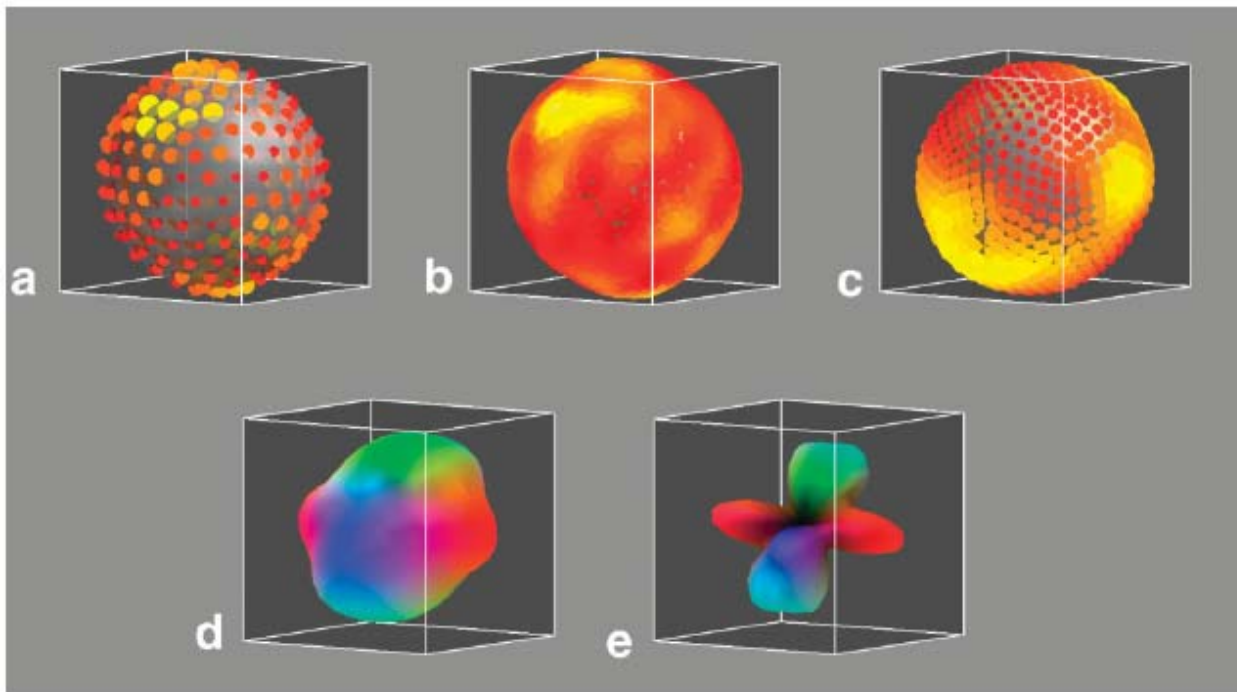


FIG. 2. Reconstruction of the diffusion ODF from the diffusion signal using the FRT. The diffusion data are taken from a single voxel from the data set described under Methods. The sampling and reconstruction schemes are also described under Methods. (a) Diffusion signal sampled on fivefold tessellated icosahedron ($m = 252$). The signal intensity is indicated by the size and color (white yellow red) of the dots on the sphere. (b) Regridding of diffusion signal onto set of equators around vertices of fivefold tessellated dodecahedron ($k = n = 48 = 755 = 36240$ points). (c) Diffusion ODF calculated using FRT. (d) Color-coded spherical polar plot rendering of ODF. (e) Min-max normalized ODF.

Q-Ball Imaging

David S. Tuch^{1,2*}

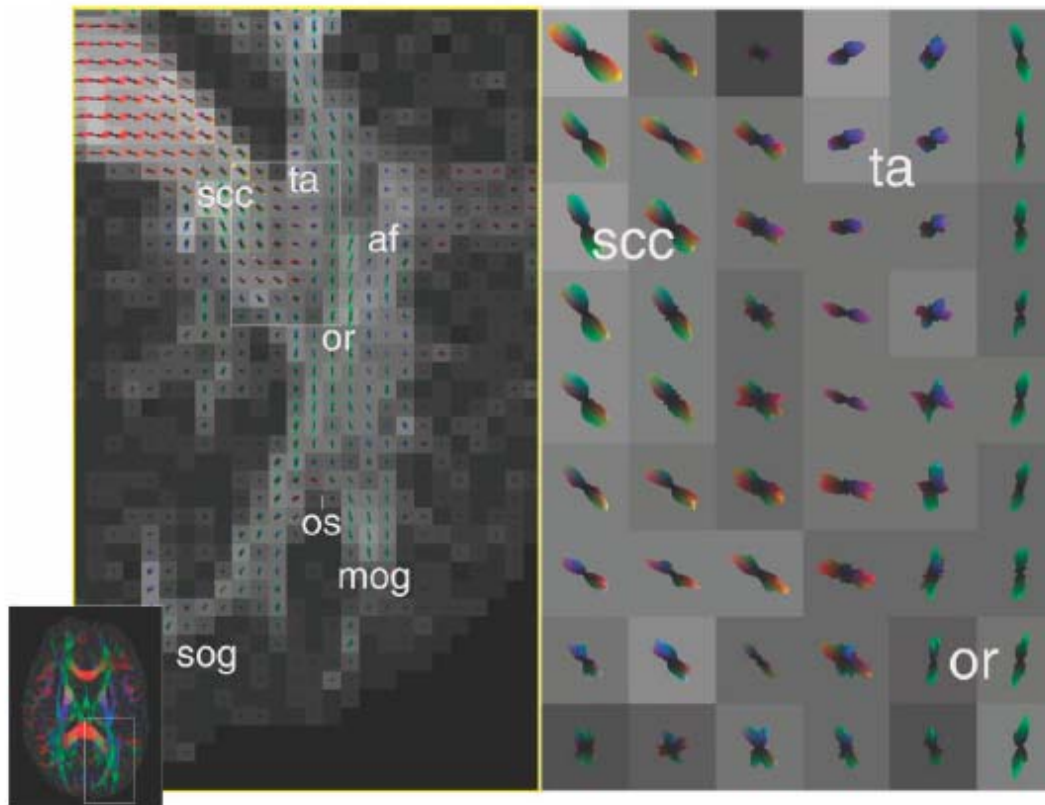


FIG. 7. ODF map of the intersection between the optic radiation and the splenium of the corpus callosum. The ODFs are rendered according to the scheme described in Theory, Visualization. The magnified view at right shows the crossing between splenium of the corpus callosum, the tapetum, and the optic radiation. af, arcuate fasciculus; mog, middle occipital gyrus; or, optic radiation; os, occipital sulcus; scc, splenium of the corpus callosum; sog, superior occipital gyrus; ta, tapetum.

Statistics of DTI data

The largest statistical problems (noise sources) are

- Registration of data between observers
- Image artifacts
- Image noise

The main statistical approach has been based on using the tensor parameters or derived quantities (e.g., FA).

I explain a new method that I think has good theory and great promise (Schwartzman, Dougherty, Taylor).

The problem with positive definite matrices

(Schwartzman, dissertation, 2006)

$$\begin{pmatrix} a & c \\ c & b \end{pmatrix}$$

$$a > 0, b > 0, ab - c^2 > 0$$

- The valid region of positive-definite (pd) matrices is bounded by a cone

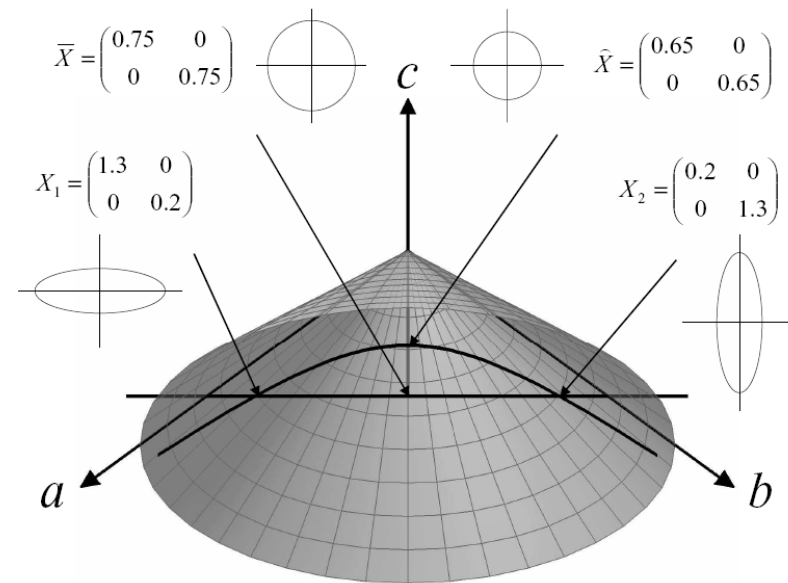


Figure 2.1: The cone of 2×2 positive definite matrices.

The problem with positive definite matrices

- The weighted sum (positive weights) of pd-matrices remains positive definite

$$x^t Q_1 x > 0$$

$$x^t Q_2 x > 0$$

$$\text{if } a, b > 0, \text{ then } x^t (aQ_1 + bQ_2)x > 0$$

- **But**, the differences between two pd-matrices may not be positive definite
- Adding even small amounts of noise to the entries of a pd-matrix may not result in a pd-matrix

Log transformation of the pd-matrix

Definition: Log and Exp of matrices

- It is advantageous to work in a representation where sums and differences, or adding symmetric noise, preserves the positive-definite characteristic
- The log transformation has these properties

$$Q = USV^t, \quad (svd)$$

$$\log(Q) = U \log(S) V^t$$

$$\exp(Q) = U \exp(S) V^t$$

$$\exp(\log(Q)) = \log(\exp(Q)) = Q$$

PD character is preserved in log domain

$$\exp(a \log(Q_1) + b \log(Q_2))$$

$$\exp(\log(Q_1) + \tilde{N})$$

Symmetric Gaussian noise



Log-normal references from INRIA

V. Arsigny, P. Fillard, X. Pennec, and N. Ayache, "Fast and simple calculus on tensors in the Log-Euclidean framework," in *MICCAI'05*, LNCS.

C. Lenglet, M. Rousson, R. Deriche, and O. Faugeras, "Statistics on multivariate normal distributions: A geometric approach and its application to diffusion tensor MRI," Research Report 5242, INRIA, 2004.

P. Fletcher and S. Joshi, "Principal geodesic analysis on symmetric spaces: Statistics of diffusion tensors.," in *CVAMIA and MMBIA*, 2004, LNCS 3117, pp. 87–98.

X. Pennec, P. Fillard, and N. Ayache, "A Riemannian framework for tensor computing," *IJCV*, vol. 66, no. 1, Jan. 2006, Also as INRIA Research Report (RR) 5255.

Definition: Log and Exp of matrices

$$Q = USV^t, \quad (svd)$$

$$\log(Q) = U \log(S)V^t$$

$$\exp(Q) = U \exp(S)V^t$$

$$\exp(\log(Q)) = \log(\exp(Q)) = Q$$

PD character is preserved in log domain

$$\exp(a \log(Q_1) + b \log(Q_2))$$

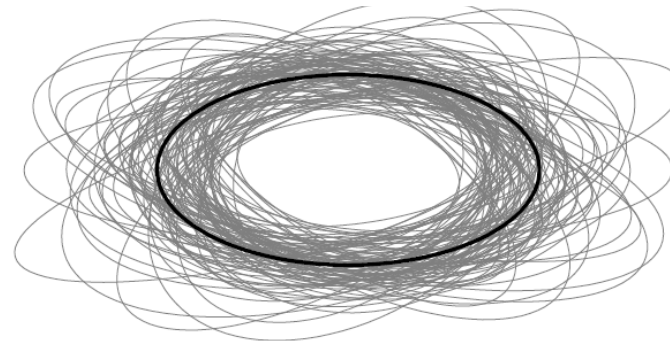
$$\exp(\log(Q_1) + \tilde{N})$$

 Symmetric Gaussian noise

Log-normal distribution from Stanford

(Schwartzman, et al. 2006)

- Schwartzman et al. model tensor (positive-definite matrix) noise as Gaussian noise in the log-transform domain



One hundred random ellipses generated from a log-normal distribution based on the original matrix

Statistical Analysis Tools for the Full Diffusion Tensor:

A Log-Normal Approach

Armin Schwartzman

Department of Statistics, Stanford University

Robert F. Dougherty

Department of Psychology, Stanford University

Jonathan E. Taylor

Department of Statistics, Stanford University

May 30, 2006

$$X = \begin{pmatrix} 4 & 0 \\ 0 & 1 \end{pmatrix} \quad X = \exp(\log(X) + \tilde{N})$$

Example: Symmetric Gaussian noise, variance 0.25.

Log-normal distribution

(Schwartzman, et al. 2006)

- Schwartzman et al. model tensor (positive-definite matrix) noise as Gaussian noise in the log-transform domain

Using this model they develop a set of statistical tests to compare the full tensor. These are:

- Omnibus test
- Eigenvalue tests
- Eigenvector tests

Statistical Analysis Tools for the Full Diffusion Tensor:

A Log-Normal Approach

Armin Schwartzman

Department of Statistics, Stanford University

Robert F. Dougherty

Department of Psychology, Stanford University

Jonathan E. Taylor

Department of Statistics, Stanford University

May 30, 2006

Atlases

- DTI measurements do not have equal statistical power throughout the white matter; partly measurement and partly processing
- The processing required to compare two groups includes steps (co-registration) have a significant impact on the result
- A good atlas will
 - Summarize the mean data after co-registration
 - The reliability of the 'typical' measurement.
 - May be built for different groups (adults vs. children; female vs. male; so forth)
 - Be available freely for download

DTI atlases

(Dougherty et al., 2005, NYAS)

A slice from an atlas summarizing 53 children's DTI measurements (N=53).

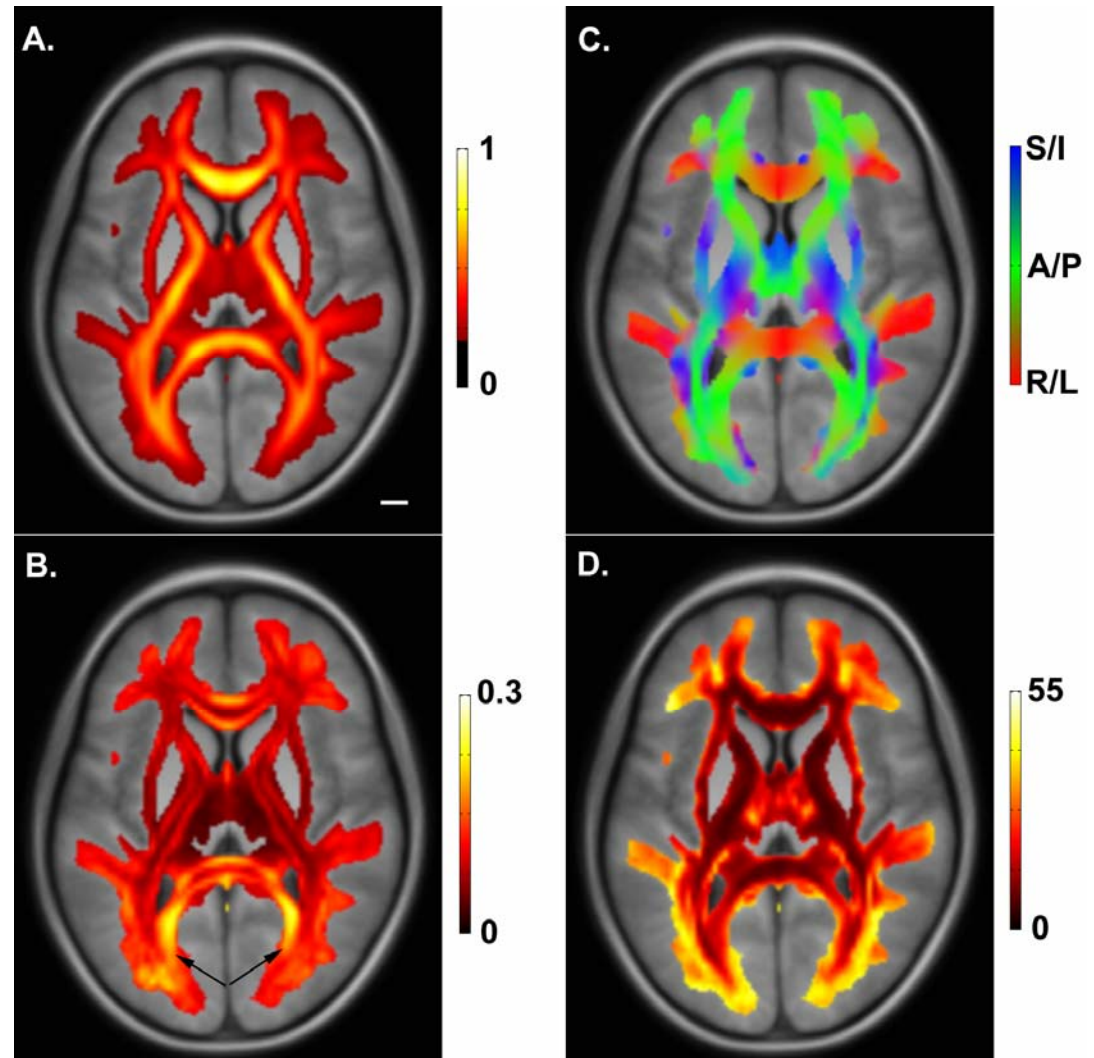
(A) Mean fractional anisotropy (FA).

(B) Standard deviation of FA.

(C) The principal diffusion direction (PDD): S/I, superior/inferior; A/P, anterior/posterior; R/L, right/left.

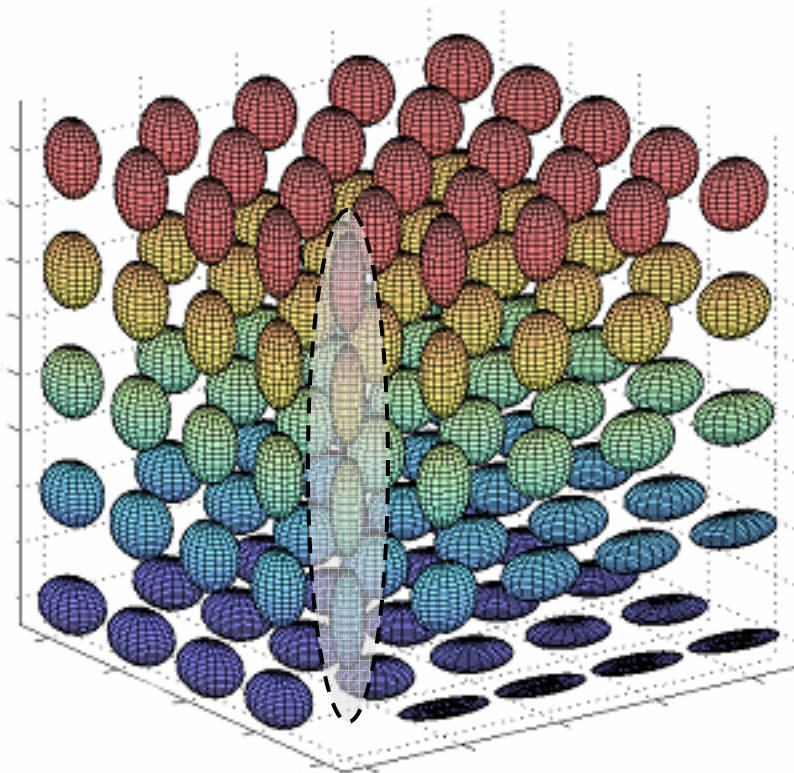
(D) PDD reliability is represented by the angular dispersion (in degrees).

Scale bar: 1 cm.



Fiber Tractography

Can We Understand These Data By Estimating Fiber Tracts (DTI-FT)?

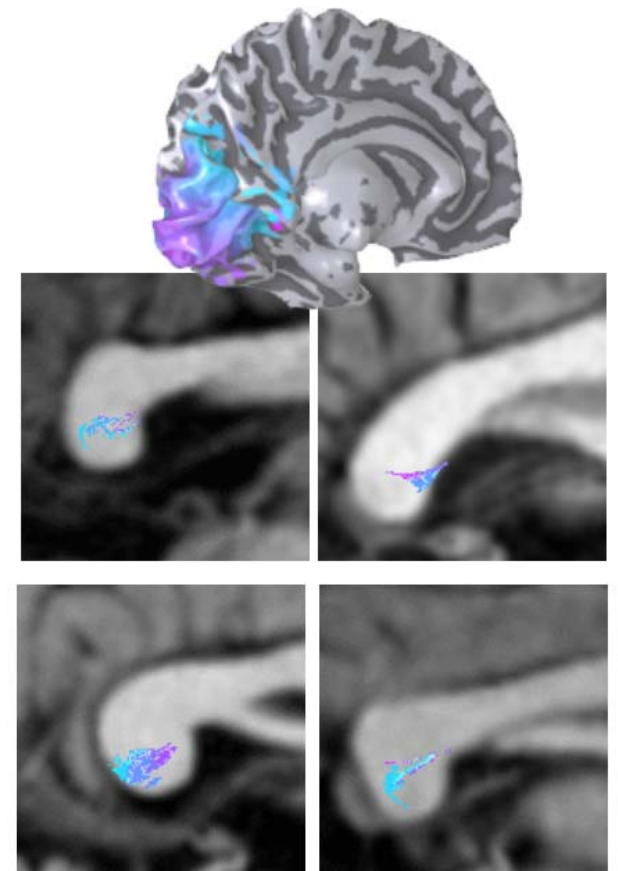


Many interesting algorithm issues

- Algorithm thresholds (direction, FA)
- Confidence intervals, probabilistic reasoning
- Spatial sampling
 - Samples are sparse, but directions are fine
 - Interpolation to intermediate positions
- Spatial co-registration between modalities (T1, fMRI) and subjects
- Validation needed

Fiber Tractography Overview

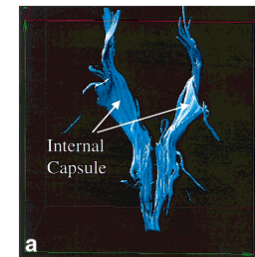
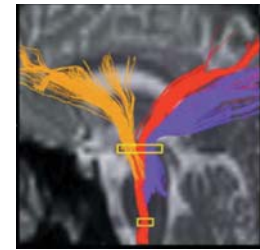
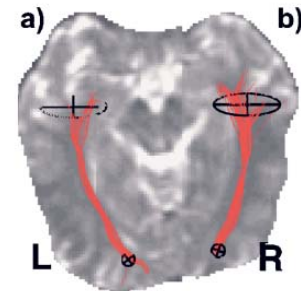
- Background - Deterministic algorithms (Conturo, Mori, Basser)
- Current developments - Probabilistic algorithms
- # mathematicians > # empirical validations
- Fiber tractography statistics and metrics an open field



Deterministic methods

Streamline Tracking Techniques (STT)

- Connect-the-voxels (Conturo)
- FACT (Mori, [DTIStudio](#))
- Path-integral method (Basser, Tuch)

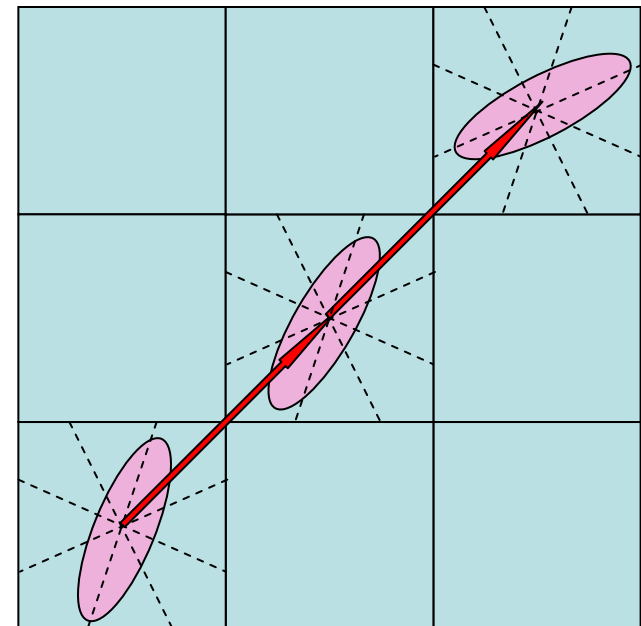


Connect-the-Voxels

(Conturo et al., 1999; PNAS)

- Super-samples the tensor field (e.g., resample from 2.5 mm to 0.5mm)
- Bi-directionally follow voxels in PDD direction (on the grid)
- Stopping rule: Tensor anisotropy becomes small.

0.5 mm super-sampled data

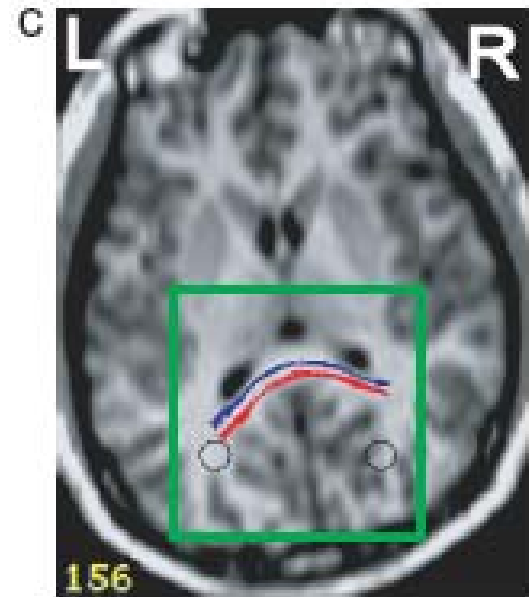


Connect-the-Voxels

(Conturo et al., 1999; PNAS)

- Super-samples the tensor field (e.g., resample from 2.5 mm to 0.5mm)
- Bi-directionally follow voxels in PDD direction (on the grid)
- Stopping rule: Tensor anisotropy becomes small.

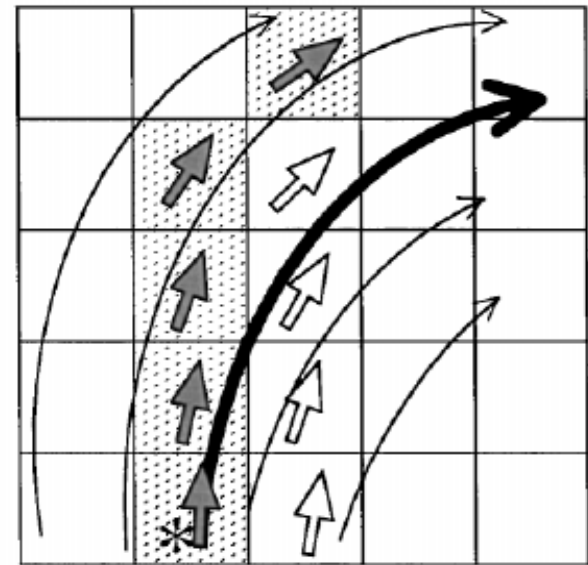
0.5 mm super-sampled data



Fiber Assignment by Continuous Tracking (FACT; Mori et al., 1999)

- Starting in a seed voxel, step in PDD until voxel edge
- Use tensor from the next voxel
- Continue in PDD until the next edge (variable step size)
- Paths fall between data samples; separates tensor sampling resolution and path resolution

Critique of Connect-the-voxels



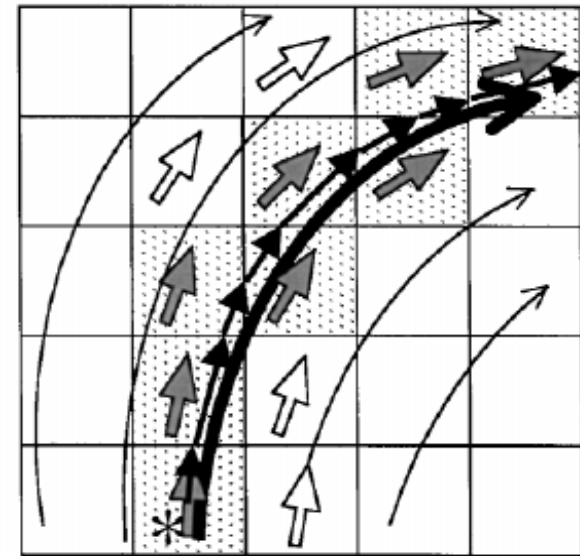
• Mori et al. (1999). *Three-Dimensional Tracking of Axonal Projections in the Brain by Magnetic Resonance Imaging*. *Annals of Neurology*.

• Xue et al. (1999) *In Vivo Three-Dimensional Reconstruction of Rat Brain Axonal Projections by Diffusion Tensor Imaging*. *MRM*.

Fiber Assignment by Continuous Tracking (FACT; Mori et al., 1999)

- Starting in a seed voxel, step in PDD until voxel edge
- Use tensor from the next voxel
- Continue in PDD until the next edge (variable step size)
- Paths fall between data samples; separates tensor sampling resolution and path resolution

Modified algorithm



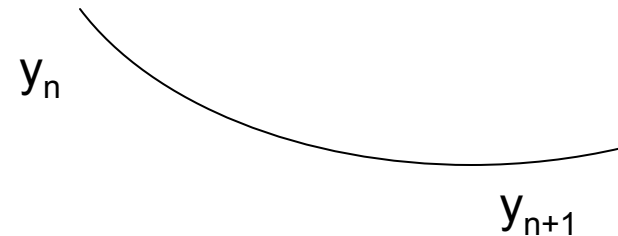
• Mori et al. (1999). *Three-Dimensional Tracking of Axonal Projections in the Brain by Magnetic Resonance Imaging*. *Annals of Neurology*.

• Xue et al. (1999) *In Vivo Three-Dimensional Reconstruction of Rat Brain Axonal Projections by Diffusion Tensor Imaging*. *MRM*.

Path-Integral Method

(Basser et al., 2000)

- Treat principal diffusion direction (PDD) as path tangent
- Uses tensor interpolation
- Estimate path integral using:
 - Euler method (simple)
 - Runge-Kutta (4th order typical)



Numerical Recipes
(Press et al., p. 711) $h = \text{step size}$

$$k_1 = hf(x_n, y_n)$$

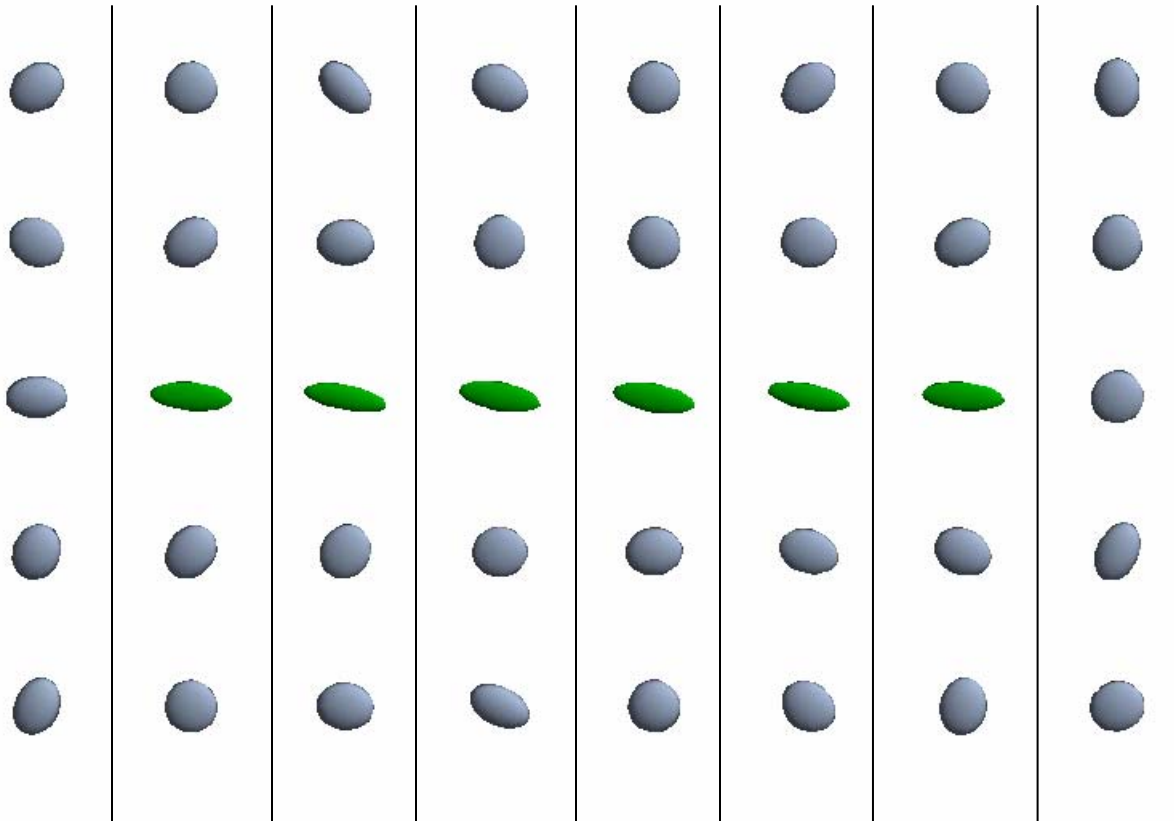
$$k_2 = hf\left(x_n + \frac{h}{2}, y_n + \frac{k_1}{2}\right)$$

$$k_3 = hf\left(x_n + \frac{h}{2}, y_n + \frac{k_2}{2}\right)$$

$$k_4 = hf(x_n + h, y_n + k_3)$$

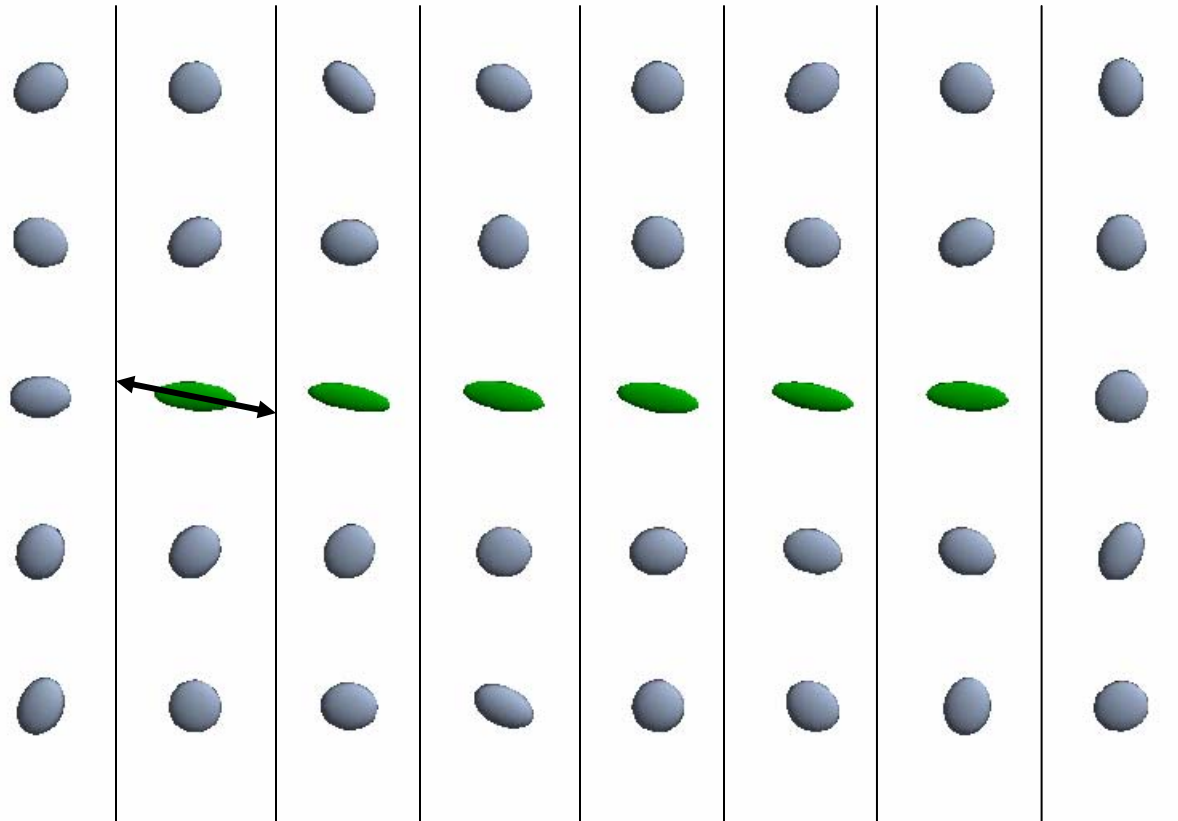
$$y_{n+1} = y_n + \frac{k_1}{6} + \frac{k_2}{3} + \frac{k_3}{3} + \frac{k_4}{6} + O(h^5)$$

Tensor data

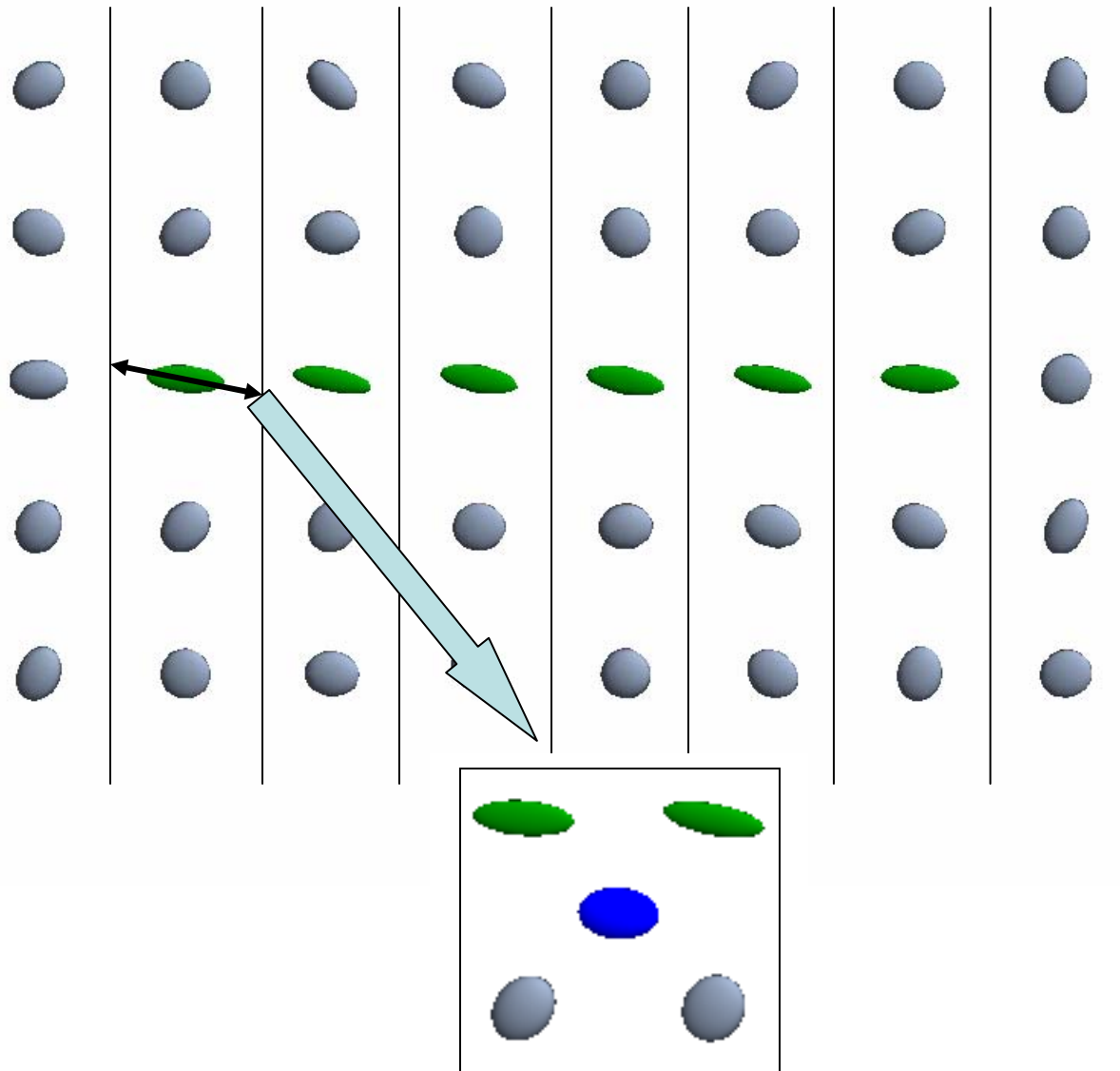


Start the path in the PDD at a seed

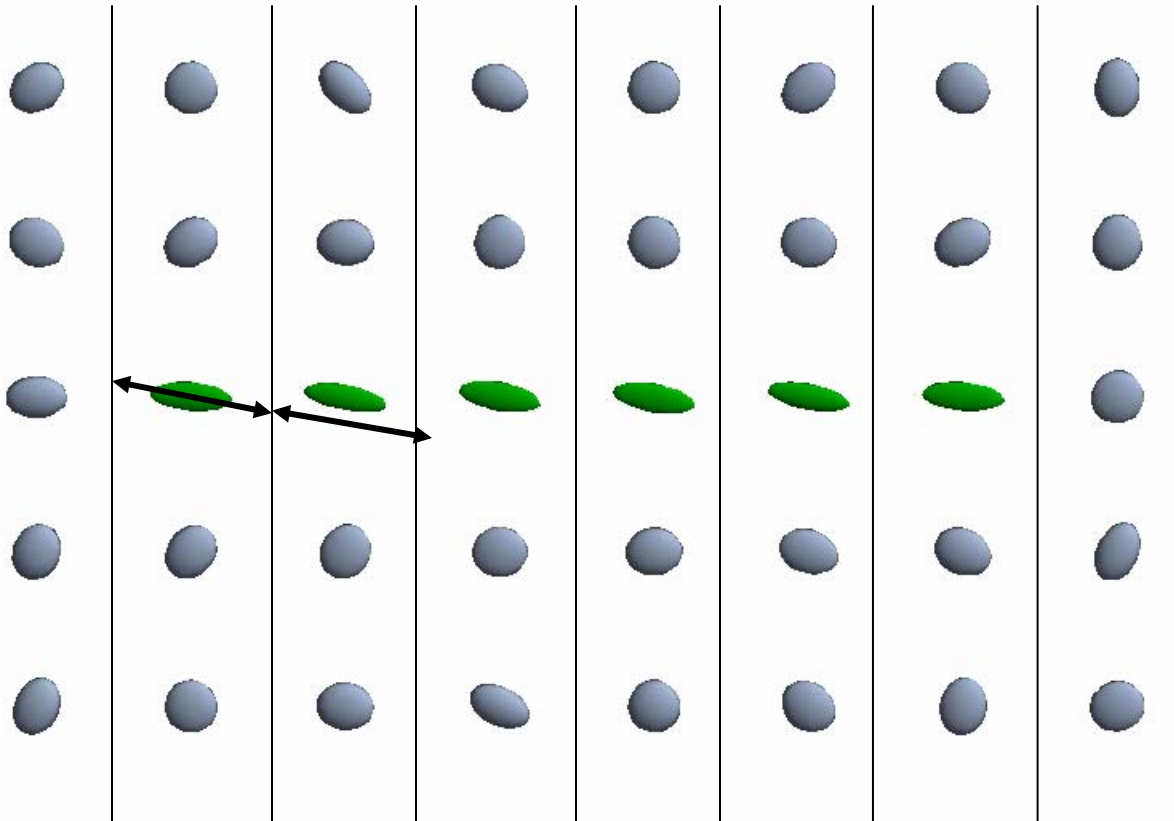
Many seeds will be used



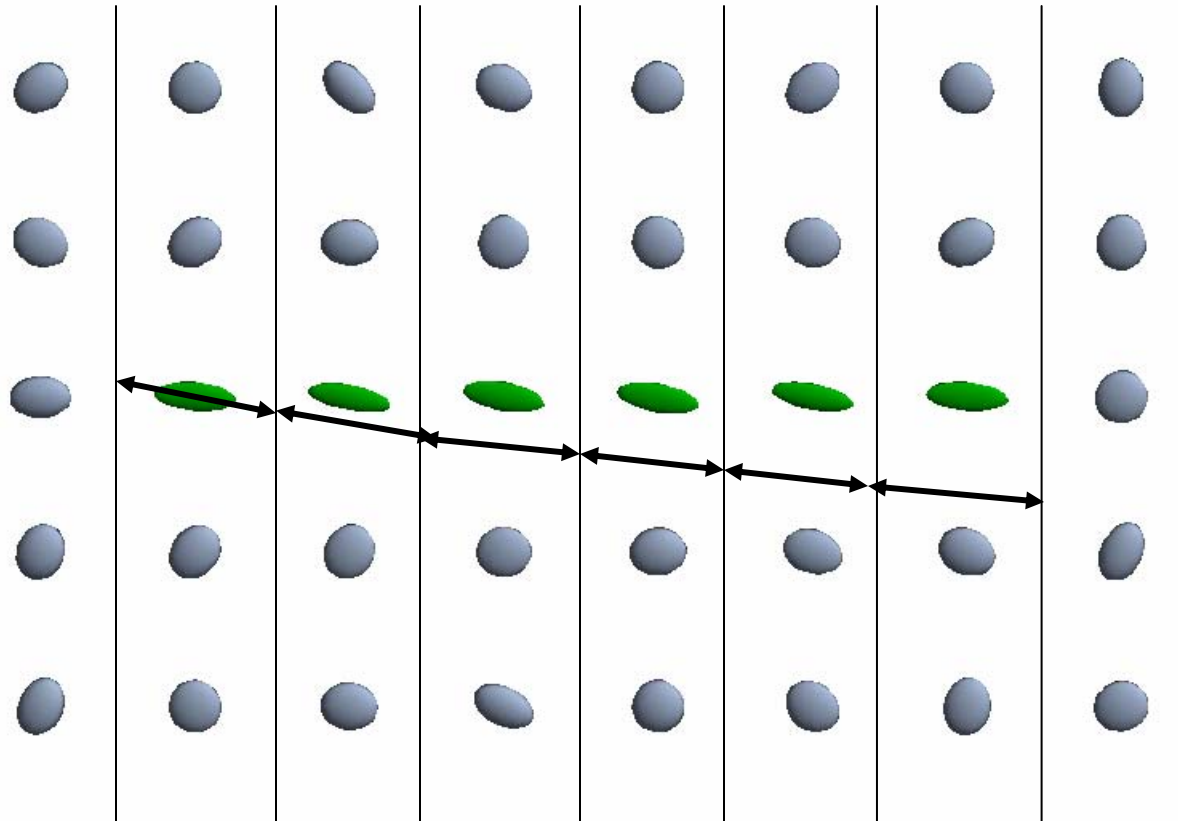
Interpolate a new tensor at path endpoint



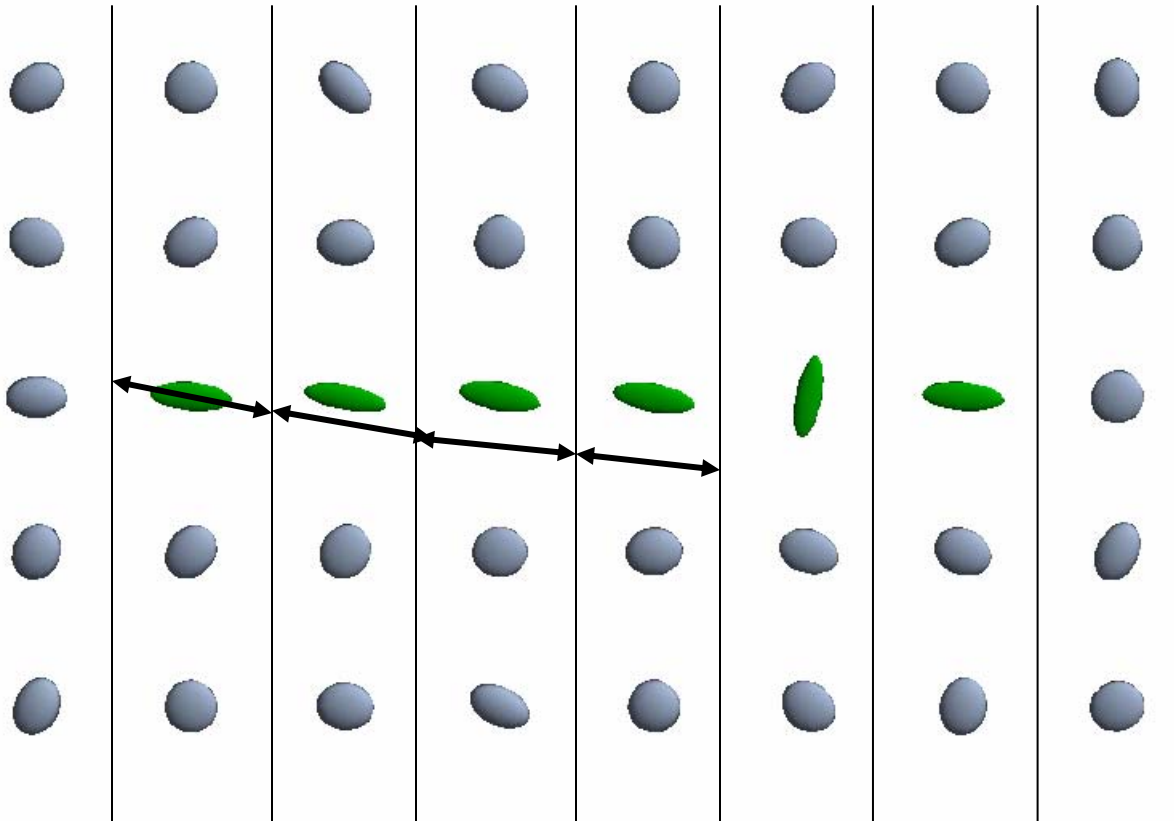
Take next step based on interpolation



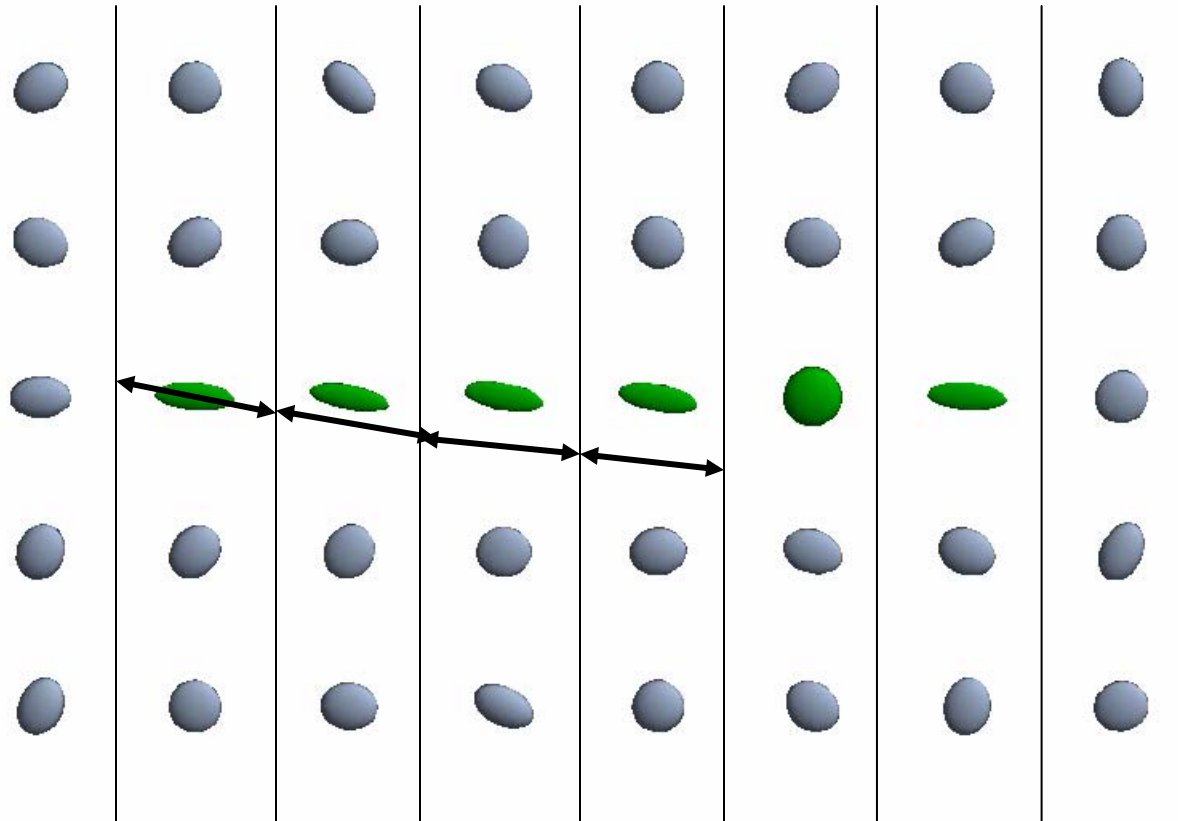
Repeat until termination condition



Terminates for angle



Terminates for isotropy



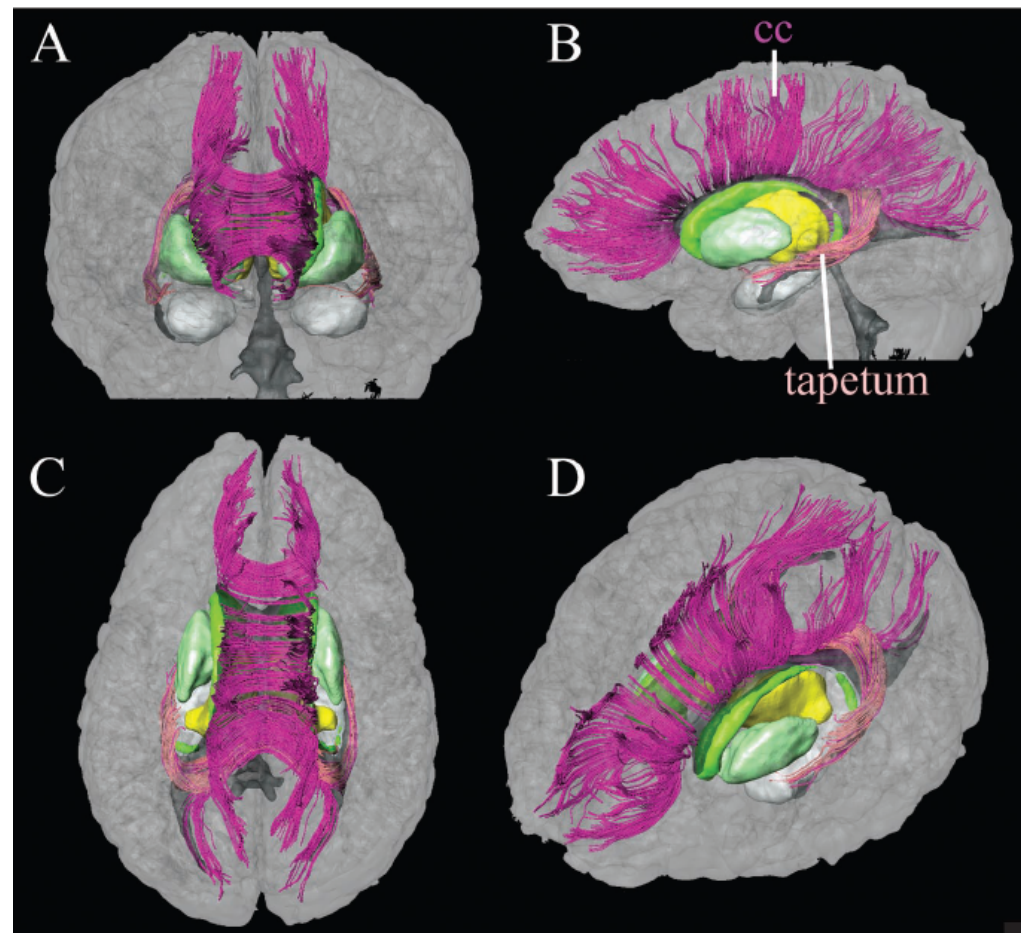
Validation and Examples

Setsu Wakana, MD
Hangyi Jiang, PhD
Lidia M. Nagae-Poetscher,
MD
Peter C. M. van Zijl, PhD
Susumu Mori, PhD

Fiber Tract-based Atlas of Human White Matter Anatomy¹

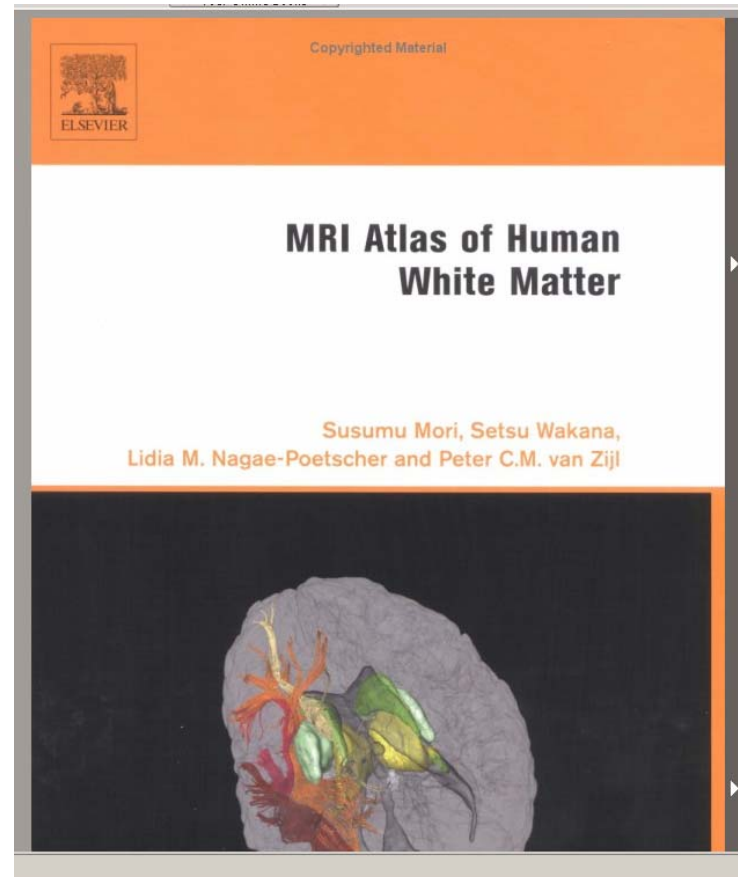
Two- and three-dimensional (3D) white matter atlases were created on the basis of

Figure 6. Four viewing angles show 3D depictions of callosal fibers. *A*, Anterior view; *B*, left lateral view; *C*, superior view; *D*, oblique view from right anterior angle. Corticocortical connections through corpus callosum (*cc*) are magenta. Subset of the tracts that project to temporal lobe (*tapetum*) are pink.



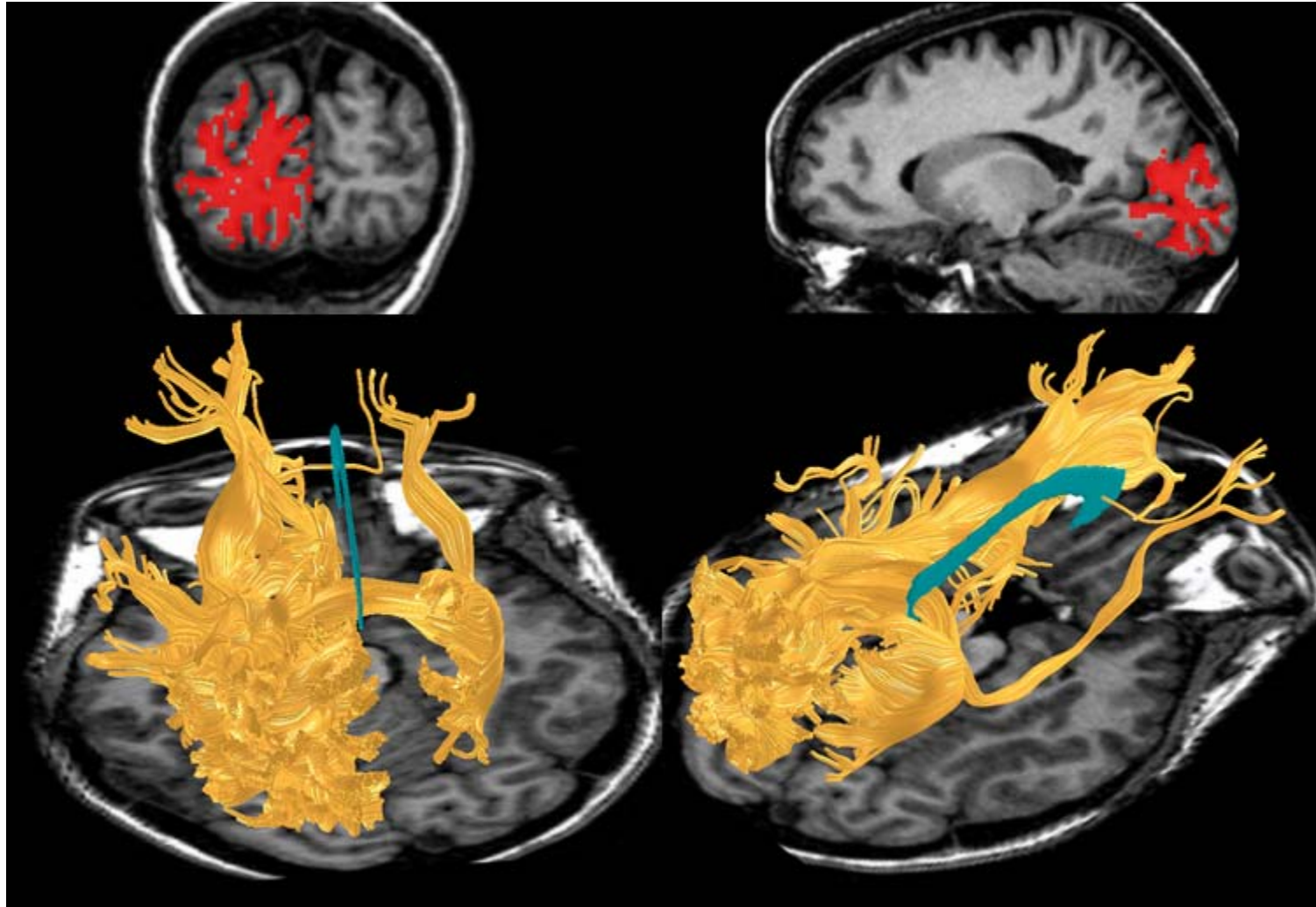
Atlas of human white matter

(Mori and collaborators)

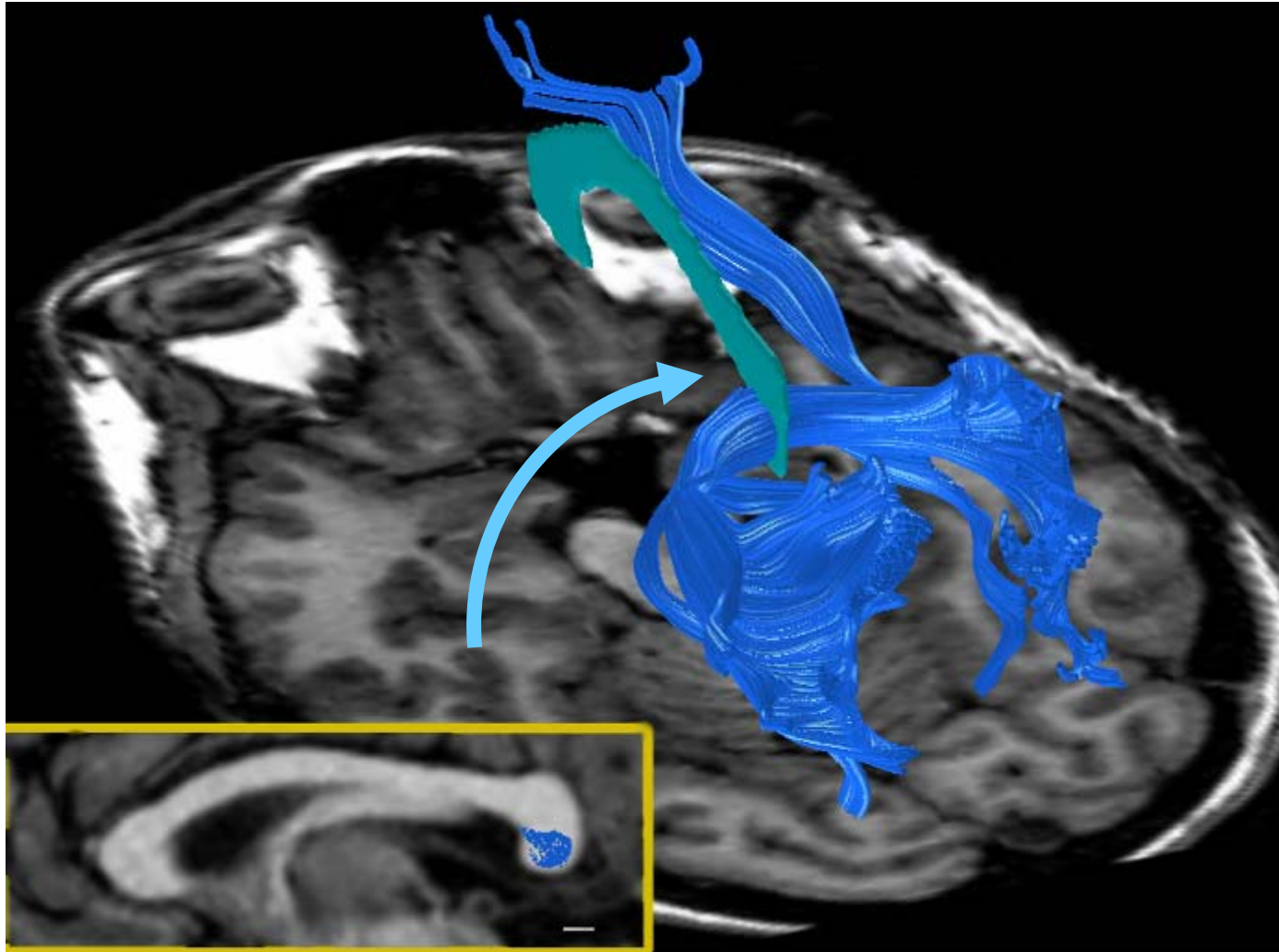


FT Estimates from left occipital seeds

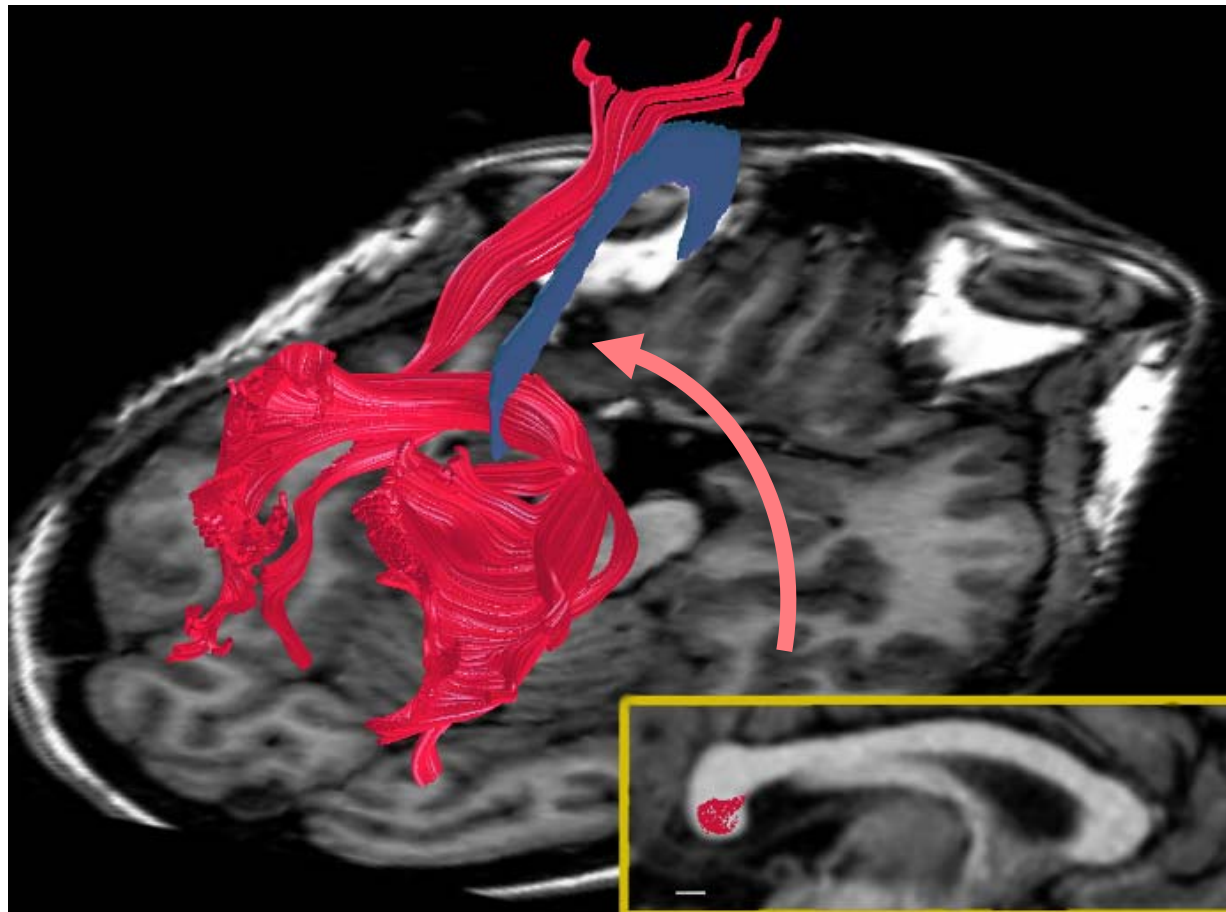
(Dougherty et al., PNAS, 2005)



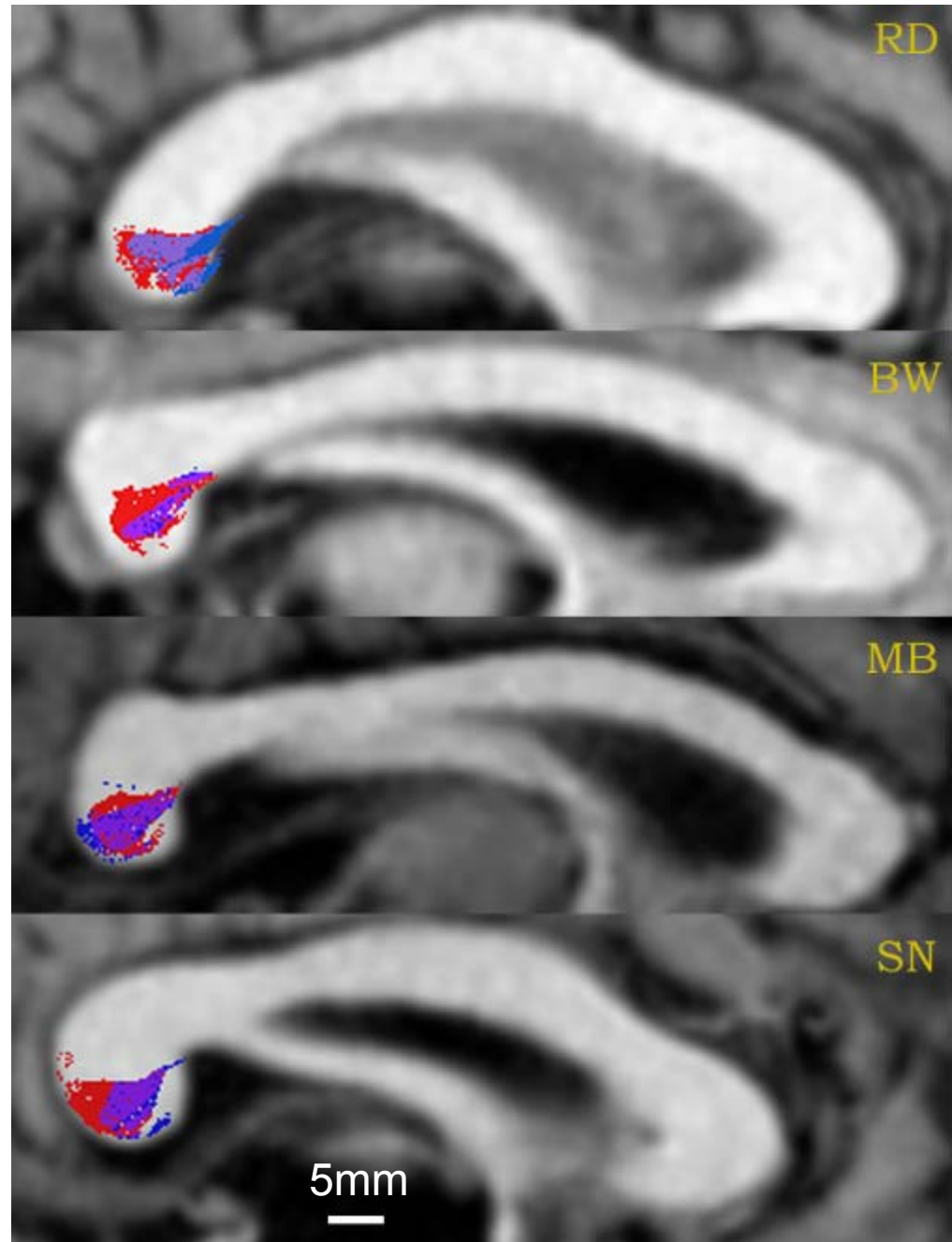
FTs from left occipital that pass through CC



Same calculation using right hemisphere data

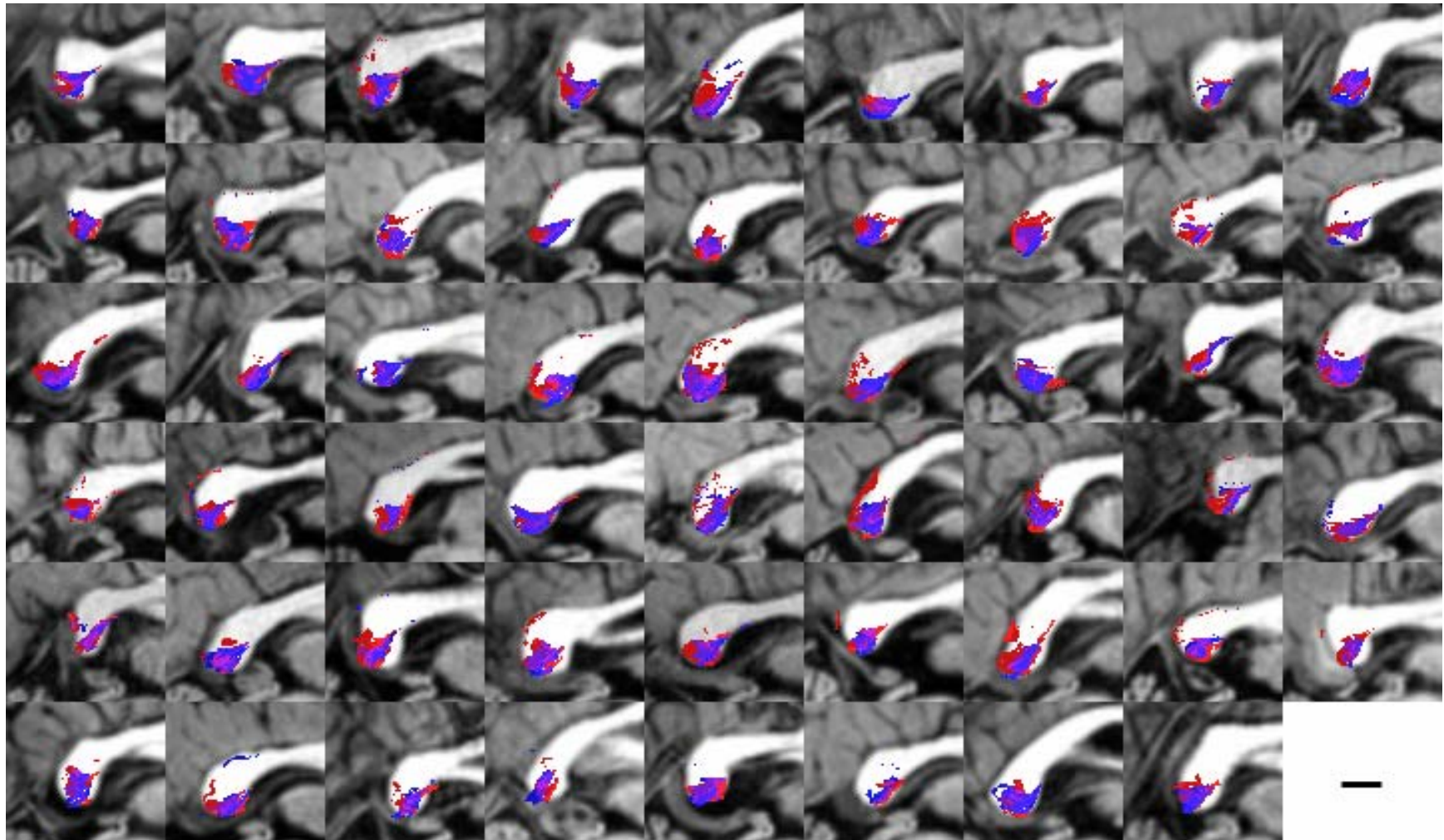


Excellent overlap
(centroid $\sim 0.5\text{mm}$)
in CC from
independent left
and right occipital
estimates;
50 children, too
(Dougherty, PNAS, 2005)



Repeated in group of 50 children

(Dougherty, NYAS, 2005)

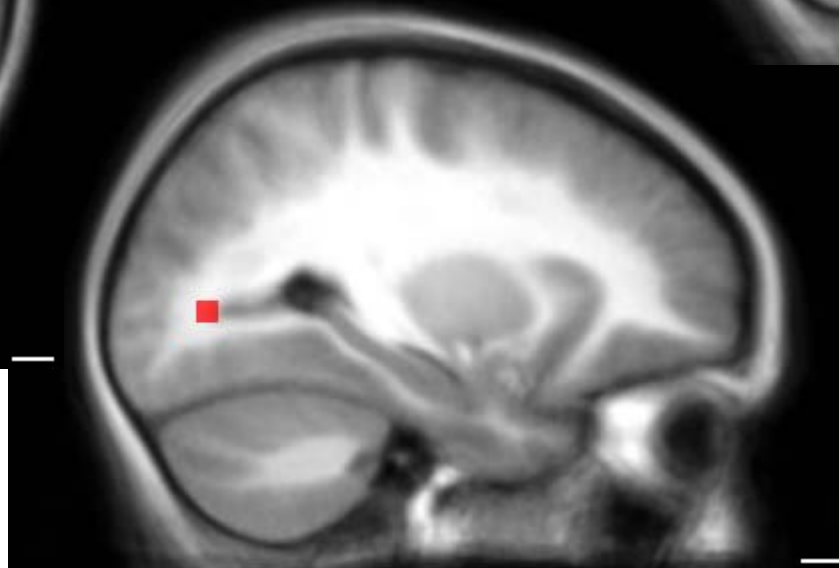
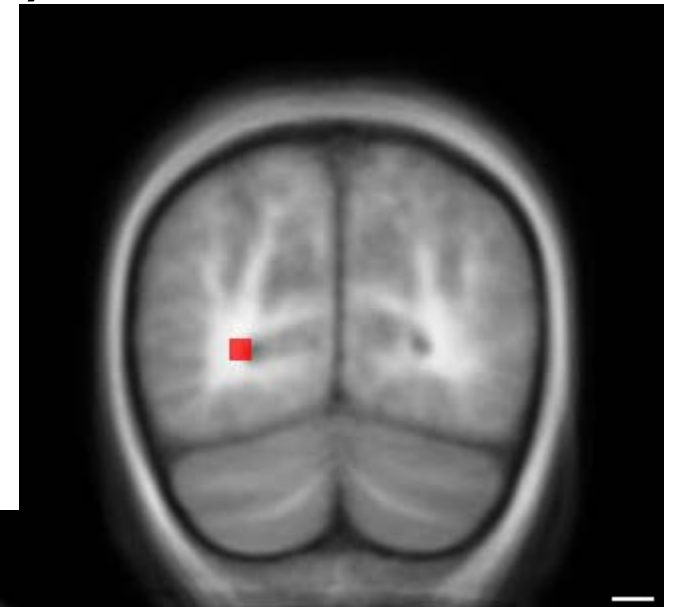


Acquired alexia: Callosal Lesion

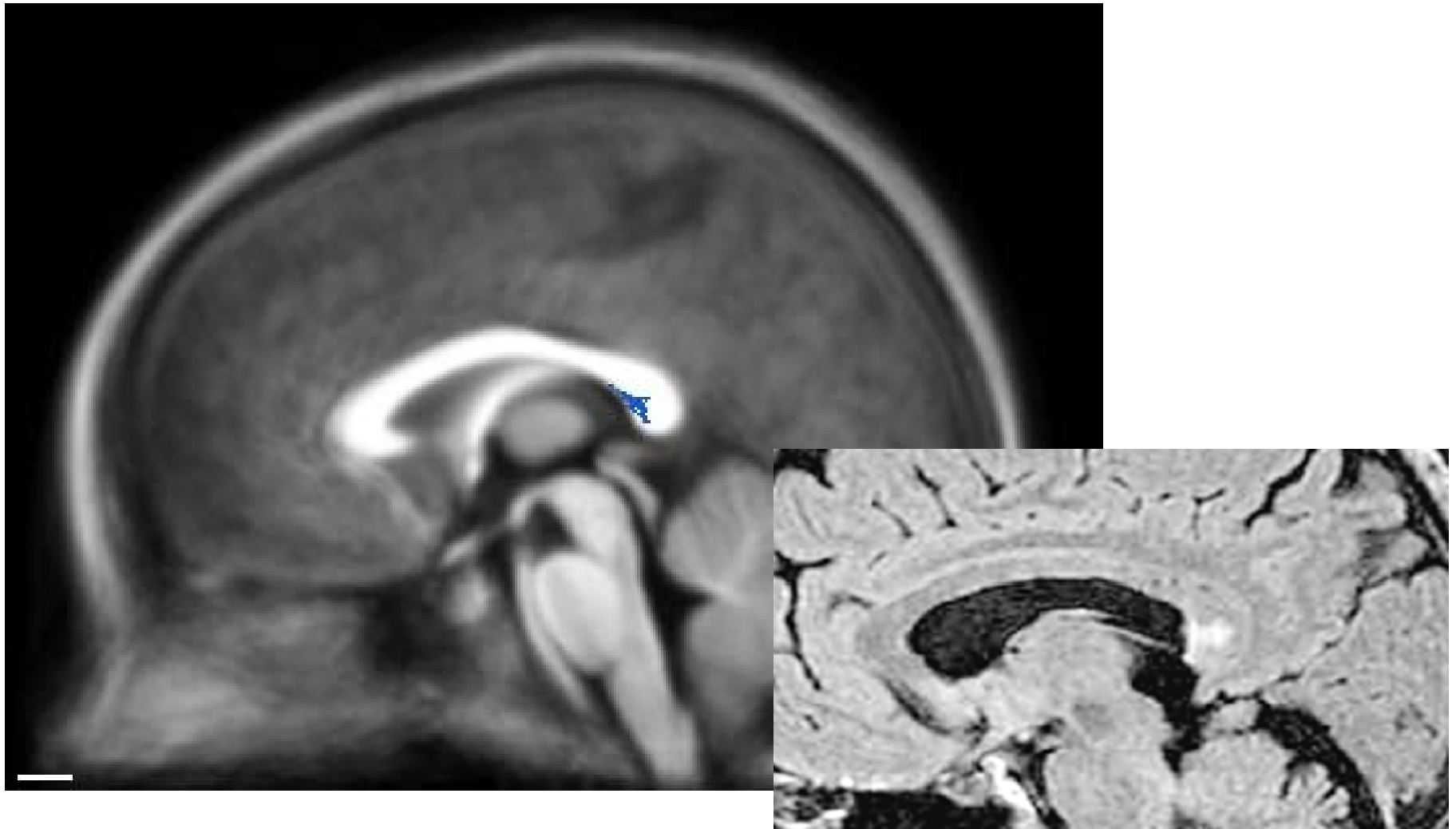


Figure 1 from Mao-Draayer & Panitch (2004), Alexia without agraphia in multiple sclerosis...

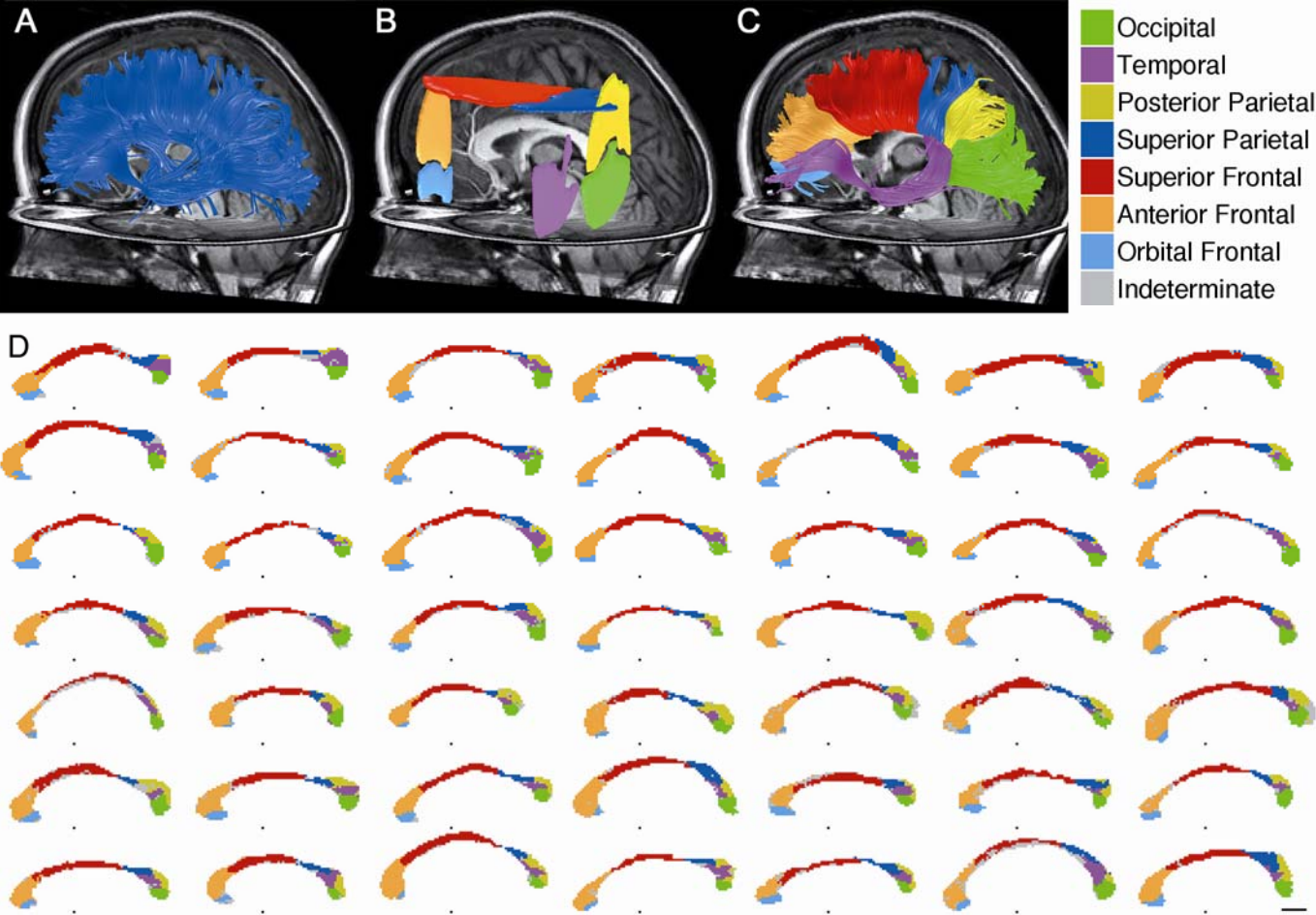
Forceps lesion location (average brain)



Fiber tracts predict lesion in callosum



Fiber tract dissection reveals a consistent organization of commissural fibers within the corpus callosum



Dougherty, xxx

Probabilistic methods

Many proposed algorithms. See references and keep going from there.

- Connection probabilities
- Find the most likely paths

Characterization and Propagation of Uncertainty in Diffusion-Weighted MR Imaging

(Behrens et al., 2003, MRM)

“... we may draw a sample from the posterior *pdf* on fiber direction at each point in space and construct the streamline (henceforth referred to as a “probabilistic streamline”) from A given these directions. Computationally, this process is extremely cheap. Samples from the local *pdfs* at each voxel have already been generated, so to generate a single probabilistic streamline from seed point A , referring to the current “front” of the streamline as \mathbf{z} , it is sufficient simply to start \mathbf{z} at A and:

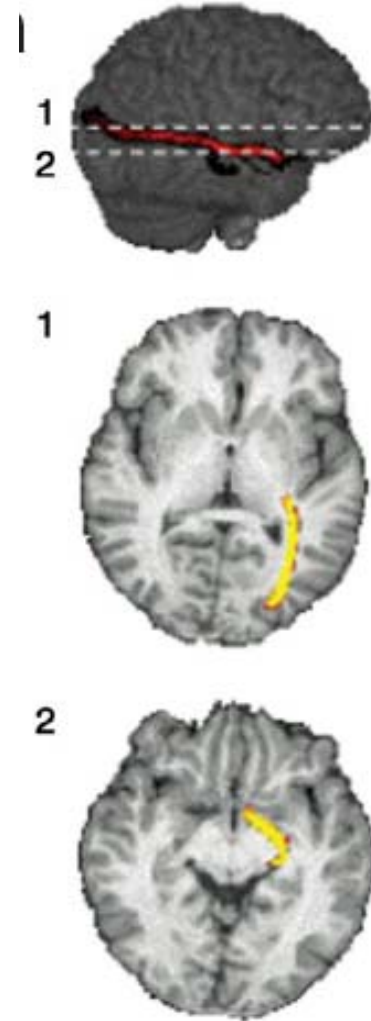
- Select a random sample, (θ, φ) from $P(\theta, \varphi | \mathbf{Y})$ at \mathbf{z} .
- Move \mathbf{z} a distance s along (θ, φ)
- Repeat until stopping criterion is met.

This probabilistic streamline is said to connect A to all points B along its path. By drawing many such samples, we may build the *spatial pdf* of $P(A \rightarrow B | \mathbf{Y})$ for all B . **We may then discretize this distribution into voxels by simply counting the number of probabilistic streamlines which pass through a voxel B , and dividing by the total number of probabilistic streamlines.** (p. 1084)”

Non-invasive mapping of connections between human thalamus and cortex using diffusion imaging

T E J Behrens^{1,2,4}, H Johansen-Berg^{1,4}, M W Woolrich^{1,2}, S M Smith¹, C A M Wheeler-Kingshott³, P A Boulby³, G J Barker³, E L Sillery¹, K Sheehan¹, O Ciccarelli³, A J Thompson³, J M Brady² & P M Matthews¹

“Tracing connectivity distributions from individual seed voxels. Voxels are color-coded according to whether the probability of pathways traveling through that voxel is high (yellow) or low (red). ... From a voxel in putative LGN, the connectivity distribution was traced anteriorly along the optic tract, and posteriorly to the visual cortex, consistent with the well established anatomy of the visual system.
“(Figure 1, caption)

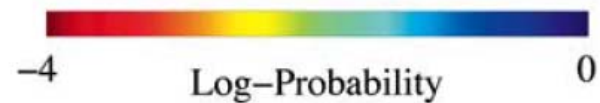
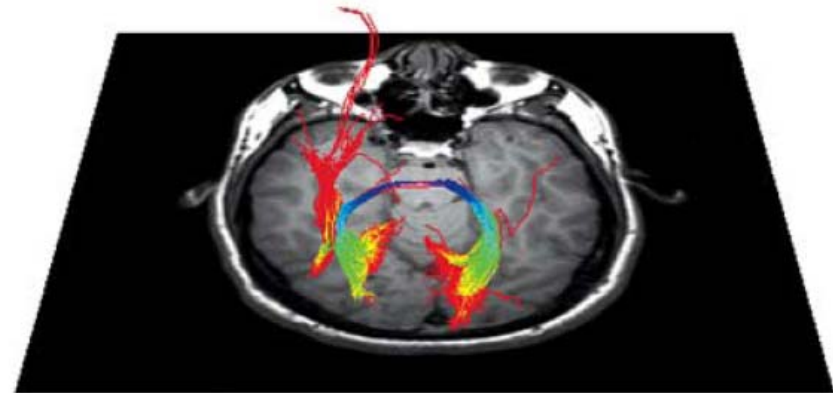
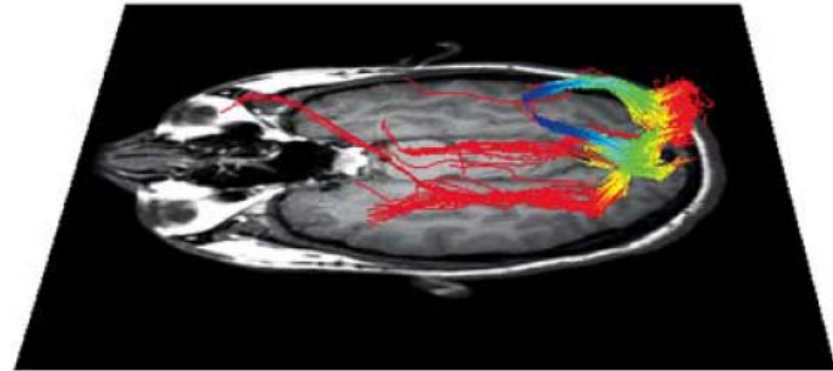


Example of probability along the path

(Friman et al., IEEE-TMI, 2006)

Three thousand fiber samples initiated in the splenium of Corpus callosum. The coloring indicates how the probability evolves along the fiber paths according to Jones et al.

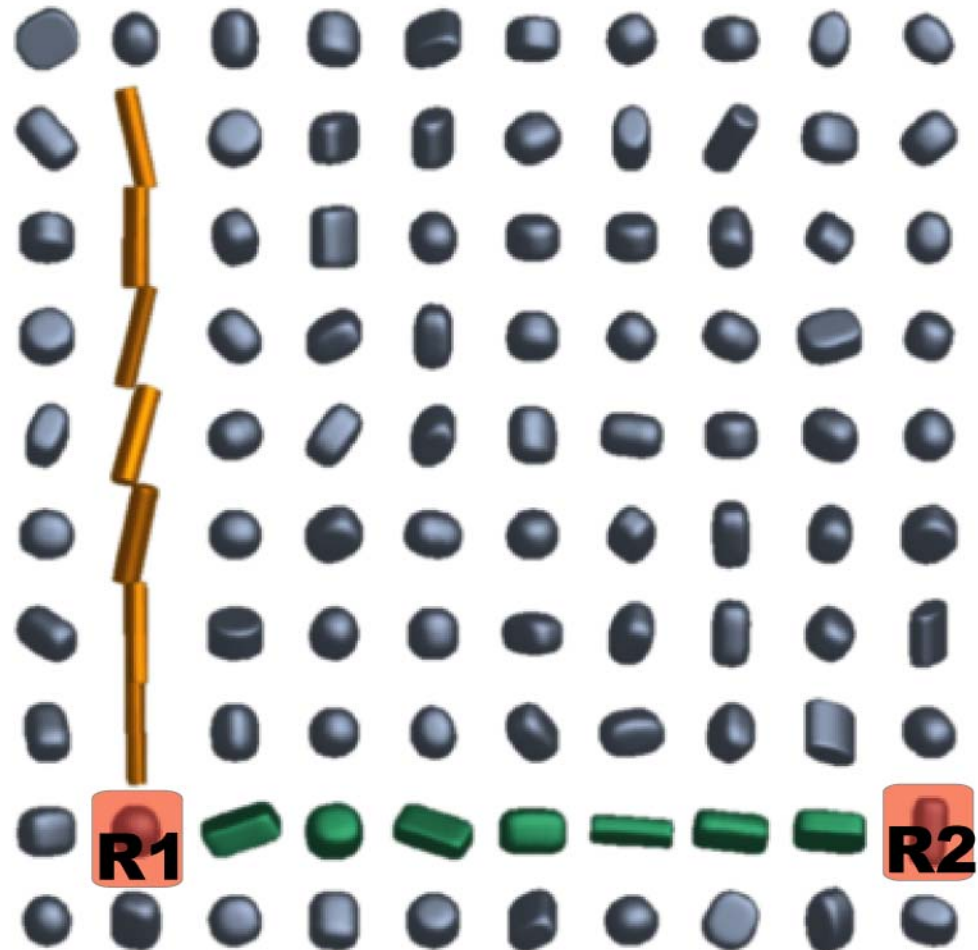
Jones et al., "Determining and visualizing uncertainty in estimates of fiber orientation from diffusion tensor MRI," *Magn. Reson. Med.*, vol. 49, no. 1, pp. 7–12, 2003.



MetroTrac: Finding the most likely paths

(Sherbondy et al., 200N)

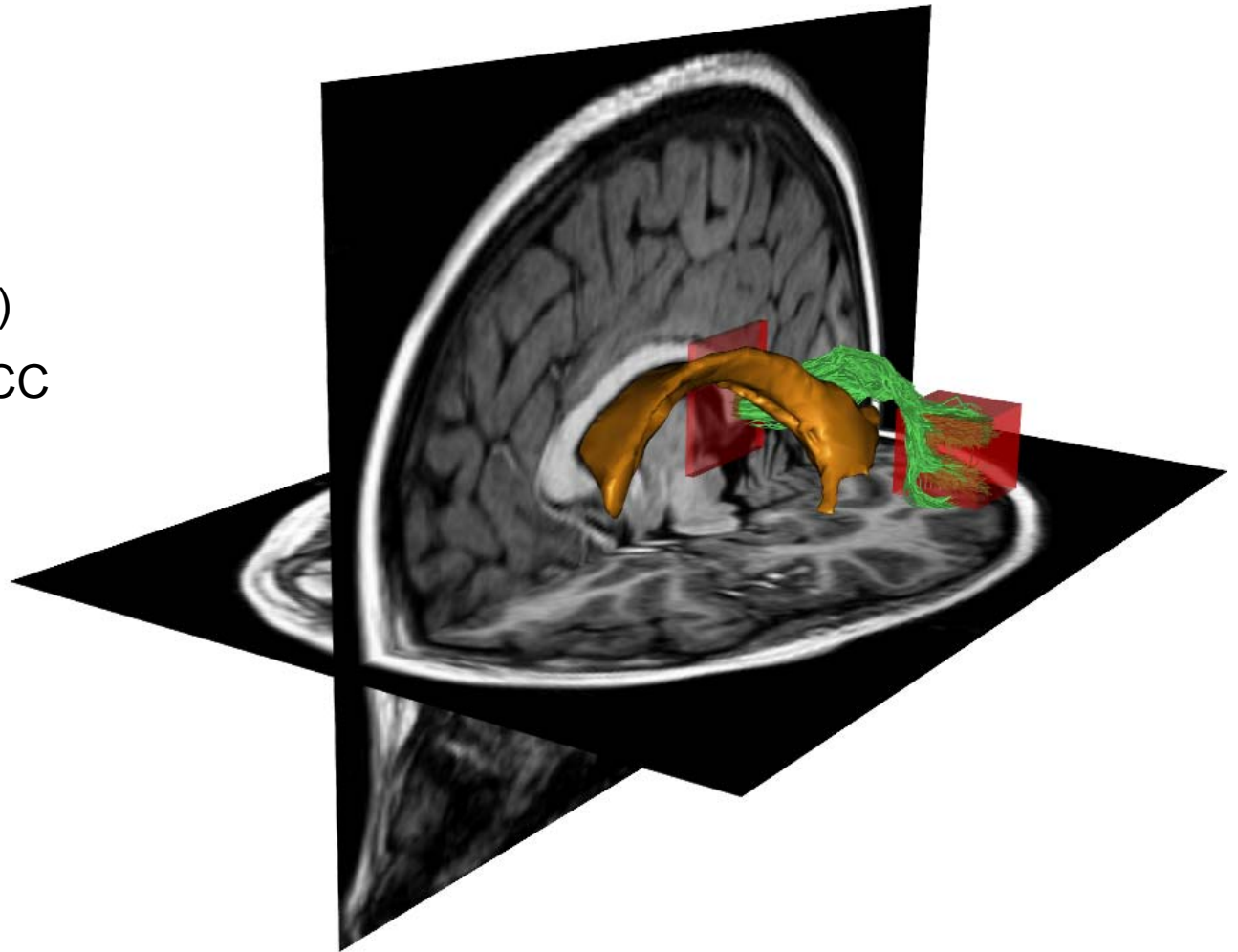
- Scoring
 - Symmetry
 - Independence
- Samplers
- Inference



MetroTrac: MT-CC connections

(Sherbondy et al., 200N)

- 2 ROIs (red)
 - Ventricle (gold)
 - MetroTrac path (green)
- estimate from hMT+ to CC



DTI and Fiber Tractography Software

- **FMRIB** (<http://www.fmrib.ox.ac.uk/fsl/>)
- **DTIStudio**(<http://lbam.med.jhmi.edu/DTIuser/DTIuser.asp>)
- **dtiQuery** (<http://graphics.stanford.edu/projects/dti/dti-query/>)
- **Camino** (<http://www.cs.ucl.ac.uk/research/medic/camino/>)
- **NAMIC** (http://www.na-mic.org/Wiki/index.php/Main_Page)

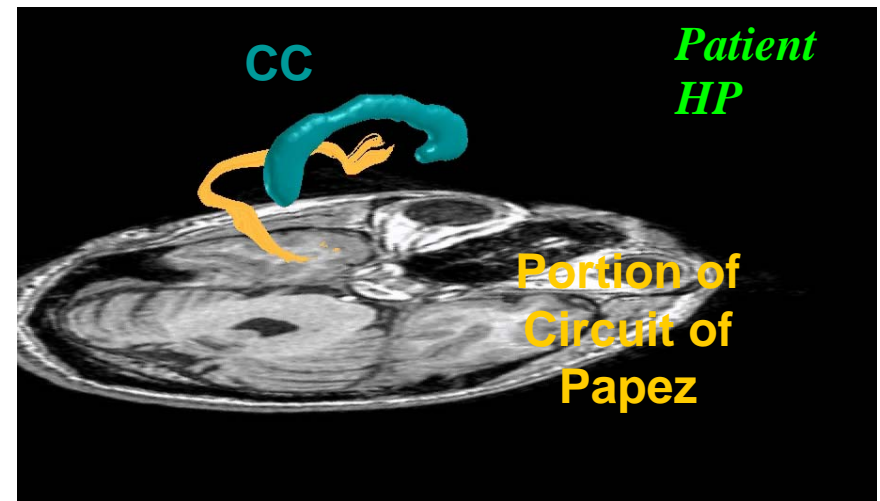
End

Example: Epilepsy

- Intractable epilepsy
 - Candidate for resection
 - Identification of seizure locus
- Measure seizing circuits
 - In human using (MR)
 - Cellular basis in animal models
- Theory: Span the measurement scales
 - Predict mean diffusivity post- and inter-ictal based on cellular (neural/glial) mechanisms from animal models
 - Optimize MR sequences for diagnosis

**A Portion of Circuit of Papez,
often implicated in MTL epilepsy**

From Brian Wandell

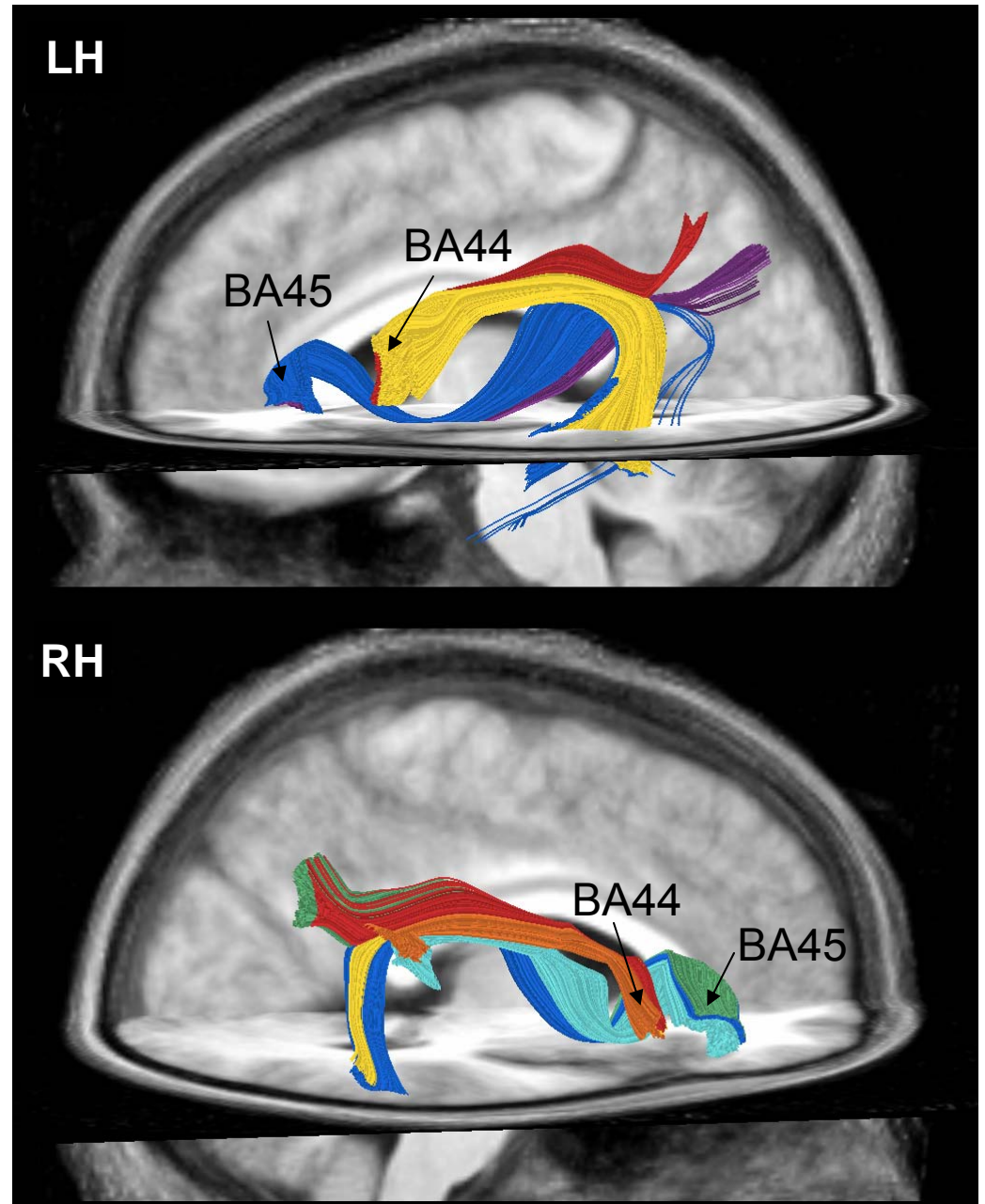


**Visualized using
diffusion tensor imaging
and fiber tractography**

Postmortem dissections provide coarse mapping of white matter



Fiber tract dissection reveals separate routes that connect Brodmann areas 44 and 45 with posterior language areas



Ben-Shachar, Eckert, Dougherty, in preparation

Diffusion tensor imaging references

Textbook

Functional Magnetic Resonance Imaging
Huettel, Song and McCarthy
Sinauer Press
(Huettel et al., 2004)

The Basics of MRI
Joseph Hornak
<http://www.cis.rit.edu/htbooks/mri/>

Reviews

(Basser, 1995; Basser and Jones, 2002)
(Basser and Pierpaoli, 1996)
(Le Bihan et al., 2001)
(Beaulieu, 2002)
(Tuch et al., 2002; Tuch, 2004)

Additional References, as if you need more

Applications

(Basser et al., 2000; Deutsch et al., 2005) – Reading Development
(Beaulieu et al., 2005) – Reading development
(Gross et al., 2006) - Epilepsy
(Jones et al., 2005) - Schizophrenia

Fiber Tractography

(Basser et al., 2000)
(Dougherty et al., 2005a; Dougherty et al., 2005b)
(Conturo et al., 1999)
(Mori et al., 1999; Mori et al., 2001; Wakana et al., 2004)
(Catani et al., 2002; Jones et al., 2002; Catani et al., 2003)
(Westin et al., 2002; Friman and Westin, 2005; Friman et al., 2006)

Conference links

International Society for Magnetic Resonance in Medicine
<http://www.ismrm.org/06/Session62.htm>

2006 IEEE Symposium

References

- Basser PJ (1995) Inferring microstructural features and the physiological state of tissues from diffusion-weighted images. *NMR Biomed* 8:333-344.
- Basser PJ, Pierpaoli C (1996) Microstructural and physiological features of tissues elucidated by quantitative-diffusion-tensor MRI. *J Magn Reson B* 111:209-219.
- Basser PJ, Jones DK (2002) Diffusion-tensor MRI: theory, experimental design and data analysis - a technical review. *NMR Biomed* 15:456-467.
- Basser PJ, Pajevic S, Pierpaoli C, Duda J, Aldroubi A (2000) In vivo fiber tractography using DT-MRI data. *Magn Reson Med* 44:625-632.
- Beaulieu C (2002) The basis of anisotropic water diffusion in the nervous system - a technical review. *NMR Biomed* 15:435-455.
- Beaulieu C, Plewes C, Paulson LA, Roy D, Snook L, Concha L, Phillips L (2005) Imaging brain connectivity in children with diverse reading ability. *Neuroimage* 25:1266-1271.
- Catani M, Howard RJ, Pajevic S, Jones DK (2002) Virtual in vivo interactive dissection of white matter fasciculi in the human brain. *Neuroimage* 17:77-94.
- Catani M, Jones DK, Donato R, Ffytche DH (2003) Occipito-temporal connections in the human brain. *Brain* 126:2093-2107.
- Conturo TE, Lori NF, Cull TS, Akbudak E, Snyder AZ, Shimony JS, McKinstry RC, Burton H, Raichle ME (1999) Tracking neuronal fiber pathways in the living human brain. *Proc Natl Acad Sci U S A* 96:10422-10427.
- Deutsch GK, Dougherty RF, Bammer R, Siok WT, Gabrieli JD, Wandell B (2005) Children's reading performance is correlated with white matter structure measured by diffusion tensor imaging. *Cortex* 41:354-363.
- Dougherty RF, Ben-Shachar M, Bammer R, Brewer AA, Wandell BA (2005a) Functional organization of human occipital-callosal fiber tracts. *Proc Natl Acad Sci U S A* 102:7350-7355.
- Dougherty RF, Ben-Shachar M, Deutsch G, Potanina P, Bammer R, Wandell BA (2005b) Occipital-callosal pathways in children: Validation and atlas development. *Ann N Y Acad Sci* 1064:98-112.
- Friman O, Westin CF (2005) Uncertainty in white matter fiber tractography. *Med Image Comput Comput Assist Interv Int Conf Med Image Comput Comput Assist Interv* 8:107-114.
- Friman O, Farneback G, Westin CF (2006) A Bayesian approach for stochastic white matter tractography. *IEEE Trans Med Imaging* 25:965-978.
- Gross DW, Concha L, Beaulieu C (2006) Extratemporal white matter abnormalities in mesial temporal lobe epilepsy demonstrated with diffusion tensor imaging. *Epilepsia* 47:1360-1363.
- Huettel S, Song A, McCarthy G (2004) *Functional magnetic resonance imaging*. Sunderland, Mass.: Sinauer Associates.

- Jones DK, Griffin LD, Alexander DC, Catani M, Horsfield MA, Howard R, Williams SC (2002) Spatial normalization and averaging of diffusion tensor MRI data sets. *Neuroimage* 17:592-617.
- Jones DK, Catani M, Pierpaoli C, Reeves SJ, Shergill SS, O'Sullivan M, Maguire P, Horsfield MA, Simmons A, Williams SC, Howard RJ (2005) A diffusion tensor magnetic resonance imaging study of frontal cortex connections in very-late-onset schizophrenia-like psychosis. *Am J Geriatr Psychiatry* 13:1092-1099.
- Le Bihan D, Mangin JF, Poupon C, Clark CA, Pappata S, Molko N, Chabriat H (2001) Diffusion tensor imaging: concepts and applications. *J Magn Reson Imaging* 13:534-546.
- Mori S, Crain BJ, Chacko VP, van Zijl PC (1999) Three-dimensional tracking of axonal projections in the brain by magnetic resonance imaging. *Ann Neurol* 45:265-269.
- Mori S, Itoh R, Zhang J, Kaufmann WE, van Zijl PC, Solaiyappan M, Yarowsky P (2001) Diffusion tensor imaging of the developing mouse brain. *Magn Reson Med* 46:18-23.
- Tuch DS (2004) Q-ball imaging. *Magn Reson Med* 52:1358-1372.
- Tuch DS, Reese TG, Wiegell MR, Makris N, Belliveau JW, Wedeen VJ (2002) High angular resolution diffusion imaging reveals intravoxel white matter fiber heterogeneity. *Magn Reson Med* 48:577-582.
- Wakana S, Jiang H, Nagae-Poetscher LM, van Zijl PC, Mori S (2004) Fiber tract-based atlas of human white matter anatomy. *Radiology* 230:77-87.
- Westin CF, Maier SE, Mamata H, Nabavi A, Jolesz FA, Kikinis R (2002) Processing and visualization for diffusion tensor MRI. *Med Image Anal* 6:93-108.